Titre: Title:	Metal Oxides for Ion-Gated Transistors
Auteur: Author:	Arunprabaharan Subramanian
Date:	2021
Type:	Mémoire ou thèse / Dissertation or Thesis
Référence: Citation:	Subramanian, A. (2021). Metal Oxides for Ion-Gated Transistors [Ph.D. thesis, Polytechnique Montréal]. PolyPublie. https://publications.polymtl.ca/9994/

POLYTECHNIQUE MONTRÉAL

affiliée à l'Université de Montréal

Metal Oxides for Ion-Gated Transistors

ARUNPRABAHARAN SUBRAMANIAN

Département de génie chimique

Thèse présentée en vue de l'obtention du diplôme de *Philosophiæ Doctor*

Génie des matériaux

Décembre 2021

POLYTECHNIQUE MONTRÉAL

affiliée à l'Université de Montréal

Cette thèse intitulée :

Metal Oxides for Ion-Gated Transistors

présentée par **Arunprabaharan SUBRAMANIAN**

en vue de l'obtention du diplôme de *Philosophiæ Doctor*

a été dûment acceptée par le jury d'examen constitué de :

Ludvik MARTINU, président
Fabio CICOIRA, membre et directeur de recherche
Clara SANTATO, membre et codirectrice de recherche
Federico ROSEI, membre
Luisa PETTI, membre externe

RÉSUMÉ

Les transistors sont les éléments constitutifs fondamentaux des circuits électroniques. Le silicium est un matériau semi-conducteur largement utilisé dans la fabrication de transistors en raison de ses excellentes propriétés électriques ajustables. Malheureusement, les applications des transistors à base de silicium sont limitées en raison des difficultés d'altération des propriétés optiques et mécaniques du silicium. Récemment, les matériaux à base d'oxydes métalliques émergent comme des candidats alternatifs pour le silicium. Les performances électriques sont similaires à celles du silicium, mais les propriétés optiques et mécaniques intrinsèques des oxydes métalliques sont ajustables. De plus, les conditions de synthèse des oxydes métalliques sont réalisables à des températures plus basses en utilisant des procédés plus simples que dans la synthèse du silicium.

Après le développement de l'oxyde d'indium-gallium-zinc amorphe (a-IGZO) traité à température ambiante, l'électronique à base d'oxyde a suscité un grand intérêt. L'IGZO possède des propriétés uniques, telles qu'une mobilité élevée à l'état amorphe, une transparence optique, une stabilité dans les conditions ambiantes et un faible courant de fuite drain-source, qui confèrent à ce matériau des performances et des caractéristiques appropriées pour la commercialisation dans de nombreuses technologies d'affichage. Un inconvénient important des IGZO est l'augmentation rapide de la demande d'indium provoquant une pénurie dans la croûte terrestre, limitant l'offre de transistors à base d'IGZO. Des recherches récentes visent à résoudre le problème de la rareté de l'indium en trouvant un substitut d'oxyde métallique à l'indium abondant sur terre.

Cette thèse de doctorat est consacrée à la recherche et à la caractérisation d'alternatives possibles aux semi-conducteurs à base d'indium. Nous nous concentrons sur le TiO_2 et le SnO_2 en tant que candidats potentiels en raison de leur abondance, de leur transparence, de leur conductivité électrique réglable et de leur aptitude au traitement à basse température. Ces oxydes métalliques présentent des performances exceptionnelles et pourraient constituer de futures alternatives aux transistors à base d'indium.

Les transistors utilisés dans les appareils électroniques portables ou biomédicaux nécessitent de faibles tensions de fonctionnement. Pour obtenir des transistors à faible tension de

fonctionnement, nous nous sommes concentrés sur le développement de transistors à déclenchement ionique (IGT). Les IGT utilisent des oxydes métalliques (TiO_2 et SnO_2) comme matériau de canal et un liquide ionique, un gel ionique ou des électrolytes aqueux comme milieu de déclenchement ionique. En raison de la capacité élevée de la double couche électrique formée à l'interface semi-conducteur/milieu de déclenchement ionique, les IGT fonctionnent à des tensions plus basses. Le mode de fonctionnement des IGT s'explique par le dopage électrostatique (dopage surfacique) et électrochimique (dopage volumétrique). Dans le premier cas, le dopage est obtenu par la migration d'ions dans le milieu de déclenchement ionique vers l'interface semi-conductrice et induit des porteurs de charge sur la surface du semi-conducteur. Ce dernier cas est décrit par le transport de masse d'ions dans le milieu de porte d'ions sur la double couche électrique provoquant un dopage électrochimique massif sur le semi-conducteur. Comprendre et contrôler le mécanisme de dopage primaire, contrôle les propriétés électriques du transistor et donne des informations précieuses sur le transport des charges.

Tout d'abord, nous avons étudié le mécanisme de dopage dans les IGT en utilisant des films de TiO_2 poreux et compacts exposés à deux liquides ioniques contenant des ions de tailles différentes. Pour chaque condition, nous avons mesuré les caractéristiques électriques des IGT TiO_2. Les films compacts présentent un courant de drain source plus élevé que les films poreux en raison de la conductivité plus élevée du canal lorsqu'il est en contact avec un milieu de déclenchement contenant de gros ions. La présence de petits ions dans le liquide ionique augmente le courant drain-source des films poreux, mais il n'y a pas eu de changement significatif dans le courant drain-source des films compacts.

Deuxièmement, des films SnO_2 transparents et cristallins sur des substrats PET ont été synthétisés par une technique de croissance aqueuse contrôlée à basse température (95 °C). Nous avons préparé des IGT à base de films SnO_2 en utilisant deux méthodes : des électrodes de source et de drain Au à motifs photolithographiques et des électrodes de source et de drain d'Ag imprimées. Les IGT à base de SnO_2 utilisant un milieu de déclenchement d'électrolytes liquides ioniques ou aqueux fonctionnaient sous 1 V. Nous avons démontré que les IGT SnO_2 sous contrainte de traction, à l'état courbé, ne présentaient aucune variation significative des caractéristiques électriques.

Troisièmement, nous avons fabriqué des films de TiO_2 en utilisant une approche chimique humide et démontré leur comportement de transistor dans des électrolytes liquides ioniques et aqueux à température ambiante. Le comportement de détection du pH a été démontré en utilisant des solutions tampons comme support de déclenchement pour les IGT. En raison de la nature de type n du film de TiO_2, l'augmentation des ions H^+ dans les solutions à faible pH permet aux IGT de s'allumer à des tensions plus basses. De plus, nous avons fabriqué des films TiO_2 sur des substrats PET flexibles par traitement en solution et une température de traitement maximale de 120 °C. Nous avons montré que les performances des transistors des IGT TiO_2 sur un substrat PET flexible n'étaient pas significativement affectées par la flexion.

Nous avons étudié le mécanisme de dopage des IGT en analysant les caractéristiques électrochimiques de l'appareil, développé plusieurs IGT en utilisant des matériaux abondants en terre et des méthodes de traitement durables. Nous avons démontré des performances électriques stables des IGT SnO_2 (utilisant un liquide ionique) à l'état plat et sous différents rayons de courbure (R = 20 mm et R = 10 mm), et avons montré le fonctionnement du milieu de déclenchement aqueux des IGT SnO_2. Enfin, nous avons démontré une application des IGT TiO_2 en tant que capteur de pH, en mesurant la tension d'activation dans des solutions tampons de pH dans la plage acide, neutre et basique en tant que support de déclenchement ionique. Nous pensons que nos appareils peuvent être utilisés en remplacement des transistors à base d'indium pour une électronique et des capteurs flexibles et peu coûteux.

ABSTRACT

Transistors are the fundamental building blocks of electronic circuits. Silicon is a semiconducting material widely used in the fabrication of transistors because of its excellent, tunable electrical properties. Unfortunately, the applications of silicon-based transistors are limited due to the difficulties of altering the optical and mechanical properties of silicon. Recently, metal oxide materials are emerging as alternative candidates for silicon. The electrical performance is comparable to polycrystalline silicon, but the intrinsic optical and mechanical properties of metal oxides are tunable. In addition, the synthesis conditions of metal oxides are achievable at lower temperatures using simpler processes than in silicon processing.

After the development of room temperature-processed, amorphous indium-gallium-zinc-oxide (a-IGZO), oxide-based electronics have attracted great interest. The IGZO possesses unique properties, such as, high mobility in an amorphous state, optical transparency, stability in ambient conditions, and low drain-source leakage current, that impart this material with suitable performance and characteristics for commercialization in many display technologies. A significant drawback of IGZO is the rapid increase in indium demand causing scarcity in the earth's crust, limiting IGZO-based transistor supply. Recent research aims to solve the problem of indium scarcity by finding a metal-oxide replacement for indium that is earth-abundant.

This PhD thesis is devoted to finding and characterizing possible alternatives to indium-based semiconductors. We focus on TiO_2 and SnO_2 as potential candidates due to their abundance, transparency, tunable electrical conductivity, and low temperature processability. These metal oxides show exceptional performance, and may be future alternatives for indium-based transistors.

Transistors used in wearable electronics or biomedical devices require low operating voltages. To achieve transistors with a low operating voltage, we focused on developing ion-gated transistors (IGTs). IGTs use metal oxides (TiO_2 and SnO_2) as a channel material and ionic liquid, ionic-gel, or aqueous electrolytes as the ion-gating medium. Due to the high capacitance of electrical double layer formed at the semiconductor/ion-gating medium interface, IGTs operates at lower voltages. The mode of operation of IGTs is explained by electrostatic (surface doping) and electrochemical (volumetric doping) doping. In the former case, doping is achieved by the migration of ions in the ion-gating medium towards the semiconductor interface and induces charge

carriers on the semiconductor surface. The latter case is described by the transport of ions in the ion-gating medium over the electrical double layer causing bulk electrochemical doping on the semiconductor. Understanding and controlling the doping mechanism, controls the electrical properties of the transistor, and gives valuable information about charge transport.

First, we investigated the doping mechanism in IGTs using porous and compact TiO_2 films exposed to two ion-gating media containing ions of different size. For each condition, we measured the electrical characteristics of the TiO_2 IGTs. Compact films show higher drain source current than porous films due to the higher conductivity of the channel when in contact with a gating medium containing large ions. Presence of small ions in the ion-gating medium increases drain-source current of porous films, but there was no significant change in the drain-source current of compact films.

Second, transparent, crystalline SnO_2 films on PET substrates were synthesized by a controlled aqueous growth technique at low temperature (95 ˚C). We prepared IGTs based on SnO_2 films using two methods: photolithographically-patterned Au source and drain electrodes and printed Ag source and drain electrodes. The SnO_2-based IGTs employing a gating medium of ionic liquid or aqueous electrolytes operated under 1 V. We demonstrated the SnO_2 IGTs under tensile stress, in the bent state, showed no significant variation in the electrical characteristics.

Third, we fabricated TiO_2 films using a wet chemical approach and demonstrated their transistor behavior in room temperature ionic liquid and aqueous electrolytes. The pH sensing behaviour was demonstrated using buffer solutions as a gating media for the IGTs. Due to the n-type nature of the TiO_2 film, the increase of H^+ ions in low pH solutions allows the IGTs to turn on at lower voltages. In addition, we fabricated TiO_2 films on flexible PET substrates by solution-processing and a maximum processing temperature of 120 °C. We showed that the transistor performance of TiO_2 IGTs on flexible PET substrate was not significantly affected under bending.

This PhD project reports on ion-gated transistors (IGTs) based on indium-free, earth-abundant metal oxide films (SnO_2 and TiO_2), deposited on rigid (SiO_2/p-Si) and flexible (polyethylene terephthalate) substrates, using both ionic liquids and aqueous electrolytes as the gating media. We investigated the doping mechanism of TiO_2 IGTs by analyzing the electrochemical characteristics of the device. We demonstrated stable electrical performance of

SnO_2 IGTs (using ionic liquid) in the flat state and under different bending radii (R = 20 mm and R= 10 mm), and showed the aqueous gating medium operation of SnO_2 IGTs. Finally, we demonstrated an application of TiO_2 IGTs as a pH sensor, by measuring the turn-on voltage in pH buffer solutions in the acidic, neutral, and basic range as the ion-gating media. We believe that our devices can be used as replacement for indium-based transistors for low-cost, flexible electronics and sensors.

TABLE OF CONTENTS

LIST OF FIGURES

LIST OF TABLES

LIST OF SYMBOLS AND ABBREVIATIONS

AFM	Atomic force microscopy
Ag	Silver
AMOLCD	Active matrix liquid crystal display
AMOLED	Active-matrix organic light-emitting diode
Au	Gold
BJT	Bipolar junction transistor
C	Capacitance
CaM	Calmodulin
CdS	Cadmium sulphide
CV	Cyclic voltammetry
D	Drain electrode
d	Thickness of dielectric
[EMIM][TFSI]	1-ethyl-3-methylimidazolium bis(trifluoromethylsulfonyl)imide
EGT	Electrolyte gated transistor
FET	Field effect transistor
G	gate electrode
Ga	Gallium
HOT	Highly optimized tolerance
I_d	Drain current
IGT	Ion gated transistor
IGZO	Indium gallium zinc oxide
I_{off}	Current in off state of transistor
I_{on}	Current in on state of transistor
ISFET	Ion-sensitive field effect transistors

ITO	Indium tin oxide
k	dielectric constant
KCl	Potassium chloride
$KClO_4$	Potassium perchlorate
KPF_6	Potassium hexafluorophosphate
L	Channel length
LiTFSI	lithium bis(trifluoro-methane-sulfonyl)imide
MOSFET	Metal-oxide-semiconductor field-effect transistor
NaCl	Sodium chloride
PBS	Phosphate-buffered saline
PEDOT:PSS	Poly(3,4-ethylenedioxythiophene):polystyrenesulfonate
PET	Polyethylene terephthalate
PSSH	Poly(styrene sulfonic acid)
Pt	Platinum
PVA	Poly(vinyl alcohol)
PVDF	Polyvinylidene fluoride
P(VP–EDMAEMAES)	poly[(1-vinylpyrrolidone)-co-(2-ethyldimethylammonioethyl methacrylate ethyl sulfate)]
S	Source electrode
SnO_2	Tin dioxide
TFT	Thin film transistor
Ti	Titanium
TiO_2	Titanium dioxide
V_d	Drain voltage
V_g	Gate voltage
V_{th}	Threshold voltage
W	Channel width
WO_3	Tungsten trioxide
XRD	X-ray diffraction
ZnO	Zinc oxide

ε	Vacuum permittivity
μ	Charge carrier mobility

LIST OF APPENDICES

CHAPTER 1 INTRODUCTION

1.1 Oxide electronics

The era of electronics starts after the invention of transistors in 1947.[1] Silicon-based semiconductors are most widely used in electronic devices, ruling the electronic industry since the invention of transistors, because of silicon's abundancy, stability, tunable electrical conductivity, uniformity, and high mobility.[2] In the last decade, demand for consumer electronics (Internet Of Things) has sharply increased. Some causes of increased consumer interest in electronics are due to adding functionality to existing electronics, such as, transparency, flexibility, and stretchability. However, Si-based devices are rigid and opaque (bandgap ~ 1.1 eV) and difficult to be employed in transparent and flexible electronics. The Si-based semiconductors used to process flexible electronics show moderate performance due to a lower mobility value observed in amorphous silicon, ~ 1 cm^2/Vs.[3-5] The mobilities of single crystalline and polycrystalline silicon are ~1000 cm^2/Vs and ~100 cm^2/Vs, but require high processing temperature that deteriorates the flexible substrate.[6] Oxides are a new class of material: an inorganic, wide-bandgap solid, with an electrical conductivity that can be tuned from insulating to conducting by changing the doping level. [7, 8] Thin films of oxides are transparent, flexible, air processable and thermodynamically stable in ambient conditions.[8] An important breakthrough in oxide electronics occurred in 2004 by Hosono et al., who developed room temperature processable, amorphous indium gallium zinc oxide (a-IGZO) on flexible substrates with a mobility value of 10 cm^2/Vs.[9] Room-temperature processable a-IGZO-based devices exhibit flexibility, transparency, high mobility, and uniformity.[3] This cutting-edge technology has been commercialised in display technologies since 2010 (Sharp, Samsung and LG).[4] The AMOLED (active-matrix organic light-emitting diode) and AMOLCD (active matrix liquid crystal display) are employing a-IGZO because of the improved properties compared to amorphous hydrogenated silicon as a result of the room temperature processability, lower leakage current, high resolution, low power consumption and low processing cost of a-IGZO.[5] In addition to display technologies, IGZO is targeted for use in wearable electronics, photodetectors, solar cells, memory devices, and chemo/bio-sensing platforms.[10] IGZO-based devices are stable under a severe bending radius of ~13 μm without significant change in the mobility, making them excellent for use in flexible electronic applications.[11, 12] Recently, IGZO-based devices have demonstrated high stretchability for use in wearable electronics. Human skin typically undergoes

~20 - 70% strain, so the electronic device needs to be able to withstand 70% strain or more while maintaining electrical properties. A recent development in stretchable IGZO achieved this performance under 200% strain, and the IGZO was comfortably attached to a human hand.[13] Due to these excellent properties, the demand for the IGZO has been continuously increasing over the years. As a result, it will be critical to continue supplying the IGZO raw materials if the demand for IGZO persists. Unfortunately, the elements, In and Ga, are considered as critical raw materials by the European commission.[14] Both materials are often employed in transparent conductors and as active channels for thin-film transistors. The high usage levels of these materials makes maintaining supply over time difficult. Thus, there is an immediate necessity to find an alternative to IGZO that demonstrate comparable properties to IGZO. The new materials should be In and Ga free, earth abundant, low cost, sustainable, and non-toxic. The current research is based on exploring new materials, considered non-critical, such as earth-abundant oxide semiconductors (Ga and In free) that are cost-effective, with low temperature processability and high-performance.[15-17]

1.2 Motivations

Indium-free metal oxides such as TiO_2 and SnO_2 are promising active channel materials for transistors and are expected to find applications in displays, wearable electronics, and sensors. Ion-gating employs ionic liquid, ion-gel and aqueous saline solutions as the gating media and allows the transistor to work under low voltages due to the high capacitance of the electrical double layer formed at the semiconductor and ion-gating medium interface. Understanding the working mechanism (electrostatic or electrochemical doping) of an ion-gated transistor (IGT) is a challenging issue. Ion insertion and charge transport properties at the gating media-semiconductor interface and semiconductor-electrode interface need to be studied to understand their impact on the working mechanism of IGT. Exploring the working mechanism of IGTs by using different channel morphologies (compact or porous) and types of mobile ions in the gating medium provides information about the oxide/ion-gating medium interface and determines the application of IGTs (e.g. displays, memory devices, ring oscillators and chemo/bio sensing). The development of new fabrication techniques to process transparent, crystalline metal oxides on polymeric substrates at low temperatures, paves the way for indium-free transparent and flexible displays and wearable electronics. Achieving stability under ambient and aqueous environment conditions, will allow

metal oxide-based IGT usage for water quality monitoring (e.g. pH sensors). In this thesis, earth-abundant metal oxides are prepared on flexible substrates at low temperatures and their transistor properties in the flat and bent state was demonstrated. Finally, the working mechanism of the transistor is analyzed by varying morphologies of the semiconductor and the mobile ions in the gating medium.

1.3 Objectives

The main objectives of this PhD thesis are: i) to deposit semiconductors on rigid/flexible substrates and fabricate high-performance devices and measure their transistor properties and ii) explore their working mechanism. These objectives were achieved by synthesizing earth-abundant metal oxide-based channel materials using a wet chemical approach, choosing the proper gating media, tuning the morphology of channel material, and selecting the appropriate size of mobile ions in the ion-gating medium. Using ion-gating allows transistors to operate at lower voltages. The morphology of channel material and mobile ions in the gating media were demonstrated to affect the working mechanism of transistors. The device performance was investigated by transfer and output transistor measurements. Cyclic voltammetry was used to explore the working mechanism of IGTs.

Specific objectives

To accomplish the main objectives, the subsequent specific objectives have been completed.

(i) To fabricate porous and compact channel materials using TiO_2 films and exploring the doping mechanism

We have fabricated TiO_2 based IGTs based on evaporated, and solution processed films and characterized their morphological, structural, and electrical properties. Ion-gating allows transistors to operate at lower potentials due to the formation of the electrical double layer and (or) electrochemical doping at the semiconductor/ion-gating media interface. Electrical characterizations showed that the transistor performance depends on the morphology of the TiO_2 films. The size of the mobile ions in the gating media and the morphology of the semiconductor affect the working mechanism of transistors. Cyclic voltammetry was carried out to understand the doping mechanism on TiO_2 films with different morphologies.

(ii) To synthesize crystalline metal oxide channel materials at low temperatures, using controlled aqueous growth for high performance, flexible IGTs.

Fabricating high performance flexible transistors is of great interest for flexible displays and wearable electronics. Generally, a high temperature is necessary to synthesize crystalline metal oxides, which hinders the applicability in flexible electronics. Controlled aqueous growth makes deposition of crystalline SnO_2 possible at low temperatures (~ 95 ˚C) on flexible substrates, such as polyethylene terephthalate (PET). Comparison of transistor measurements in ionic liquid under no bending and in the bent state shows no significant change in the transistor behaviour. In addition, we demonstrated the transistor behaviour using a cellulose membrane soaked in NaCl aqueous solution as the ion-gating medium. Further, we printed metal electrodes on SnO_2 deposited PET substrates and assembled the IGTs with an aqueous electrolyte to make them more sustainable.

(iii) To develop pH sensors and flexible ion-gated transistors using solution-processed metal oxide films

Metal oxides are stable in ambient and aqueous environments, making them suitable for sensing applications. We synthesized TiO_2 films using a sustainable wet chemical method employing green alcohol solvents (ethanol and isopropanol). We assembled the transistors using ionic liquid and aqueous electrolytes, and demonstrated the successful operation at low voltages. We tested the pH sensing ability of TiO_2 IGTs in pH buffer solutions at different pH levels. Increasing the gate-source voltage shift with respect to the reference drain-source current was observed when the pH of the analyte solution increases. In addition, we prepared TiO_2 films on flexible substrates and assembled the transistors using ionic liquid. We showed that there are no significant changes in the electrical characteristics of the IGT under moderate bending.

1.4 Organization of the work

This PhD thesis contains 8 chapters. Chapter 1 discusses the background of oxide electronics, the research project motivation, and objectives of this PhD work. Chapter 2 is devoted to the literature review in which a brief history of transistors, field effect transistors and their working principle and characteristics, ion-gated transistors and their working principle, and metal oxides

for flexible electronics and sensing. Chapter 3 discusses the methodology used in this PhD thesis. Chapter 4, 5 and 6 are about the three articles where I am the first author.

Article 1: Arunprabaharan Subramanian, Ben George, Sanyasi Rao Bobbara, Irina Valitova, Irene Ruggeri, Francesca Borghi, Alessandro Podestà, Paolo Milani, Francesca Soavi, Clara Santato, and Fabio Cicoira, Ion-gated transistors based on porous and compact TiO_2 films: Effect of Li ions in the gating medium, AIP Advances, **2020**, 10, 065314.

Article 2: Arunprabaharan Subramanian, Mona Azimi, Clara Santato and Fabio Cicoira, Combining Aqueous Solution Processing and Printing for Fabrication of Flexible and Sustainable Tin Dioxide Ion-Gated Transistors, Advanced Materials Technologies, **2021**, 2100843.

Article 3: Arunprabaharan Subramanian, Mona Azimi, Cheng Yee Leong, Siew Ling Lee, Clara Santato and Fabio Cicoira, Solution- processed titanium dioxide ion-gated transistors (IGTs) and pH sensors using ionic liquid and aqueous saline solution, Frontiers In Electronics, **2021 (Manuscript ID: 813535, under review).**

Chapter 7 is a general discussion of all work that I did during PhD.

Chapter 8 discusses the conclusions from all the work and perspectives for future work.

.

CHAPTER 2 LITERATURE REVIEW

The aim of this section is to give a general overview of the history of transistors, discuss thin-film transistor working principles, characteristics, and figure of merits, and highlight recent accomplishments in the development of oxide based thin-film transistors, ion-gated transistors, and oxide-based ion-gated transistors.

2.1 A brief history of transistors

The first report describing the operating mechanism of field-effect transistors (FET) was accomplished by J. E. Lilienfeld in 1925, but he was not able to build a working device based on the concept.[18] In 1948, William Shockley of Bell Telephone Laboratories, invented the bipolar junction transistor (BJT), patented it in 1951, and won the Nobel Prize in 1956 along with J. Bardeen and W.H. Brittain, for their discovery of the transistor effect.[19] The BJT is a type of transistor that uses electrons and holes as charge carriers and consists of three differently doped regions of semiconducting materials, the base, collector, and emitter regions. The BJT was extensively used in the design of discrete and integrated circuits for three decades. The metal-oxide-semiconductor FET (MOSFET) was invented by Mohamed Atalla and Dawon Kahng in 1959 and then commercialized in 1963.[20] The MOSFET essentially supplanted the BJT and profoundly impacted the development of digital electronics. The first example of an electrolyte-gated transistor (EGT) was reported by J. Bardeen and W. H. Brattain, who showed that the conductivity of germanium changed when the surface of germanium came in contact with an electrolyte.[21] The first thin film FET, invented in 1961, used polycrystalline CdS as a semiconductor and SiO_2 as an insulator.[22] The invention permitted completely integrated thin-film circuits to be deposited on a glass substrate using automatic processes. The main advantage of thin film transistors is for large-area circuits in display technologies. In 2000, Z. Alferov, H. Kroemer, and J. Kilby won the Nobel Prize in Physics for developing fast opto- and microelectronic components based on layered semiconductor structures, called semiconductor heterostructures, and inventing the integrated circuit. Fast transistors built using heterostructure technology are used in radio link satellites, CD players, and laser diodes that drive the fibre-optical cables of the internet. The invention of the integrated circuit started an electronic revolution and is the basis of modern computers and processors. The integrated circuit allows many transistors to be connected to

resistors, capacitors, diodes, etc. through metal interconnects on one chip, which led to the miniaturization of electronics.[23]

Modern electronics relies on integrated circuits and microprocessors in which FETs are the fundamental building blocks. Recently, transistor miniaturization has been pushed to nanometer size scales. MOSFET technology (especially Fin-FET) can process nanometer dimension transistors resulting in 173 million transistors/mm^2. Recent iPhones (iPhone 13, A15 bionic chip) and the Macbook Pro (M1 Max processor) contains 15 and 57 billions of transistors in their processor, respectively, prepared using the TSMC's (Taiwan Semiconductor Manufacturing Company) 5 nm process.[24]

Current research in transistor technology is mainly focused on the production of lightweight, transparent, flexible, stretchable and biocompatible electronics for a variety of applications, such as wearable and textile integrated systems, medical implants, flexible displays and artificial skins.[25] These applications require transistors to have flexible and stretchable materials used in all the transistor components, while maintaining high levels of stable performance.

2.2 Field-effect transistor (FETs)

A transistor is a semiconductor device consisting of at least three electrodes that switches or amplifies electrical signal or power. Transistors are divided into two main categories that are used slightly different in circuits: field-effect transistors (FET) and bipolar junction transistors (BJT). FETs have been fabricated with many different types of materials and in varying structures. The most important FET in the field of electronics is the MOSFET (metal-oxide-semiconductor field effect transistor). In MOSFETs, the term "oxide" refers to the gate insulator, which is typically SiO_2. The insulating oxide is between the gate electrode and a semiconductor, forming a capacitor, which drives the transistor characteristics. A thin film transistor (TFT) is a specific type of MOSFET that is processed at low temperatures and grown on an insulating substrate such as glass. In contrast, most MOSFETs are processed on silicon wafer substrates and require high processing temperatures.

The MOSFET structure includes a substrate, that is typically semiconducting single crystalline silicon, two terminals (source and drain) formed by doping the substrate causing regions of variable

conductivity at the edges, a dielectric layer (oxide) placed onto the semiconducting substrate, and the metal gate electrode attached on top of the dielectric. The typical structure of MOSFETs and TFTs is shown in Figure 2-1.[26] TFTs are fabricated on an insulating substrate (glass, plastic and paper) and processed in solution. In the following sections, we chose TFTs to focus on in the research projects because of its solutions processability at low temperatures allowing for fabrication on a wide variety of substrates, allowing for flexible and stretchable transistors.

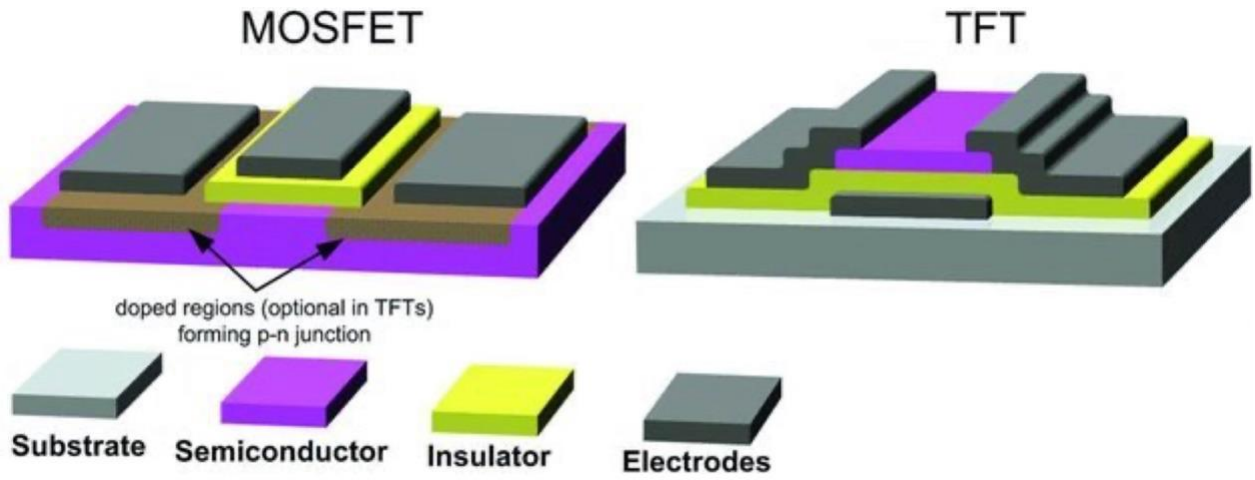

Figure 2-1 Device structures of MOSFETs and TFTs. Adapted with permission[26]

2.2.1 Operation of TFTs

The working mechanism of a TFT (n-type, where the majority charge carriers are electrons) is depicted in Figure 2-2. A capacitor is formed from the stacked gate electrode, the semiconductor and the dielectric. When the transistor is polarized by a positive bias to gate electrode (V_g), negative charge carriers accumulate on the channel, while the source electrode is grounded. The channel becomes conductive when V_g is above a certain threshold voltage (V_{th}).[26] Charge injection/extraction into/from the semiconductor takes place at the source and drain electrodes, featuring a certain interelectrode distance (L) and width (W). [27]

When a bias is applied between source and drain electrodes (V_d), a transistor current will pass between them. When V_d is increased at constant V_g, the current increases linearly to eventually reach a saturation value. In other words, when drain voltage (V_d) exceeds the effective gate voltage, V_{eff}, (i.e. $V_d > V_g - V_{th}$), V_d, compensated by V_g, leads to the *pinch off* of the channel, at the drain.

It indicates that the transistor reached the saturation state and a further increase in V_d does not have any impact on the transistor current.

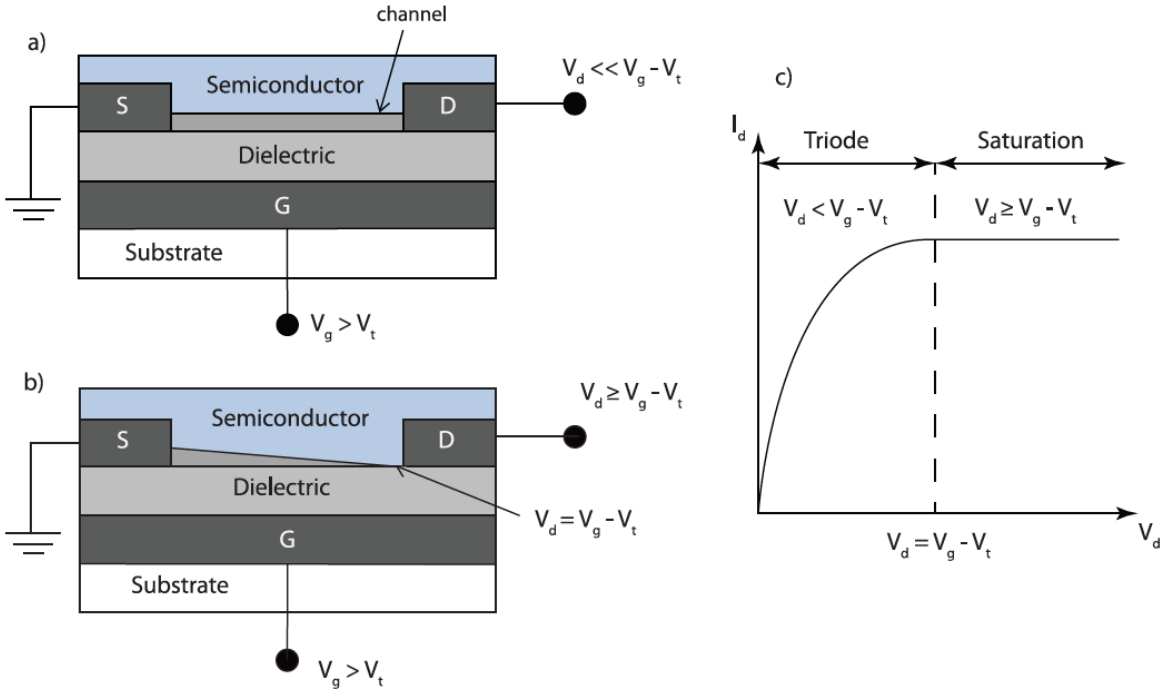

Figure 2-2 Schematic representation of operating mechanism of TFTs (the channel is the portion of the semiconductor where the conductivity is controlled by V_g): (a) linear region; (b) saturation region, at pinch-off. Current-drain voltage characteristics of a transistor (c). Adapted with permission[27]

An additional increment of V_d will just move the pinch off point towards the source, resulting in the shortening of the channel length; the current from source to drain will not increase because of the lack of charge carriers near the drain. [27, 28]

The capacitance of the dielectric is expressed as:

$$C = \varepsilon_0 k A/d \qquad (1)$$

Where ε_0 is the vacuum permittivity, k is the relative permittivity (dielectric constant), A is the area and d is the thickness of the dielectric.

The density of the mobile charge can be calculated using the following equation:

$$Q = C (V_g - V_{th}) \quad (2)$$

The transistor current in the linear and saturation regions can be described by the approximation equations:

$$\text{(Linear)} \quad I_d = (W\mu C/L) (V_g - V_{th}) V_d \quad (3)$$

$$\text{(Saturation)} \quad I_d = (W\mu C/L) (V_g - V_{th})^2 \quad (4)$$

where μ is the mobility of the charge carriers.

The charge carrier mobility is the drift velocity of a charge carrier per unit of electric field. In the linear region, it can be expressed as:

$$\mu_{lin} = \frac{L}{WCV_d} \frac{dI_{dlin}}{dV_g} \quad (5)$$

whereas in the saturation region it can be expressed as:

$$\mu_{sat} = \frac{2L}{WC} \left(\frac{d\sqrt{I_{dsat}}}{dV_g} \right)^2 \quad (6)$$

The charge carrier mobility derived from the above equations that is different from *intrinsic* mobility derived, e.g. from the Hall effect. The charge carrier transport occurs in TFTs only in the channel region, that is close to dielectric where charge scattering events can take place. [29]

Another figure of merit for transistors is the ON/OFF ratio (I_{ON}/I_{OFF} ratio), derived from transistor current vs V_g (transfer) characteristics, as shown in Figure 2-3 (a). This figure of merit is defined as the ratio between the channel current in the ON state to the current in the OFF state of the transistor. Higher value of I_{ON}/I_{OFF} are required (~ 10^6) for good switching performance.

FET can work in enhancement (accumulation) or depletion mode. In the absence of Vg, the enhancement mode transistors are in the OFF state ($I_d \approx 0$). In the absence of V_g, the depletion mode transistors are in the ON state ($I_d \neq 0$), so that V_g is needed to turn off the transistors. Enhancement mode transistors are needed for display technologies due to their low power consumption.[27]

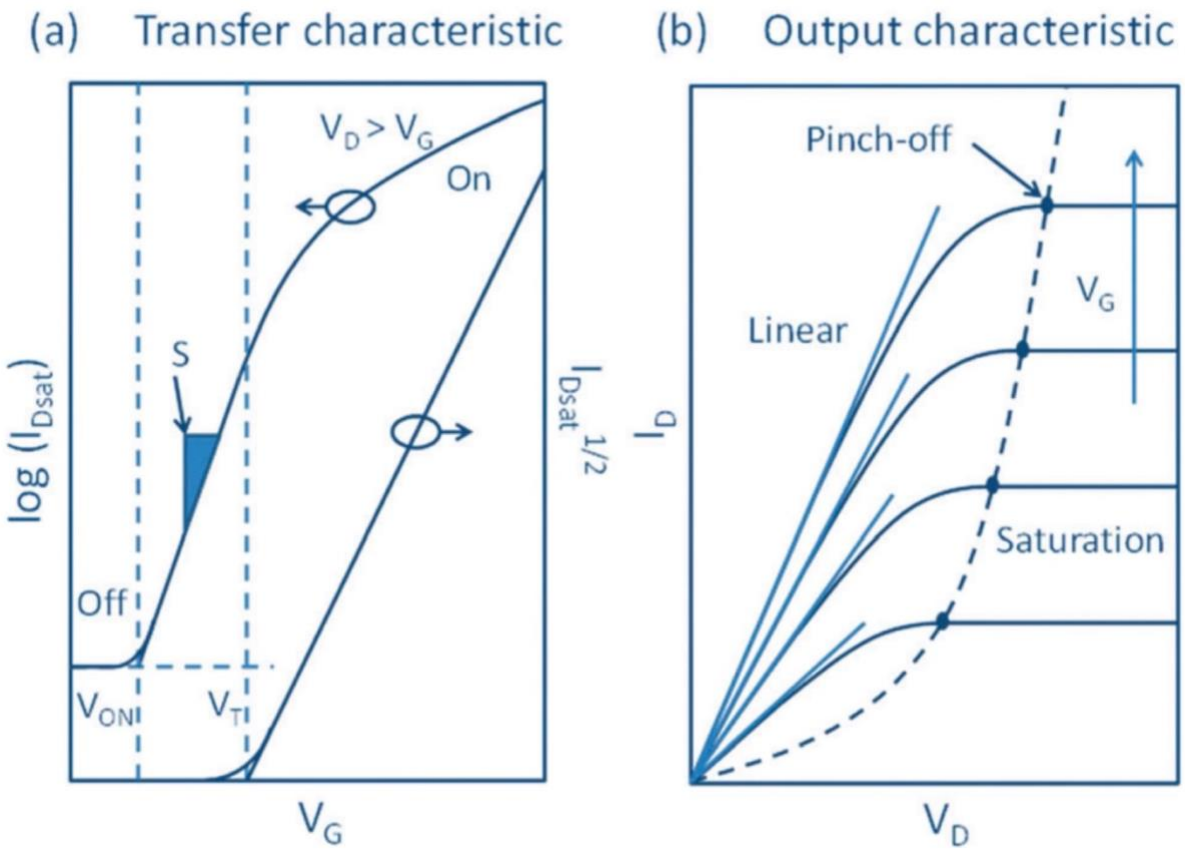

Figure 2-3 Transfer (a) and output (b) characteristics of TFTs. Adapted with permission.[30]

An important figure of merit of transistors is V_{th}, defined as the minimum V_g needed to induce a channel (and, consequently, a measurable transistor current). V_{th} depends on the semiconducting material, dielectric and device architecture. A well-established method to find V_{th} is the linear extrapolation of $I_d^{1/2}$ vs V_g in the saturation region. Generally, V_{th} is negative when the n-type FET works in depletion mode and positive when it works in depletion mode. [29]

The transconductance of a transistor is the modulation of the transistor current with respect to the change of V_g at constant V_d, described as follows:

$$g_m = dI_d/dV_g \qquad (7)$$

The subthreshold swing is calculated from the logarithmic plot of the transistor current vs V_g, at constant V_d.[30] It is directly related to the quality of the semiconductor/dielectric interface that determines how efficiently a transistor turns ON and OFF. It is expressed as:

$$S = \frac{dV_g}{d\log_{10}(I_d)} \quad (8)$$

An important characteristic of transistors is the hysteresis, observed as a difference in the transistor current observed in the forward and backward scans of V_g. Reproducibility of the current-voltage behavior give insight on the stability of the device, i.e. hysteresis should be avoided for better device stability and performance.[27]

2.2.2 Architecture of TFTs

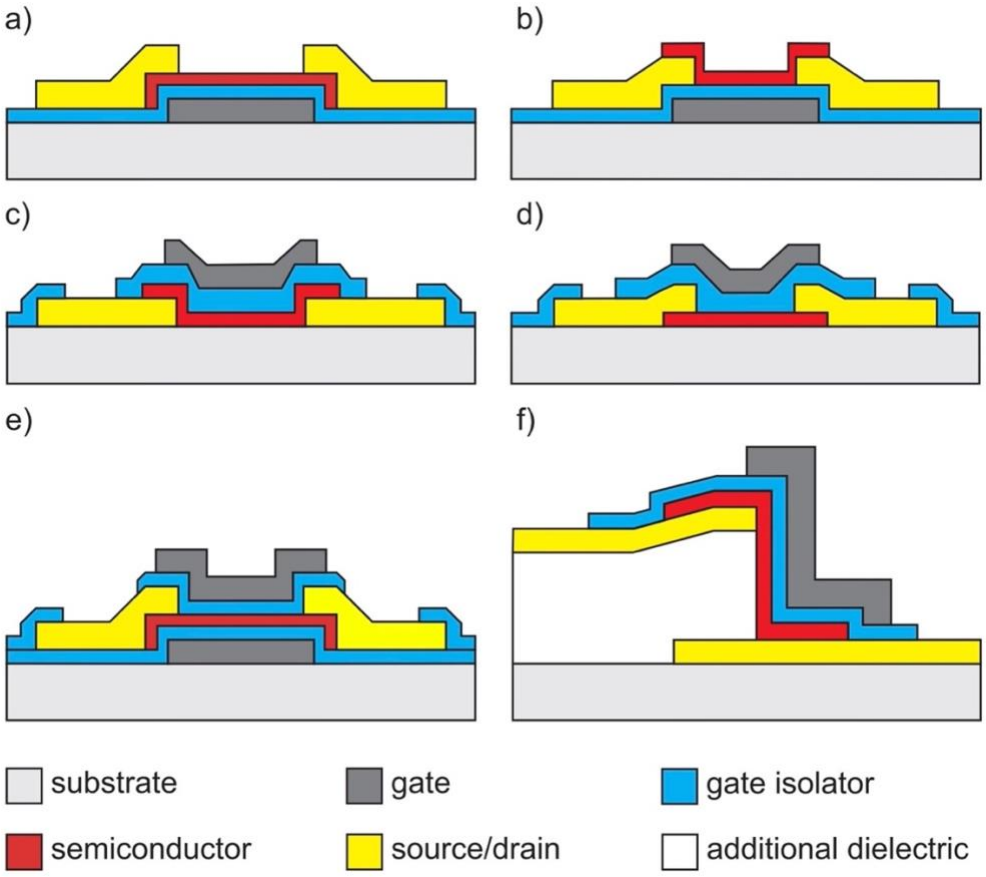

Figure 2-4 Architectures of thin film transistors (a) bottom gate top contact, (b) bottom gate bottom contact, (c) top gate bottom contact, (d) top gate top contact, (e) double gate, (f) vertical gate. Reproduced with permission[31]

The most common TFT architectures are depicted in Figure 2-4. Depending upon the position of the gate electrode, we can identify two categories, bottom gate (a-b) and top gate (c-d). Moreover, the position of source and drain contacts can result in staggered and coplanar configurations. Figure 2-4 (a) and (b) represent the bottom gate TFT with staggered and coplanar structure. Bottom gated structures might need an additional passivation layer that reduces the air exposure from the back channel and undesired instability effects. Figure 2-4(c) and (d) represents top gated structure with staggered and coplanar configurations, where the gate dielectric acts a passivation layer. Figure 2-4(e) represents double gated architecture in which a larger portion of the semiconductor channel is effectively controlled by V_g, through an additional gate electrode. Figure 2-4 (f) represents a vertical TFT in which the channel is not patterned through photolithography (see methodology) but, instead of this, it is defined by the gate or the semiconductor thickness.[26]

2.3 Metal oxides for TFTs

In transistor technology, metal oxides are studied for use as the electrodes, semiconductor, and insulator material. The semiconductor material in the transistor channel is the most important transistor component in determining device performance. Metal oxides are excellent transistor channel material for flexible and transparent TFTs due to their combined electrical and optical properties, as well as impressive reliability.[32] Amorphous metal oxides with post transition metal cations exhibits degenerate band conduction and higher mobility (> 10 cm^2/Vs). In addition, the mechanical properties of the amorphous metal oxides are superior than the polycrystalline one due to their uniformity and processing temperature.[9]

Metal oxides are essentially insoluble in any solvent at room temperature and require highly acidic/basic conditions, at high temperature to become soluble in a solvent. This problem makes metal oxides difficult to be deposited on a substrate using room temperature solution-processing methods and not suitable for solution processing of the semiconductor component of the transistor.[33] In contrast, organic semiconductors can be dissolved in a suitable solvent and thin films of semiconducting material can be formed on a substrate at low temperatures.

2.3.1 InGaZnO

A breakthrough in metal oxide devices was accomplished by Hosono et al., who developed amorphous indium gallium zinc oxide (a-InGaZnO or a-IGZO) at room temperature by pulsed laser deposition, rapidly growing interest in metal oxide electronics.[9] Hosono et al., fabricated room temperature a-IGZO (30 nm thick) on flexible PET (200 μm thick) substrates. TFTs based on a-IGZO show a charge mobility of 10 cm^2/Vs which is one order of magnitude higher than hydrogenated amorphous silicon. a-IGZO was deposited using polycrystalline $InGaZnO_4$ as a target material with pulsed laser (Krypton fluoride laser) deposition at room temperature in an oxygen atmosphere. The prepared films are 80% transparent in the visible and near infrared region (390–3200 nm, bandgap of ~ 3 eV). Source, drain, and gate were ITO (Sn-doped indium oxide) and the dielectric was Y_2O_3 (140 nm, dielectric constant is 80), which were all deposited using pulsed laser deposition at room temperature on PET substrates. The length and width of the channel was 50 and 200 μm, respectively. The initial mobility of TFTs was maintained throughout repetitive cycles of bending to 30 mm. These transistor demonstrated a low leakage current (0.1 nA) and high on/off ratio of 10^3. [9] The a-IGZO based TFTs were eventually commercialized by SHARP corporation and IGZO technology was adapted in laptops, tablets, and mobile phones. Currently, a-IGZO TFTs are employed to manufacture large area displays with 8 K resolution. Recently, there has been several examples of IGZO based TFTs in flexible and rollable displays. [8, 34]

The a-IGZO TFTs are extensively studied with the aim to move from rigid electronics to light weight, soft and flexible electronics. The following studies were IGZO TFTs based on different substrates, processing routes, thermal treatments, and substrate pre-treatments. Recently, work has been done to partially or fully print devices based on a-IGZO TFTs.[35]

Münzenrieder et al., fabricated RF sputtered a-IGZO-based TFTs on a 1 μm-thick parylene substrate with a maximum processing temperature of 150 ˚C.[13] These a-IGZO TFTs are stretchable up to 200 % while maintaining the initial electrical performance (Figure 2-5). a-IGZO TFTs showed the threshold voltage of 0.4 V and mobility of 11 cm^2/Vs. The wrinkle formation in the elastomeric substrate mimics human skin. The device was made on prestretched substrates and

then the devices were released and stretched and relaxed for >4000 cycles. The electrical performance was retained up to 4000 cycles.

Cantaralla et al., fabricated a-IGZO TFTs on a wrinkled biocompatible substrate (1 µm thick parylene).[12] Electrical characteristics of the a-IGZO TFTs were not significantly changed when the devices were bent to 13 µm and stretched up to 4 %. The a-IGZO TFTs showed a mobility of 14 cm^2/Vs and a threshold voltage of 0.1 V.

Facchetti et. al., demonstrated IGZO nanofibers by blow spinning on a 1.5 µm thick polyimide substrate. They carried out repetitive bending on the TFTs for more than 10000 cycles, and the mobility of ~ 1 cm^2/Vs was maintained with respect to the original state. [36]

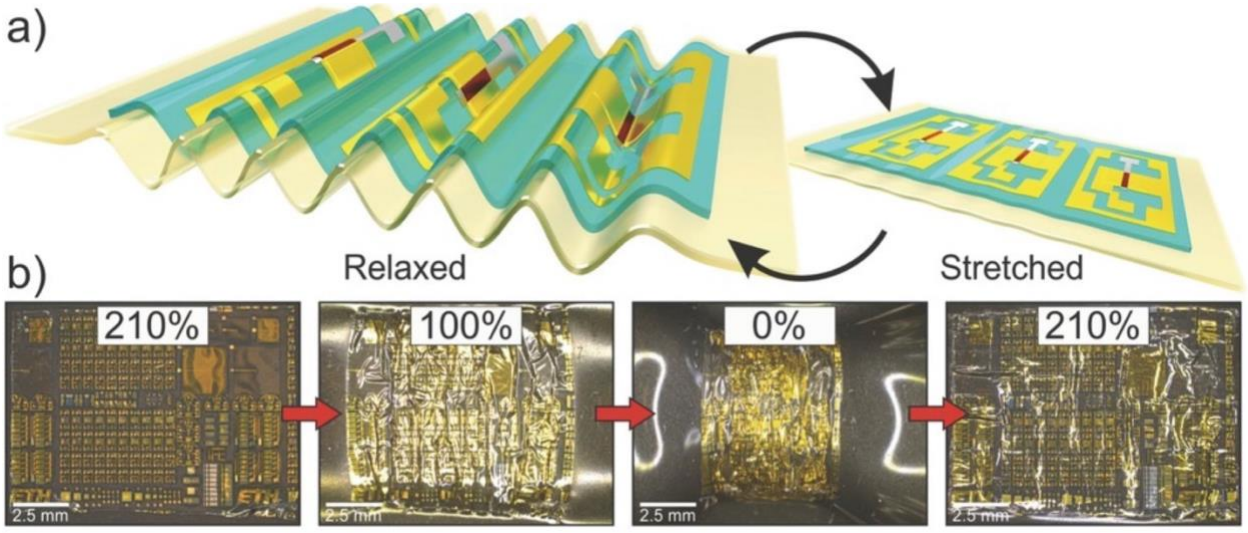

Figure 2-5 (a) Stretchable electronics on a buckled (wavy) substrate (relaxed ↔ stretched) (b) a-IGZO TFTs on the prestressed substrate to strains of 210%, released to 0% strain, and stretched to 210% strain. The formation of wrinkle appears when the strain is reduced from 210% to 100 % and 100% to 0%. Adapted with permission. [13]

2.3.2 Indium-free metal oxides

Indium-based materials have a significant advantage over amorphous silicon-based transistors. While indium has several advantages over other materials, the demand for indium is greater than what is available in the earth crust. The scarcity creates an urgent need to find alternatives for indium-based devices. The materials ZnO, SnO_2, TiO_2 have been examined to

possibly replace indium. Among them SnO_2 and TiO_2 stand out due to their transparency, abundancy, and low cost. However, the fabrication and processing of those metal oxides are not compatible with flexible electronics since a high temperature is required to process the films. The properties of the channel material depend not only on its chemical composition, but also on the method that is used for fabrication, e.g. sputtering, e beam evaporation, pulsed laser deposition and solution-processing. [16]

2.3.3 Tin dioxide

Tin dioxide (SnO_2) is widely used in gas sensors, thin-film transistors and transparent electrodes due to its abundancy, electrical conductivity, optical transparency and solution-processability.[37] SnO_2 films in TFT configuration prepared using physical and chemical methods, exhibit a field of mobility of >100 cm^2/Vs. [38-42] Due to its high conductivity and transparency, SnO_2 finds application in transparent conducting electrodes. The conductivity of the SnO_2 can be modulated by tuning the doping with foreign elements. The preparation methods for fabrication of SnO_2 will affect the TFT performance. Thickness of the SnO_2 films affects its crystallinity and also affects the operation mode of the transistors. [43, 44] Room-temperature fabricated flexible SnO_2 exhibits good electrical performance in TFT in the bent state. [45] TFTs based on SnO_2 nanowire can withstand stretchability up to 40%.[46] The above-mentioned properties makes SnO_2 an excellent alternative for the Indium-based materials.

2.3.4 Titanium dioxide

Titanium dioxide (TiO_2) is an abundant metal oxide, widely used in the food industry, cosmetics, medicine, water treatment, and electronic devices. TiO_2 is of interest for next-generation indium-free thin-film transistors due to its tunable optoelectronic properties, ambient stability, and solution processability.[47] Due to its insulating property, TiO_2 is used as a dielectric in TFTs. The conductivity of TiO_2 can be tunable to a limit. Recently, TiO_2 is investigated as an active channel material for TFTs. TFTs fabricated using TiO_2 as the active channel exhibits a mobility range from 0.05 to 10 cm^2/Vs.[48-54]

2.4 Ion-gated transistors

Typical thin film transistor operates at high voltage (> 10 V) due to the low capacitance of the dielectric. The specific capacitance of typical dielectric materials, such as SiO_2 (k~3.9) and Si_3N_4 (k~7) is in the range of 5-10 nF cm^{-2}, depending on the thickness of the dielectric and its dielectric constant, e.g. the specific capacitance is ~11 nF/cm^2 for 300 nm thick SiO_2. The capacitance is inversely proportional to the thickness of the dielectric, i.e. ultra-thin dielectrics exhibits higher capacitance. The use of ultra-thin conventional dielectric materials might cause leakage currents and reliability issues.[55] ZrO_2 (k~20), Ta_2O_5 (k~25), and TiO_2 (k~40) are high-k dielectric material, and can increase the capacitance value without resulting in a significant leakage current.[56] Another solution to lower the operating voltage is to use as the gating medium an ion-transporting material such as those used in ion-gated transistors (IGTs). Ionic liquids, ion gels, aqueous electrolytes, polymer electrolytes, polyelectrolytes and oxide electrolytes are used as gating media for ion-gated transistors.[57] Ions are responsible for charging the semiconductor in IGTs. IGTs are suitable for sensing and bio-interface application due to its operation under aqueous electrolytes. Compared to the dielectric, ion-gating medium has several advantageous such as high transconductance, larger electric field, higher charge carrier concentration and low operating voltage. Under the application of V_g, ions in the ionic medium redistribute at the electrolyte/semiconductor interface, resulting in the formation of an electrical double layer (EDL). The EDL thickness is very low (few nanometers thick) leading to high capacitances (~ 1-10 μF cm^{-2}), and allowing transistors to operate at low voltage (< 2 V). [58, 59]

In an electrode/ion-gating medium/semiconductor structure, electrical double layers are formed at the electrode/ion-gating medium and ion-gating medium/semiconductor interfaces during application of gate voltage. The potential drops that occur at the interfaces are confined within ultrathin regions, and this allows a high charge carrier density accumulation in the transistor channel.[58] At least two doping mechanisms are proposed in IGT: electrostatic or electrochemical

doping, as shown in Figure 2-6. A double layer is formed at the ion-gating medium/semiconductor interface and the mechanism is like that of FET when the semiconductor is impermeable to ions (Figure 2-6 (a) and (b)). The current modulation is due to reversible redox reactions accompanied by ion penetration into the film when the semiconductor is permeable to ions (Figure 2-6 (c)). This effect changes the charge carrier density and conductivity of the film. Electrostatic and electrochemical doping may happen simultaneously in real devices. [60]

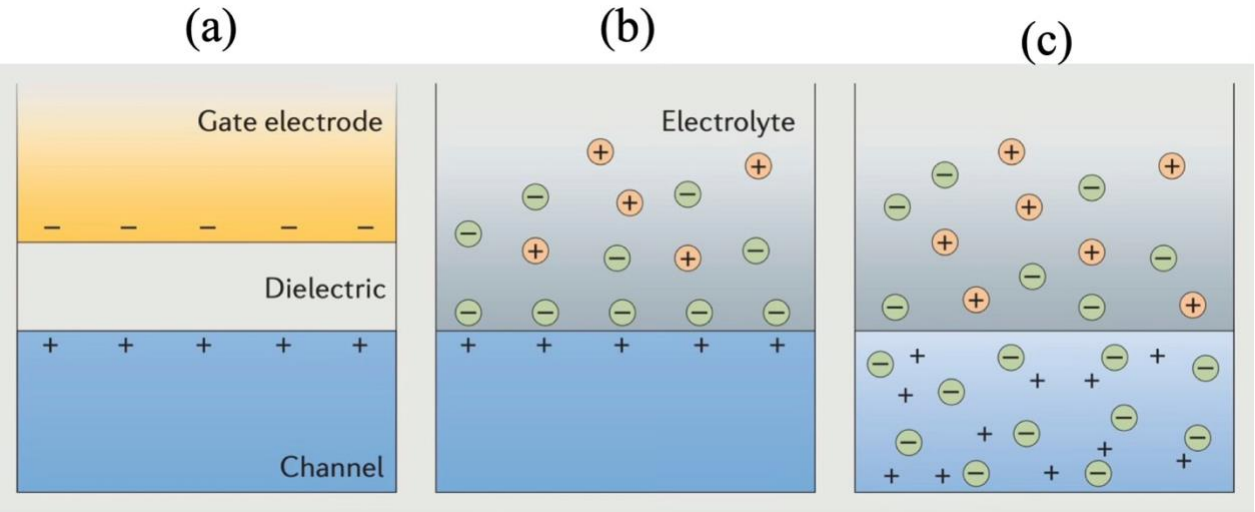

Figure 2-6 Operating mode of (a) FET, (b) electrical double layer transistor and (c) electrochemical transistors for p-type channel material. Adapted with permission [61]

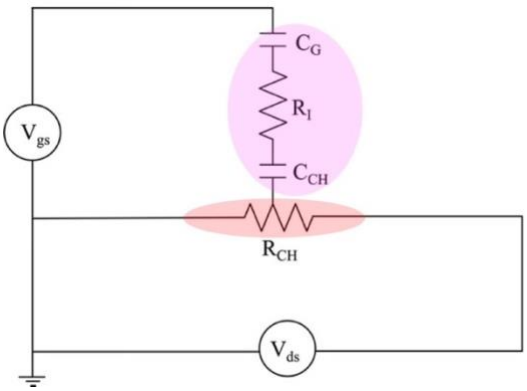

Figure 2-7 The equivalent circuit corresponds to the ionic (magenta region) and electronic (red region) circuit in IGTs. Adapted with permission[57]

Figure 2-7 shows the simple equivalent circuit of IGTs. Two electrical double layers contribute to the total capacitance of the gate/ion-gating medium/semiconductor stack. C_{CH} and C_G are the double layer capacitance at the ion-gating medium/semiconductor interface and ion-gating medium/gate electrode interface. R_I is the resistance of the ion-gating medium. R_{CH} is the resistance of the channel material that is modulated by C_{CH}. The gate voltage drop across the channel during the gate bias is influenced by the nature and geometry of the gate electrode. Capacitance at the gate electrode/ion-gating medium interface should be ~10 times larger than the capacitance at the ion-gating medium interface/semiconductor to create an efficient gating ($C_G >> C_{CH}$). When there are two capacitors in series, the capacitor with lower capacitance dominates the total capacitance of the system, so the gate electrode/ion-gating medium capacitance should be larger than the ion-gating medium/semiconductor capacitance for efficient gating. [57] Electrostatic and electrochemical doping exhibit the capacitance value of 1-10 μF/cm^2 and 10-100 μF/cm^2 respectively. [62]

2.4.1 Ion-gating medium for IGTs

Different physical and chemical properties of the ion-gating medium influence the performance of IGTs, and determine the application the IGTs would be suitable for, according to the needs of the application. Chemical and biological sensors based on IGTs requires a liquid ion-gating medium, usually aqueous electrolytes. Polymer-based electrolytes have several advantages over aqueous electrolytes due to a wider electrochemical potential window, tunable viscosity and printability. Inorganic oxide electrolytes have high stability at increased temperatures and a wide potential stability window. We discuss briefly the ion-gating mediums that are available for IGTs. Table 2-1 shows the properties of the ion-gating medium that are used in IGTs.[57]

2.4.1.1 Ionic liquid

Ionic liquids are molten salts that are in a liquid state at room temperature. Ionic liquid has several advantages when used as an ion-gating medium in IGTs, such as a wide electrochemical stability window (~ 3V), high boiling point (> 400 ˚C) and low melting point (< 20 ˚C). Ionic liquids are widely used in IGTs due to their above excellent properties. Some drawback of ionic liquids are sensitivity to moisture, which lead to reactions that decrease the window of

electrochemical stability, and biological toxicity of most of the ionic liquids rendering them not biocompatible.

Zaumseil et al., studied the effect of chemical structure of the imidazolium-based ionic liquids used in the ZnO based IGTs and inferred those ionic liquids based IGTs are more stable in nitrogen atmosphere. In addition, they found that the mobility of the transistors decreases with increased capacitance of the ionic liquid. [63]

2.4.1.2 Ion-gels

Ion-gel gating medium is a polymer network, prepared by cross-linking the polymer with ionic liquids. Ion-gels are prepared using chemical, physical, and photochemical methods. Ion-gel has an advantage of functioning in the solid states and printability.

Frisbie et.al, investigated an ion-gel based ion-gating medium for ZnO IGTs. They prepared the ion-gel using PS-PMMA-PS triblock copolymer and ionic liquid, [EMIM] [TFSI]. ZnO IGTs operated at lower voltage with an ion-gel thickness of ~ 1μm.[64]

2.4.1.3 Aqueous electrolytes

Aqueous electrolytes are prepared by dissolving salt in an aqueous solution. The most common aqueous electrolytes contains sodium chloride (NaCl), potassium chloride (KCl), phosphate-buffered saline (PBS), potassium perchlorate ($KClO_4$), potassium hexafluorophosphate (KPF_6) and lithium bis(trifluoro-methane-sulfonyl)imide (LiTFSI). Due to the bio-compatible nature of sodium chloride (NaCl), potassium chloride (KCl), phosphate-buffered saline (PBS), they are employed in IGTs for detecting physiological signals, bio-interfacing and health monitoring.

Park et. al. prepared a-IGZO IGTs based on aqueous solutions of NaCl, KCl and KBr.[65] The IGTs operated at lower voltages (< 0.5 V) with faster response time.

2.4.1.4 Polymer electrolytes

Polymer electrolytes are made up of salt dissolved in ion-coordinating polymer. Poly(ethylene oxide) (PEO) is widely studied as a ion-coordinating polymer, since PEO backbone contains oxygen lone pairs that can coordinate efficiently with positive ions. This leads to strong

coupled ionic movement and polymer backbone reorganization during the presence of an applied electric field.

Dasgupta et al. fabricated ZnO based IGTs with printed polymer electrolyte. Polymer electrolyte consists of polyvinyl alcohol and propylene carbonate and $LiClO_4$, in which propylene carbonate acted as a platicizer [66]

2.4.1.5 Polyelectrolytes

Polyelectrolytes are polymers, consisting of repeating units of an ionizable group. According to the charge type on the polymers, it can be classified into two types, namely, polycations and polyanions. Poly(styrene sulfonic acid) (PSSH) with H^+ as the counterion, poly(styrene sulfonic acid sodium salt) (PSSNa) with Na^+ as the counterion, and poly[(1-vinylpyrrolidone)-co-(2-ethyldimethylammonioethyl methacrylate ethyl sulfate)] [P(VP–EDMAEMAES)] with ethyl sulfate as the counterion, are used in polyelectrolyte-based ion-gating mediums, widely studied in IGTs. Natural polymer derivates such as chitosan, carboxymethyl cellulose and other cellulose derivates are also used as a polyelectrolyte. Polyelectrolyte is useful to tune both the electrochemical doping and electrostatic doping in organic electrochemical transistors.

Berggren et.al., controlled the mode of operation (from electrochemical to electrostatic doping) of organic electrochemical transistors using a polyelectrolyte, i.e., polyanionic proton-conducting electrolyte. [67] Due to the immobile nature of the anions in the ion-gating medium, it resists the penetration of anions into the organic semiconductor when the gate is negatively biased. This effect prevents the electrochemical doping in the channel. [67]

2.4.1.6 Oxide electrolytes

Oxide electrolytes are extensively studied in batteries and fuel cells due to its more reliable and wider operating temperature. Very few reports are based on oxide electrolytes for IGTs due to its relatively complex fabrication process.

Katz et.al., fabricated zinc tin oxide based IGTs with Sodium β-alumina (contains mobile Na^+ ions) as an ion-gating medium. Transistors work at lower voltages due to higher capacitance,

but longer response time is needed to utilize the complete capacitance from the ion-gating medium.[68]

Table 2-1 Ion-gating medium for the IGTs.[57]

Gating medium	*Capacitance* *($\mu F\ cm^{-2}$)*	*Thickness* *(μm)*	*Highest applied voltage* *(V)*	*Working temperature* *(°C)*
Ionic liquids	2–2000	NA	**~3**	<400
Ion gels	1–200	0.05–400	**~3**	<300
Aqueous electrolytes	1–10000	NA	**~1**	<100
Polymer electrolytes	1–100	0.1–500	**~3**	<300
Polyelectrolytes	0.2–3000	0.05–100	**~3**	<300
Oxide electrolytes	0.5–1.6	0.02–1	**Can be > 5 V**	<700

2.4.2 IGTs for printed electronics

Printing is simple technique compared to the conventional manufacturing. The difference between printing and microfabrication for side-gated IGTs (i.e. with semiconductor channel and gate electrode in the same plane) is shown in Figure 2-8. The main advantage of printing are: short processing time, low cost, and low material waste. The printing process doesn't need complex instruments and the process is fast compared to the microfabrication, paving the way for on-demand manufacturing of electrical components.[69]

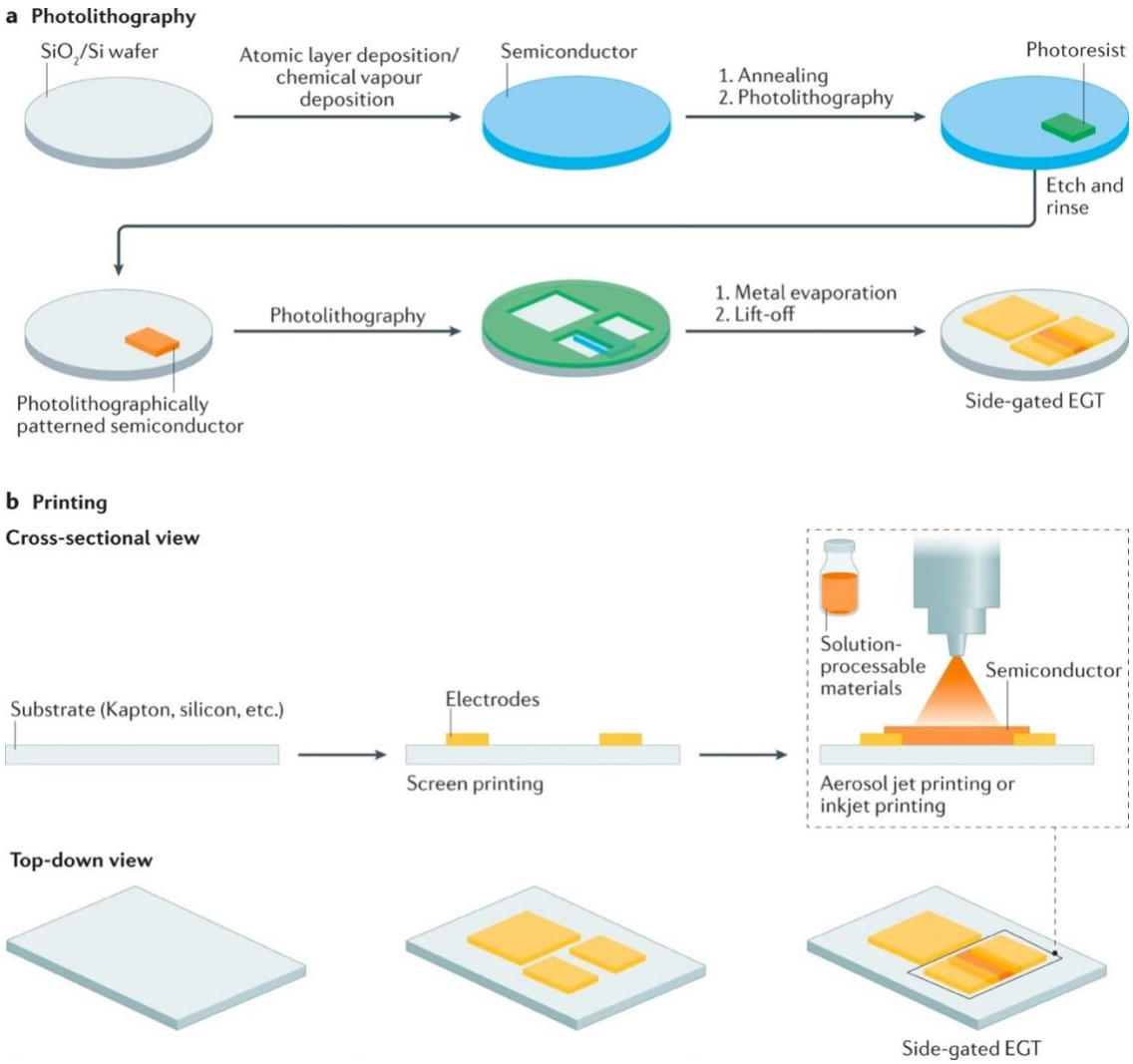

Figure 2-8 Fabrication of side-gated IGTs by (a) photolithography and (b) printing. Reproduced with permission.[69]

In a typical photolithography process (Figure 2-8) initially the active material is deposited on the substrates (e.g. wafers, glass and plastic) and then subjected to the thermal treatment. Afterwards, the semiconductor is patterned using photolithography and an etching process. After patterning the semiconductors, the photoresist is deposited using a spin-coater and then exposed with UV-exposure through a mask aligner, followed by photoresist development. The electron-beam evaporation is carried out to deposit metal contacts and followed by a lift-off process (Figure 2-8 (a)). Depending on specific requirements, these processes can be tuned. Conversely, in a printing process, the metal contacts and semiconductor are deposited using liquid ink. Compared to the lithography process, printing produces similar results while reducing the number of steps. Initially, the metal contacts are deposited using a printer (e.g. screen printer, inkjet printer and aerosol jet printer) and then followed by thermal treatment to attain maximum conductivity. Afterwards, the printer is aligned to print the semiconductor between the source and drain contacts using a semiconductor suspension. In addition, the ion-gel gating can be printed on the semiconductor to make fully printable IGTs.

2.4.2.1 Recent advancements in printed IGTs based on metal oxides

Recently, metal oxide IGTs prepared using printing techniques are comparable to the state of the art of the devices prepared using lithography process. Frisbie et al. demonstrated a low voltage ZnO IGTs on polyimide substrates using aerosol jet printing. They printed ion-gel (PS-PMMA-PS triblock copolymer and [EMIM][TFSI] ionic liquid in ethyl acetate) and demonstrated the bending behaviour (curvature radius ~ 25 mm and ~ 5 mm) of IGTs. ZnO-based IGTs shows a mobility and threshold voltage of 1.6 cm^2V^{-1} s^{-1} and 0.97 V, respectively, without any significant change in electrical characteristics under bending.[64] Dasgupta et. al., fabricated In_2O_3 IGTs by printing In_2O_3 and a composite solid polymer electrolyte on a glass substrate at room temperature. The In_2O_3 IGTs showed a mobility of ~12.5 cm^2/Vs. [70, 71] Recently, Frisbie et. al., showed a printable ion-gel using a screen printer to fabricate ZnO IGTs and demonstrated a ring oscillator circuit using IGTs. [72]

2.4.3 IGTs for sensors

IGTs can be used as a chemical and biosensors due to their ability to function as an ion/electron converter. Oxide semiconductors are stable in air and water, an essential requirement for sensors (chemical/biological) to work under ambient conditions. [73-76] The analyte is in contact with the gate dielectric in conventional ion-sensitive field effect transistors (ISFET) and the analyte is in direct contact with the semiconductor channel, allowing IGTs to work under lower applied voltages.

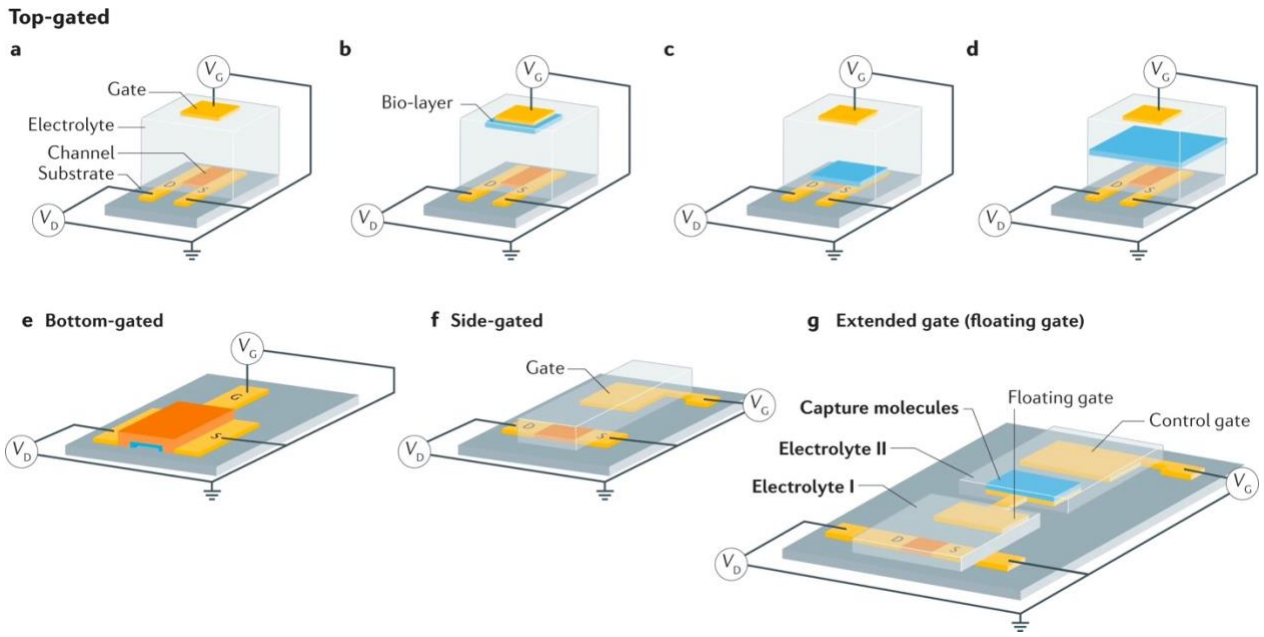

Figure 2-9 Device configuration of IGTs for sensing. (a) top-gate configuration (b) top-gate configuration with bio-layer on the gate electrode (c) top-gate configuration with bio-layer on the channel (d) top-gate configuration with biolayer between the gate and channel (e) bottom-gate configuration (f) side-gate configuration (g) extended-gate configuration. Reproduced with permission. [69]

Ion-gated transistors can be constructed in several ways depending on the position of gate electrode and the semiconductor. The top-gate configuration involves placing the gate over the channel in Figure 2-9 (a). This IGT architecture has application in ion detection, electrophysiology and neuromorphic applications. Top-gate transistors with a biolayer coating on the gate electrode are used for label-free biosensors, where protein probes were selectively detected. (Figure 2-9 (b)).

The biolayers such as antibodies, nucleic acids, peptides and enzymes are essential for specific biosensing applications. The most used design in biosensors and cell monitoring is the top-gate configuration with a biolayer positioned on top of the channel (Figure 2-9 (c)). In another design, the biolayer lies in the electrolyte with absolutely no contact to the both the gate and the semiconductor surface (Figure 2-9 (d)). This design is applied to monitor the integrity of cell membrane tight junctions and for selective ion detection. The less commonly used bottom gate configuration transistor with an ion-conducting solid electrolyte membrane that separates the semiconductor channel from the metallic gate is used in bioelectronics (Figure 2-9(e)). The gate and semiconductor are placed laterally on the same plane in a side gate geometry which is used in neuromorphic applications (Figure 2-9 (f)). Another transistor configuration includes the extended/floating gate configuration consisting of two compartments, namely, a sensing compartment and an IGT compartment (Figure 2-9 (g)).

2.4.3.1 Recent advancements in IGT sensors based on metal oxides

Several metal oxides such as amorphous-gallium indium zin oxide (IGZO), In_2O_3, ZnO and SnO_2 have been widely studied as an active channel material for IGTs based pH and biosensors. [77-81] This section will systematically analyze a few metal oxide materials that display sensing mechanism, their synthesis methods, and device applications. Particularly In_2O_3, ZnO and SnO_2 will be investigated because these exhibits several advantages like low-temperature processing, chemical sensitivity, and easy surface modification. The recent research on oxide-based materials for electronics and biology are discussed.

2.4.3.1.1 In_2O_3 based IGT sensors

Fumiaki N. Ishikawa et al. [82] developed the biosensors using a In_2O_3 nanowire for the detection of nucleocapsid (N) protein found in severe acute respiratory syndrome coronavirus (SARS-CoV). The metals Ti/Au (5nm/50nm) are used as source and drain metal electrodes patterned on SiO_2/Si substrates using photolithography and a lift-off process. The length and width of the transistor channel are 2.5µm and 780 µm. In_2O_3 was deposited on the SiO_2/Si substrates using a laser ablation method. In_2O_3 nanowire was functionalized with small in size (2-5 nm) antibody-mimicking proteins that can detect sub-nanomolar concentrations of the N-protein in SARS-CoV. Pt wire is used as a gate electrode. Figure 2-10 (a) shows the schematic representation

of the antibody-mimicking protein functionalised In_2O_3 biosensor. The output (Figure 2-10 (b)) and transfer (Figure 2-10 (c)) characteristics of In_2O_3 IGTs gated with 0.01 M PBS solution. The ON/OFF ratio and transconductance of the IGT were 10^3 and 4µS. A fibronectin probe molecule used as an antibody-mimicking protein was used to specifically capture the nucleocapsid (N) protein of SARS-CoV. The non-specific binding of the other elements was hindered by introducing 44 µM concentration of bovine serum albumin to the 0.01 M PBS solution. Label free detection of N-protein of SARS-CoV with a lower concentration of 0.6 mM was achieved in 10 minutes using In_2O_3 based biosensors (Figure 2-10 (d)). [82]

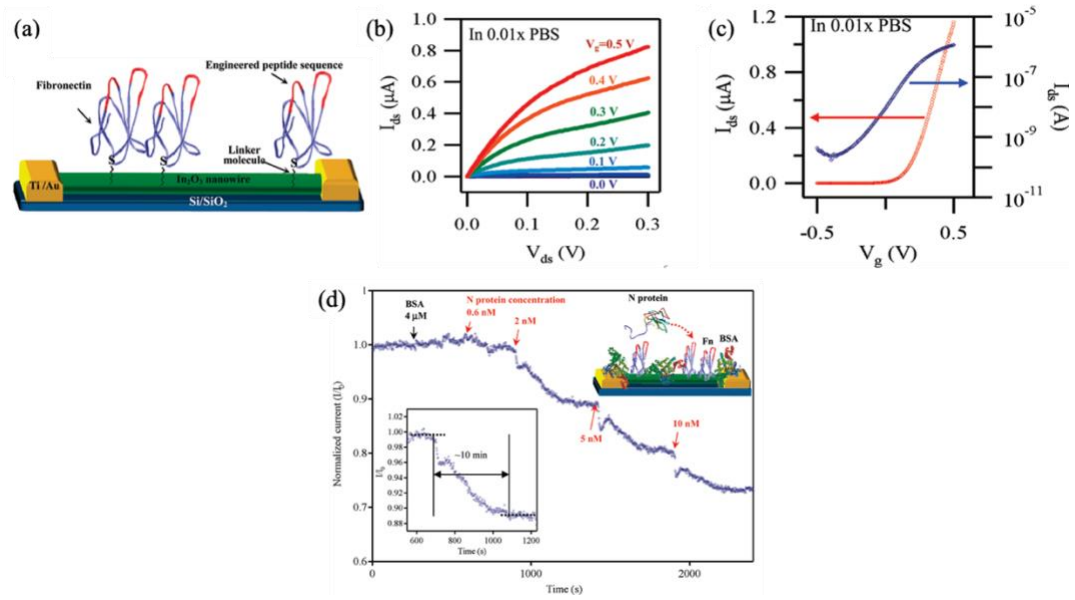

Figure 2-10 (a) Schematic representation of fibronectin functionalised In_2O_3 nanowire biosensor (b) output and (c) transfer characteristics of In_2O_3 nanowire gated with PBS solution (d) normalised current response of In_2O_3 based IGTs with different concentration of N-protein. The inset of Figure (d) shows the response time of the IGTs. Adapted with permission [82]

You Reung Rim et al. [83] fabricated a wearable, non-invasive health monitoring biosensor to detect the glucose levels in tears using solution-processed In_2O_3. Au/Cr (30/10 nm) source and drain electrodes were patterned on the polyimide or SiO_2/Si substrates using a photolithography process. The width and length of the channel are 1000 µm and of 200 µm respectively. Hexa aqua indium (III) complex was spin-coated on the polyimide substrate and heated at 250 ˚C in air. The ultrathin (3.5 nm) In_2O_3 thin films was obtained on the substrate. The mobility of 20 cm^2/Vs was

observed for the thin film transistor configuration. Figure 2-11 (a) depicts the device fabrication of In_2O_3 sensors. Figure 2-11 (b) shows the attached glucose sensor on the artificial eye and human hand. Here, they functionalized the NH_2- terminated silanes on the In_2O_3 surface to act as a pH sensor and they functionalised glucose oxidase to specifically detect the d-glucose. The transfer and output characteristics of the IGTs gated with PBS solution are shown in Figure 2-11 (c and d). Au is used as a gate electrode. The prepared device shows good conformal contact to the artificial skin (PDMS) and artificial eye (acrylic plastic). The normalised current response of the pH sensors is shown in Figure 2-11 (e). The prepared non-invasive glucose sensor can detect glucose levels in the blood (ranging from 2 - 30 mM) and tears (ranging from 0.1 – 0.6 mM). Figure 2-11 (f) shows the normalised current response of the IGTs with different concertation of d-glucose in PBS solution. [83]

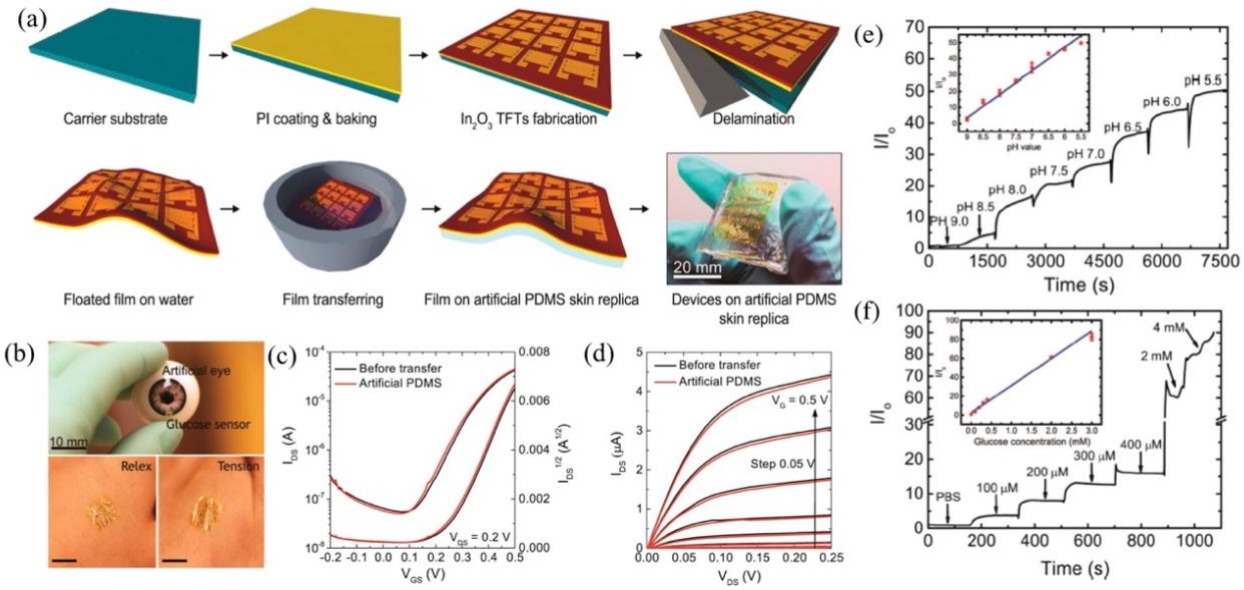

Figure 2-11 (a) Scheme of the device fabrication (b) glucose sensor on the acrylic artificial eye and the human hand, (c,d) the device response of the In_2O_3 IGTs before and after transfer on the artificial skin. A 1 M PBS solution is used as a gating medium. (e) A pH sensor prepared from In_2O_3 based IGTs shows the response with pH ranging from 5.5 to 9. (f) The detection of d-glucose concentration in the low range (i.e similar to tears) and upper range (i.e similar to blood). Adapted with permission [83]

Hsiao-Kang Chang et al. [84] fabricated In_2O_3 nanowire sensors for the detection of cancer biomarkers in body fluids (e.g. human blood). It is an electrical detection and label- free detection technique. Various cancer biomarkers were detected using In_2O_3 sensor. The Au/Cr (50nm/5nm) source and drain electrodes were prepared on SiO_2/Si substrates by photolithography and e-beam evaporation. The length and width of the transistor channel are 2.5 and 780 µm. The In_2O_3 nanowire channel was deposited through laser ablation chemical vapor deposition. The schematic representation of the In_2O_3 sensor is shown in Figure 2-12 (a). The surface passivation of amphipathic polymer (Tween 20) on the channel material was done to selectivity capture the cancer biomarker. The sensor has a selectivity towards the cancer antigen 125 (CA-125) and insulin-like growth factor II (IGF-II). The sensor shows a detection limit of 0.1 U/mL of CA-125 and 8 ng/mL of IGF-II, which is two orders of magnitude lower than the clinically relevant level (Figure 2-12 (b) and (c)). [84]

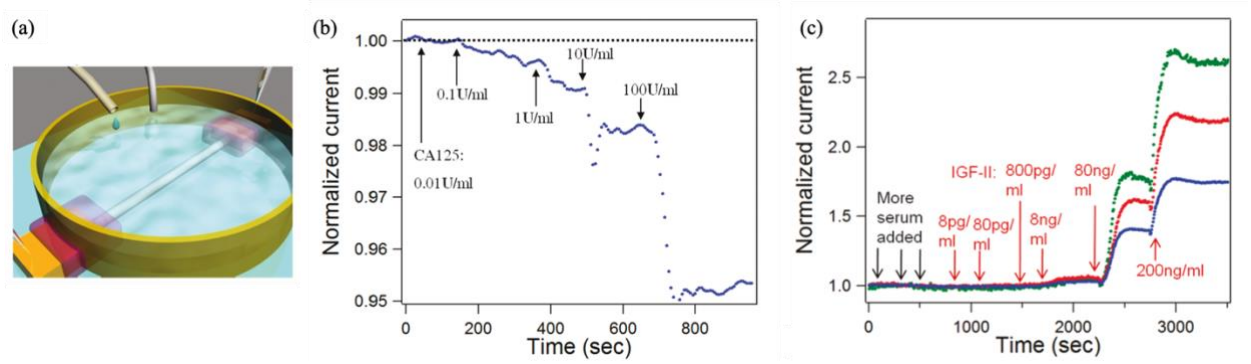

Figure 2-12 (a) Schematic representation of In_2O_3 biosensor, (b) normalised current response of the sensor during the measurement of CA125 in the blood , and (c) normalised current response of the sensor during the measurement of IGF-II in the blood. Adapted with permission [84]

Qingzhou Liu et al [85] prepared a wearable biosensors using sputtered In_2O_3 nanoribbons. Ti/Au (1nm/50nm) source, drain and gate electrodes were prepared on the PET substrates by shadow mask electron beam evaporation. The length and width of the transistor channel are 500 µm and 25 µm. The In_2O_3 was deposited through radio frequency magnetron sputtering. The on-chip gold side gate enables an easier way to detect glucose levels in artificial sweat, artificial tear and saliva. Chitosan, carbon nanotubes and glucose oxidase were dissolved in a PBS solution and then printed (inkjet printing) onto the In_2O_3 nanoribbons. Figure 2-13 (a) shows the schematic representation of the In_2O_3 sensor. After functionalising, the sensor specifically captures the

glucose in the analyte solution. Figure 2-13 (b) shows the output characteristics of the In_2O_3 based IGTs gated with a 0.1 M PBS solution. The mobility and ON/OFF ratio of the device are 22 cm^2/Vs and 10^5. The normalised current response of the device exposed to 0.1 M PBS, artificial tears, artificial sweat and saliva with respect to glucose concentration are shown in Figure 2-13 (c). The prepared glucose sensor shows a detection limit of 10 nM of glucose. [85]

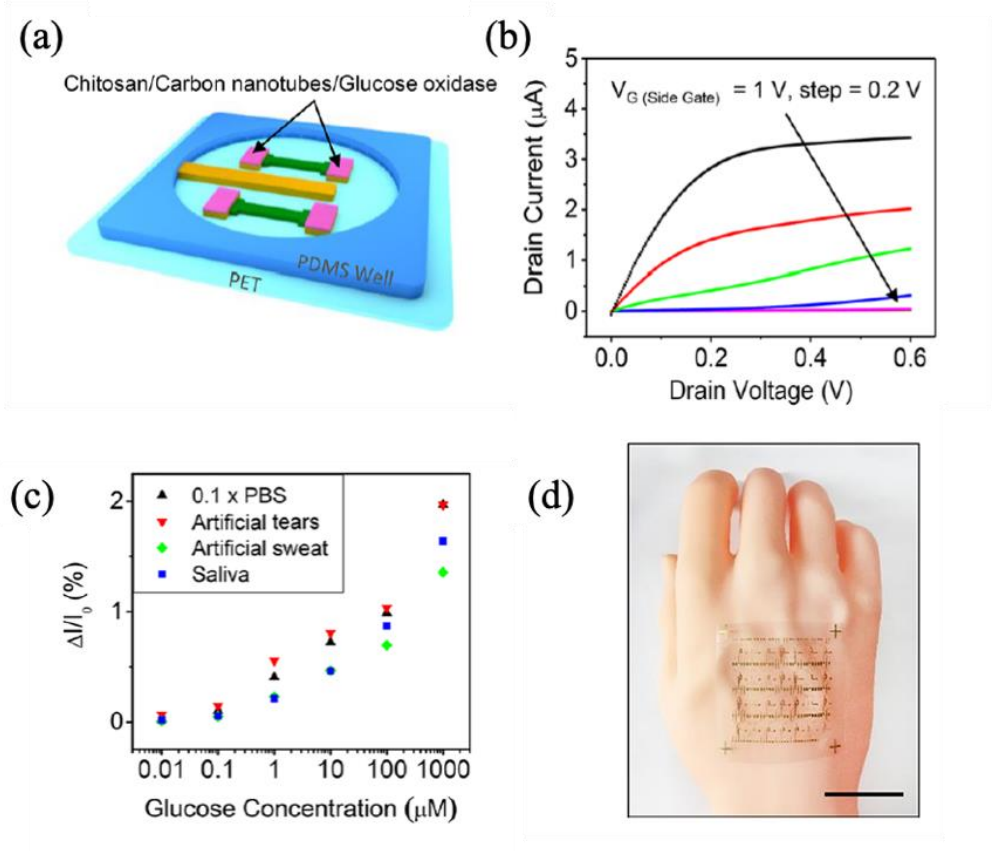

Figure 2-13 (a) Schematic representation of In_2O_3 IGTs, (b) output characteristics of IGTs gated with 0.1 M PBS solution, (c) normalised current response of the device with respect to increasing concertation of glucose, and (d) the attached biosensor on an artificial hand. Adapted with permission [85]

2.4.3.1.2 ZnO based IGT sensors

The authors, E. Bandiello et. al[76], fabricated ZnO IGTs based on aqueous gating media used for environmental and biological sensing. Ion-selective ZnO IGTs was prepared by integrating the ion-selective membrane in the transistors. Enzyme functionalization was performed to use this IGT

as a glucose sensor. The glucose sensing and ion-selective sensing was demonstrated. IGT was prepared on the glass substrates. ITO source and drain electrodes were patterned on the glass substrates with a width and length of 2000 µm and 20 µm, respectively. A ZnO nanoparticle suspension in ethanol was spin-coated on the pre-patterned glass substrates and then annealed at 450 ˚C for 30 mins in ambient air. The thickness of ZnO film is 60 nm. Glass wells were attached on the substrate to confine the gating medium. A Pt wire or Ag/AgCl pellet electrode was used as a gate electrode. Initially 0.1 M KCl solution was used as a gating media for the IGTs.

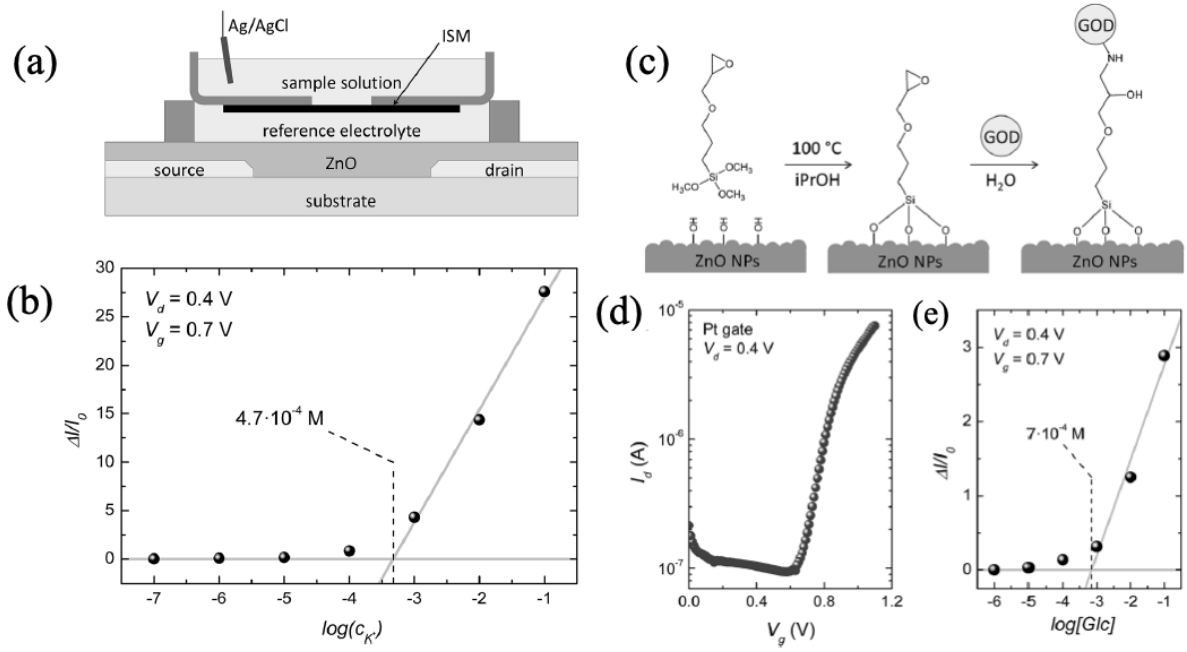

Figure 2-14 (a) Schematic representation of ion-selective IGTs. (b) IGTs response with respect to the K^+ concentration. (c) The reaction scheme of the surface functionalization of ZnO with enzyme glucose oxidase. (d) Transfer curve of IGTs functionalised with enzyme GOD. (e) IGTs response to glucose concentration. Adapted with permission [76]

The prepared device shows the mobility of 0.8 cm^2/Vs. Ion selective transistors were prepared using an ion selective membrane (membrane prepared using solution processing), which separates analyte from the reference solution. This setup (Figure 2-14 (a)) was used as an ion sensor that selectively detects K^+ ions. There is a potential shift that occurs at the reference electrolyte/ion-selective membrane interface due to changes in the concentration of the analyte solution. This leads to a drop in the electric field at the transistor channel, modulating the conductivity of the channel.

The IGTs response to different concentration of K+ ions is shown in Figure 2-14 (b). For glucose sensing, the enzyme glucose oxidase (GOD) was covalently linked with the ZnO surface using an alkoxysilane functional group (Figure 2-14 (c)). Transfer curve of IGTs functionalised with enzyme GOD measured with 0.1 M KCl is shown in Figure 2-14 (d). The analyte used here is 0.1 M KCl aqueous solution with the different d-glucose concentrations (Glc = 0.1 mM – 100mM), which is the glucose concentration in the human body (1-20 mM). IGTs response to different glucose concentrations are shown in Figure 2-14 (e). ZnO IGTs based biosensors shows the highest sensitivity above 1 mM.[76]

2.4.3.1.3 SnO_2 based IGT sensor

Zahrah Alqahtani et al. [86] fabricated SnO_2-based IGTs to detect Pb^{2+} and Cu^{2+} ions in drinking water at very low concentrations. SnO_2 was deposited using spray pyrolysis on a quartz substrate prepatterned with Au source and drain electrodes (W/L = 33.3). The substrate was heated at 400 ˚C during spray pyrolysis. Clinoptilolite embedded plasticised PVC is used here as an ion selective membrane in the IGT architecture. Tap water was filled in the bottom of the chamber and the analyte with Pb^{2+} or Cu^{2+} ions were filled in the top chamber (Figure 2-15 (a)). A tungsten needle was used as a gate electrode. The change in concentration of the ions leads to a change in the threshold voltage that follows the Langmuir–Freundlich (LF) characteristic. Figure 2-15 (b) and (c) shows the transfer curves of the SnO_2 IGTs with different concentration of Pb^{2+} and Cu^{2+} ions. The level of detection of Pb^{2+} and Cu^{2+} in the drinking water using IGTs are 0.9 nM and 14 nm.[86]

Nawal Alghamdi et al.[87] prepared SnO_2-based IGTs for the detection of benzyl alcohol. SnO_2 is deposited on Au-interdigitated-quartz substrates using spray pyrolysis. A two chamber setup is used here, and a zeolite embedded PVC membrane separates the reference and analyte solution. The membrane is selective towards benzyl alcohol. Figure 2-16 (a) shows a schematic representation of the SnO_2 IGTs. The reference solution contains DI water and the analyte contains benzyl alcohol with different concentrations. Figure 2-16 (b) shows the transfer curve of the transistor with increasing concentration of the benzyl alcohol. The limit of detection of benzyl alcohol in the water using SnO_2 IGT is 2 µM and that follows Langmuir surface adsorption.[87]

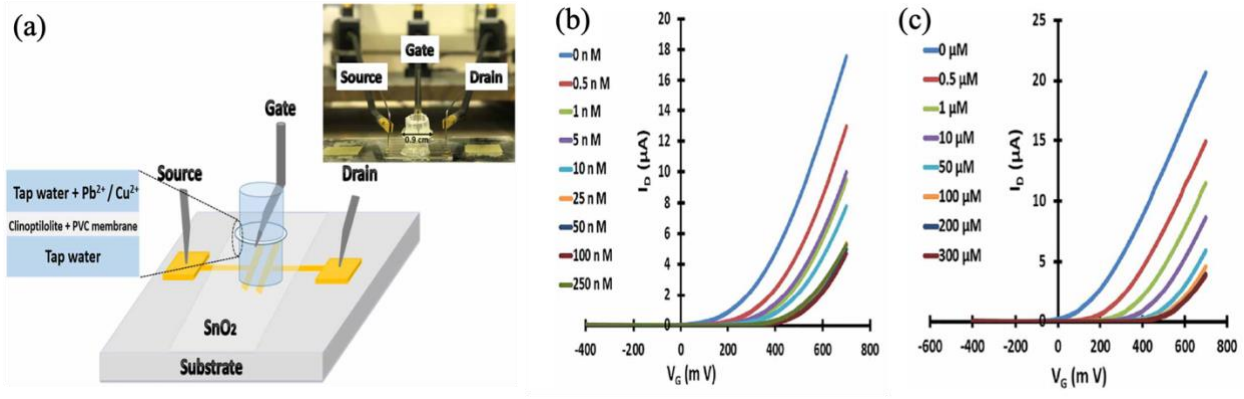

Figure 2-15 (a) Architecture of SnO_2 IGTs for Pb^{2+} and Cu^{2+} detection. (b and c) Transfer characteristics of IGTs with increasing concentrations of Pb^{2+} (b) and Cu^{2+} (c). Adapted with permission[86]

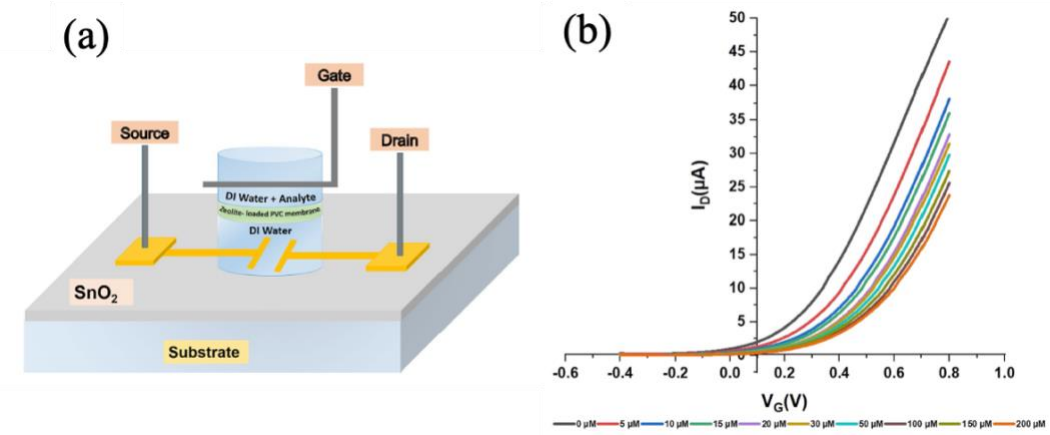

Figure 2-16 (a) Architecture of SnO_2 IGTs for benzyl alcohol detection. (b) Transfer characteristics of IGTs with increasing concentrations of benzyl alcohol. Adapted with permission[87]

CHAPTER 3 METHODOLOGY

The following methods are discussed in this chapter: gold patterning on the substrates by microfabrication, silver patterning on the substrates by printing, transistor channel material fabrication by solution processing and vacuum processing, ion-gating medium preparation, gate electrode preparation, device fabrication, and characterization of the active channel material and transistors.

3.1 Substrates

The substrate is the base in which the transistor device is built. The transistors in the experiments discussed used two different types of substrates i.e., rigid (SiO_2/p-Si) and flexible (PET) substrates. The SiO_2/p-Si substrate (WaferPro, USA) employs wet thermal oxide (~ 200 nm) grown on the front side of polished single crystalline (crystal orientation of <100>) B-doped silicon (heavily doped p-type, thickness ~500 µm, electrical conductivity ~650 S/cm), and was chosen for the rigid substrate due to its smoothness, uniformity and the high temperature tolerance of SiO_2. We used polymeric substrates for the flexible transistor preparation. Specifically, we used PET (polyethylene terephthalate) substrates (Policrom. Inc., USA) with a thickness of 175 µm with an antistatic coating on both sides. The PET substrates are thermally stable up to 150 ˚C. We cleaned the substrates prior to deposition using three rounds of ultrasonication: 10 min submerged in a bath of isopropanol, followed by 10 min in acetone, and lastly, 10 min in isopropanol. Subsequently, we treated the surface of the substrates with UV-Ozone for 15 mins to remove organic contaminants and enhance the adhesion of the channel material films on the substrate surface.[88] The UV-Ozone cleaner (Jelight, Model 30) has a low-pressure mercury vapor lamp, and a lamp intensity of ~ 30 mW/cm^2 that uses a wavelength of ~ 254 nm.

3.2 Source and drain electrode preparation

The source and drain electrodes for ion-gated transistors (IGTs) are prepared using two methods and materials: microfabrication and printing. We patterned Au source and drain electrodes using microfabrication and Ag source and drain electrodes using printing.

3.2.1 Microfabrication

Photolithography and electron beam evaporation are used to pattern Au source and drain electrodes for IGTs. Photolithography is the transfer of a geometric pattern to a substrate from a photomask.

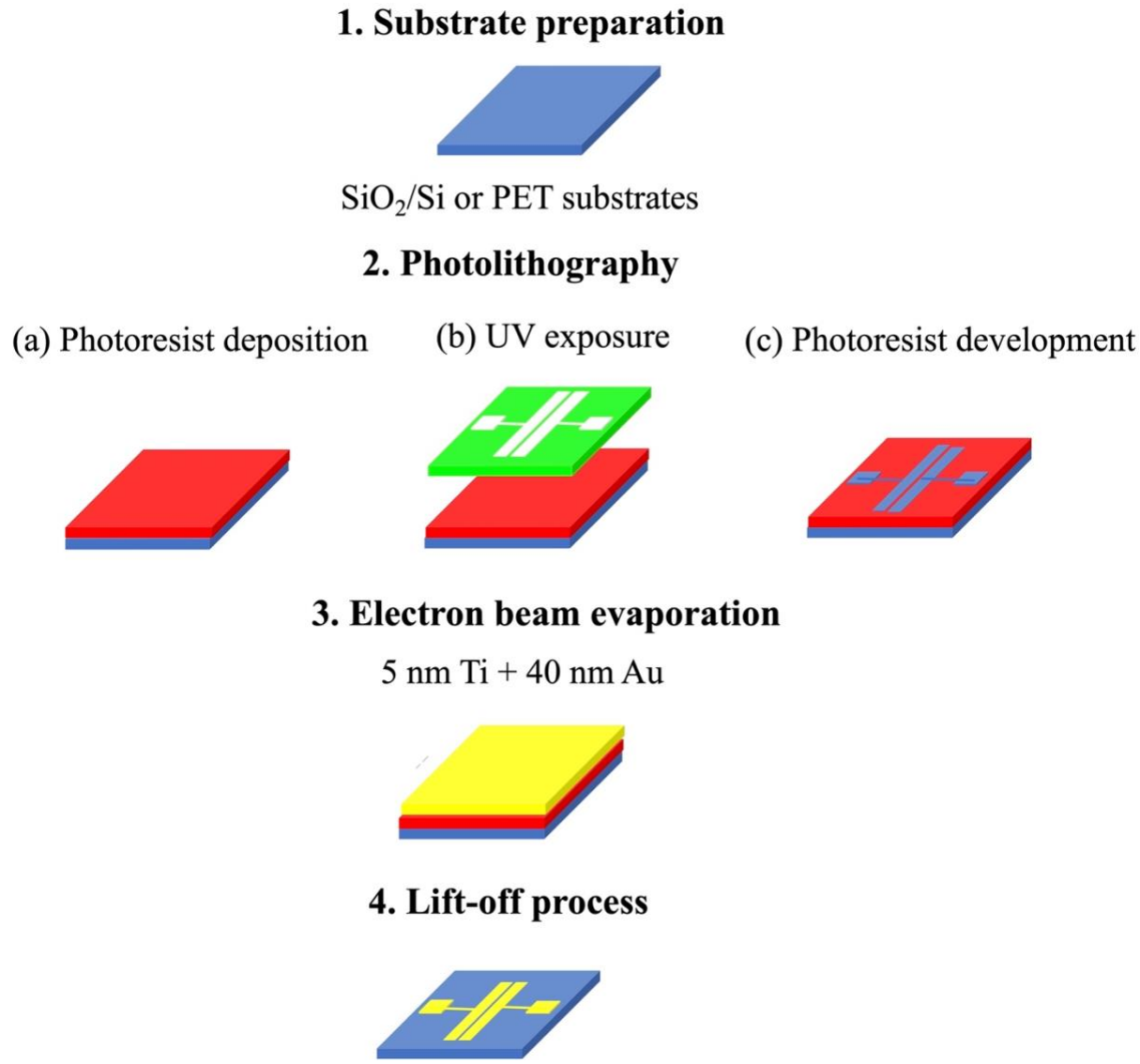

Figure 3-1 Schematic representation of Au electrodes patterning on the substrates.

To pattern the substrates using photolithography the substrates are first covered with a uniform film of photoresist using a spin-coater. The substrates are spin-coated with positive photoresist, AZ 900 MIR (consisting of diazonaphthoquinone sulfonic acid ester, ethyl lactate, n-

butyl acetate, cresol novolac resin, and phenolic polyol) at 3000 rpm, and immediately baked at 110 ˚C for 60 s. The substrate with the photoresist is placed under a photomask containing the desired pattern geometry using a Karl Suss MA6 mask aligner and exposed to UV light (i-line, 365 nm). After the exposure, the substrates undergo a post exposure bake at 90 ˚C for 60 s, and after, are submerged in a developer, AZ726 (3 % of tetramethylammonium hydroxide in a aqueous solution), which is used to dissolve the UV-exposed photoresist that, once dissolved, leaves the bare silicon substrate only in the areas exposed, resulting in the desired pattern geometry. To make the metal contacts, the substrate with the patterned photoresist is covered with 5 nm of Ti, to promote Au adhesion, followed by 40 nm of Au, deposited using e-beam evaporation at a rate of 0.5 Å /s. After the metal contact deposition, the excess metal is removed using a lift-off process: the substrates are immersed in Remover 1165 (consisting of 90-99 % of 1-Methyl-2-pyrrolidinone), the areas of the metal-covered substrate with a base layer of photoresist, not exposed to UV, are removed, leaving Ti/Au adhered to the silicon substrate in the desired geometry. The process flow for the fabrication of Ti/Au electrodes is shown in Figure 3-1. We employ two transistor device structures: 1) top gate, bottom contact and 2) top gate, top contact. The top gate, top contact device structure was necessary for transistors with channel materials prepared by controlled aqueous growth, due to the highly acidic environment of the aqueous growth environment causing the gold electrodes to detach from the substrates. Therefore, the use of top contacts, that are deposited on the top of the aqueous solution processed films, is necessary.[88, 89]

3.2.2 Printing

A printed circuit board (PCB) printer is used to pattern Ag source and drain electrodes on substrates. Initially, the source and drain electrode pattern is created using a pattern editor program in DipTrace PCB design software. Once the pattern file is created using pattern editor, it is loaded into the Voltera V-One software. The Ag ink cartridge (The nozzle size is 150 µm) is attached to the PCB printer for printing the Ag electrodes. The Ag ink (Conductor 2, Voltera Inc., Canada) contains Ag, diethylene glycol monoethyl ether acetate and mineral salts. After loading the ink cartridge, the desired pattern is automatically printed on the substrate by the Voltera controller moving the ink cartridge to the desired locations on the board and depositing a single layer of continuously printed ink, in a specified pattern, controlled by the Voltera V-One software. Due to

the resolution limitations of the printed circuit printer, we achieved a minimum ~ 110 µm channel length from the printer. We prepared top-contact Ag source and drain electrodes on SnO_2 deposited on PET substrates using the printing method.[89] Printing electrodes using a PCB printer greatly reduces the complexity and time required for photolithography and etching, and costs required in using vacuum sublimation methods.

3.3 Channel material preparation

We used the wet chemical approach described below, and vacuum sublimation to fabricate the metal oxide channel materials for IGTs. We prepared SnO_2 and TiO_2 films by the wet chemical approach, and we prepared the compact TiO_2 films by vacuum sublimation.

3.3.1 Wet chemical approach

3.3.1.1 Metal oxide films through controlled aqueous growth

Controlled aqueous growth is a technique used to deposit the metal oxides and oxy-hydroxides on either crystalline (single crystalline / poly crystalline) or amorphous substrates in one step, at lower temperatures than standard deposition techniques. The material is deposited on the substrates without any template, surfactant, applied field or an under-coat on the substrate with another material. The deposition is obtained through slow nucleation and growth of metal oxides by lowering the interfacial tension. The thermodynamically stable minimum surface energy of the system is formed by controlling pH, ionic strength and aqueous precursors. Varying the temperature and concentration of the precursors, affects the hydrolysis rate which controls kinetics of nucleation and growth.[90, 91]

In this PhD work, we deposited SnO_2 using controlled aqueous growth. The typical synthesis of SnO_2 was carried out using 100 ml aqueous solution of 0.6 M HCl, 0.97 mM tin chloride pentahydrate, and 150 mM urea and heated at 95 ˚C for 2 days.[89]

3.3.1.2 Metal oxide films through metal alkoxide processing

Metal alkoxide processing is carried out using a sol-gel method. Sol-gel method is a wet chemical method used to prepare thin-films and nanoparticles, widely used for the preparation of

metal oxides such as TiO_2 and SiO_2. In the sol-gel method, metal alkoxide undergoes hydrolysis and a polymerization reaction to form the sol. Specifically, the sol is deposited on the substrate, and then subsequent evaporation of solvents through heating, followed by high temperature annealing which provides the crystalline metal oxide film.[92]

In this PhD work, we prepared TiO_2 films by sol-gel assisted spin-coating method. The sol gel was synthesized by stirring the solution containing 1.7 mL of titanium butoxide (Alfa Aesar, 99%), 65 µL of concentrated HNO_3 (Thermo Fisher Scientific, 70%), 90 µL of deionized water (Milli-Q water purification system, resistivity of 18.2 MΩ.cm) and 19.1 mL of isopropyl alcohol. The sol gel is spin-coated on the SiO_2/Si substrates by spin-coater and then heated at 100 ˚C to evaporate the solvent. Afterwards, the film is subjected to high temperature thermal treatment (450 ˚C), to ultimately form a crystalline metal oxide film.[93]

3.3.1.3 Metal oxide films through metal oxide nanoparticle processing

The metal oxide films are deposited on the substrates using metal oxide nanoparticle ink. As compared to metal precursor processing, in metal oxide nanoparticle processing, the metal oxide nanoparticle is the starting material for the ink preparation, and does not require a precursor material. The metal oxide nanoparticle ink is prepared using metal oxide nanoparticle with a binder and solvent. The ink is deposited on the substrates by drop-casting and spin-coating methods. The morphology of the resulting material is tuned by using a suitable binder and then followed by thermal treatment. A high temperature thermal treatment, with a temperature above the decomposition temperature of the specific binder, leaves metal oxide films with a porous morphology. [94]

In this PhD work, we used two routes to prepare metal oxide nanoparticle ink. Route I) synthesis using 2 g of TiO_2 (particle size ~70 nm, Sigma Aldrich) with 0.4 g of PVDF binder and 20 mL of dimethyl formamide solvent. The prepared TiO_2 ink is deposited on the substrate by drop-casting technique. Route II) synthesis using 10 g of Aeroxide TiO_2 P25 nanoparticles (Photocatalytic standard, particle size ~ 21 nm, Millipore Sigma), 107 mL of ethanol (Commercial Alcohols Inc., Canada), 1.4 mL of deionized water and 3.7 mL of titanium tetraisopropoxide.[88, 93]

3.3.1.4 Film forming techniques

In this PhD work, the solutions for the metal oxide film formation are deposited on substrates using (i) drop-casting or (ii) spin-coating for the wet chemical approach.

3.3.1.4.1 Drop-casting

Drop-casting is a technique in which the specific amount of solution is dropped on the static substrate using a micropipette, followed baking for complete solvent evaporation, leaving a layer of film on the substrate (Figure 3-2(a)).[95] In some cases, we heated the samples at higher temperatures to tune the surface morphology by decomposing the binder.

3.3.1.4.2 Spin-coating

Spin-coating technique is a versatile method in wafer processing to create films with a thickness ranging from few nm to few µm. First, the substrate is attached to a rotating chuck, held in place by vacuum. Then, the solution is cast by dropping the solution on the substrate using a pipette, until ~75% of the substrate is covered with the solution. Afterwards, the substrate is centripetally accelerated at a rate in the range of ~ 500 to 12000 rpm, chosen depending on the solution viscosity and desired thickness, to spread the solution on the substrate by centrifugal force (Figure 3-2 (b)).[96]The viscosity of the spin-coating solution plays a vital role in depositing the films by spin-coating. In this PhD work, TiO_2 are deposited films by spin-coating using Laurell spin-coater (Model Number: WS-650HZB-23NPPB/UD3).

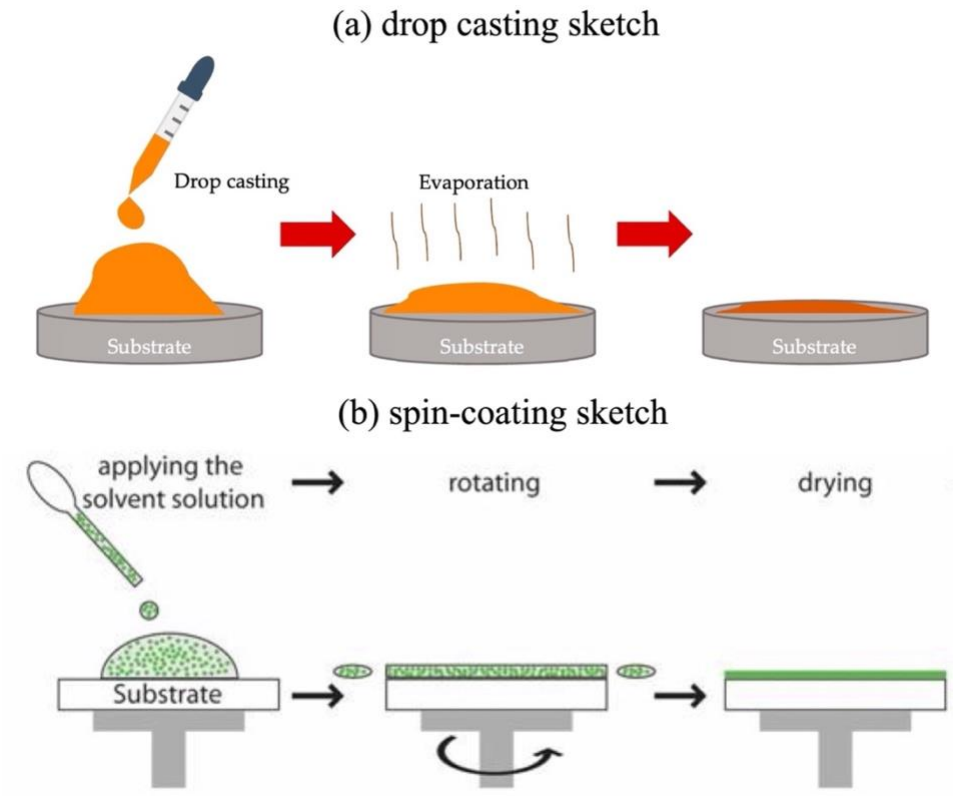

Figure 3-2 Scheme of the (a) drop-casting and spin-coating. Adapted with the permission[95, 96]

3.3.2 Vacuum sublimation

Electron-beam evaporation is carried out in the vacuum environment in which the target material strikes the substrate with high energy and intensity beams of electrons. Electron-beam evaporation takes place in a vacuum chamber, containing a metal target material, an e-beam source and a quartz crystal microbalance. When the electron beam hits the target material, there is sufficient energy to vaporize the material (sublimation, solid phase to the gaseous phase). The material, now in the gaseous phase, travels upward in the vacuum, condensing (deposition, gaseous phase to solid phase) onto the substrate surface. The quartz crystal microbalance is used to monitor the deposition rate and the thickness of the material deposited on the substrate.[97]

In this PhD work, we fabricated ~ 60 nm compact TiO_2 films on SiO_2/Si substrates using electron beam evaporation (Thermionics) with a TiO_2 target (Kurt J. Leskar, USA). [88]

.

3.4 Ion-gating medium

3.4.1 Ionic liquid

Room temperature ionic liquid is used as an ionic liquid gating medium in this work. We employed [EMIM] [TFSI] as an ionic liquid. [EMIM] [TFSI] exhibits ionic conductivity of 6.63 mS/cm, density of 1.52 g/cm^3, viscosity of 39.4 cP and a wide electrochemical stability window of 4.7 V (anodic limit of 2.6 V and cathodic limit of -2.1 V).[52, 60] If water enters the ionic liquid, it acts as an impurity in the ionic liquid, and the presence of water in the ionic liquid reduces its electrochemical potential window. Prior to device fabrication, we purified the ionic liquid in vacuum (10^{-6} Torr) and simultaneously heated at 60 ˚C for overnight.[52] This is the important step for the usage of room temperature ionic liquid for the transistors. We confined the ionic liquid by soaking the PVDF (polyvinylidene fluoride) membrane (125 µm thick) in ionic liquid and attaching it on the top of the device. The PVDF membrane has a hydrophobic nature and contains a pore size of 220 nm. When the membrane is immersed in the ionic liquid, it becomes wet with ionic liquid throughout the entire membrane volume.[88] Unless otherwise specified, wherever ionic liquid is mentioned hereafter, it corresponds to the [EMIM][TFSI].

3.4.2 Aqueous electrolyte

In this work, we used aqueous electrolytes as an ion-gating medium for the IGTs due to the ambient stability and water stability nature of metal oxides. We prepared 0.1 M NaCl in deionized water (saline solution) and used as the ion-gating medium for the transistors. We confined the aqueous gating medium by 2 ways: (1) using a PDMS (polydimethylsiloxane) rectangular well, in which the PDMS well (i.e, rectangular cuboid) is attached to the device and the ion-gating medium is filled with the micropipette, (2) using a hydrophilic cellulose membrane (i.e. cotton linters), in which the cellulose membrane (220 µm thick, pore size ~20 µm) is soaked with electrolyte and then attached to the device.[89, 93]

3.5 Gate electrode preparation

Activated carbon on the porous, graphitized, resin bonded carbon fiber paper (Spectracarb 2050A, Fuel Cell Store, USA) is used as a gate electrode for IGTs. Porous, graphitized, resin

bonded carbon fiber paper (shortly carbon paper hereafter) has the thickness of 381 µm, density of 0.5 g/cm^3, porosity of ~78 %, conductivity of 185 S/cm (in-plane) and 65 S/cm (through plane). We deposited a chemically activated (chemically activated using phosphoric acid) wood carbon (Norit, Chemically activated) on the conductive carbon paper using two methods, chosen depending on whether ionic liquid (hydrophobic) or aqueous electrolyte (hydrophilic) ion-gating medium is used.[89]

Activated carbon ink for the ionic liquid gated IGTs are prepared using activated carbon (28 mg mL^{-1}) and PVDF (1.4 mg mL^{-1}) in N-methyl pyrrolidone. Activated carbon ink for the aqueous electrolyte gated IGTs are prepared using activated carbon (28 mg mL^{-1}) and Nafion (1.4 mg mL^{-1}) in isopropyl alcohol. The activated carbon inks are drop-casted on the carbon paper and heated at 60 ˚C to remove the solvent traces.[89]

3.6 Device Assembly

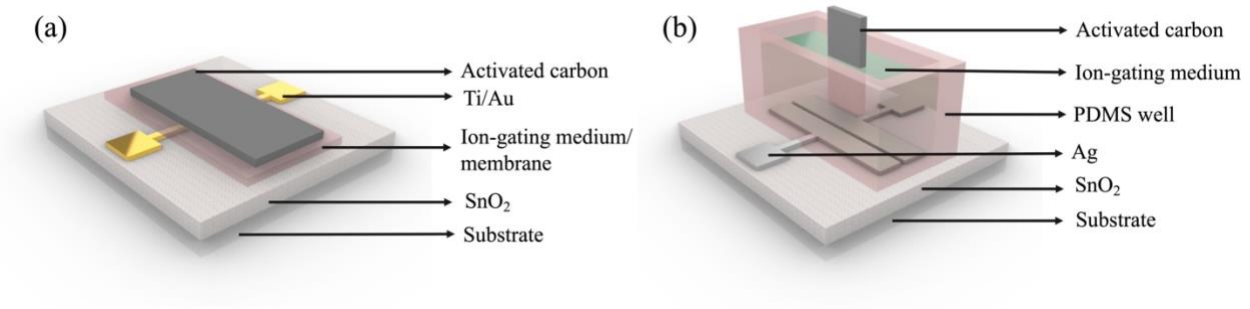

Figure 3-3 Schematic representation of SnO_2 IGTs. (a) IGTs with Au patterned electrodes with the ion-gating medium confined with a membrane; (b) IGTs with Ag patterned electrodes with the ion-gating medium confined with a PDMS well.

For ionic liquid gated transistor, the ionic liquid soaked PVDF membrane is placed on top of the semiconductor and then activated carbon gate electrode is placed on the top of the ionic liquid soaked PVDF membrane. For the IGTs with cellulose membrane, the saline solution-soaked cellulose membrane is placed on top of the semiconductor and then gate electrode is placed on top of the ion-gating medium. For the IGTs with PDMS well, we attached PDMS well on top of the device and filled the well with the ion-gating medium using a micropipette. The activated carbon gate electrode is immersed in the ion-gating medium during the measurements.[89, 93] The schematic

representation of SnO_2 IGTs is shown in Figure 3-3, the ion-gating medium is confined with a membrane (a) or a PDMS well (b).

Unless otherwise noted, the devices with ionic liquid, are assembled in N_2-purged glove box and measured in the N_2-purged glove box. In addition, all the devices with aqueous electrolytes are assembled and measured in the ambient condition unless otherwise specified.

3.7 Film characterization

3.7.1 Atomic force microscopy

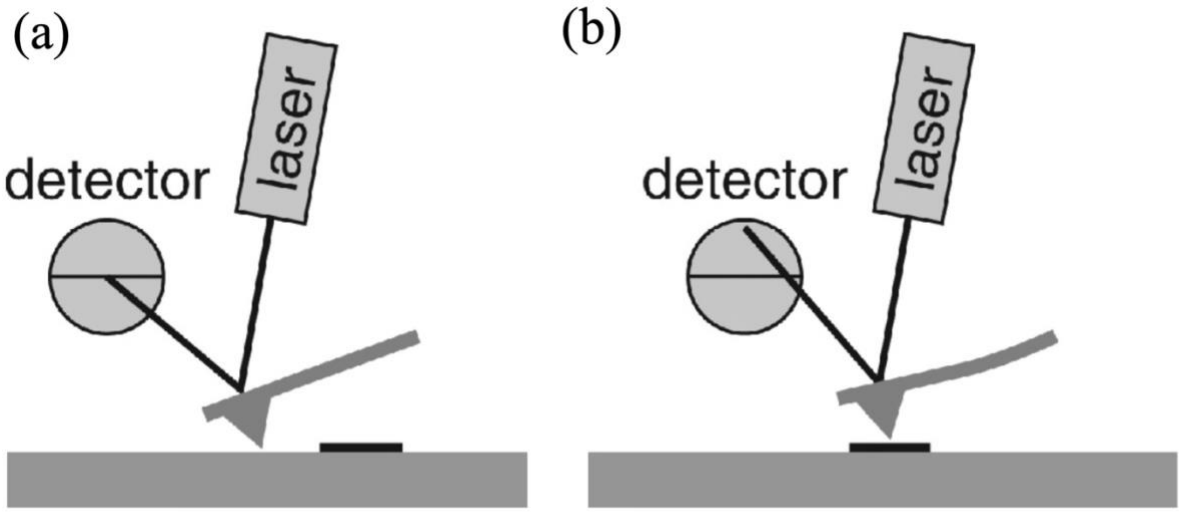

Figure 3-4 Schematic representation of cantilever deflection (a) before and (b) during the interaction with surface feature, and the reflection of the laser on the detector associated with the cantilever deflection.[98] Adapted with the permission.

Atomic force microscopy (AFM) is the topographical surface characterization technique to study the surface features of films at nanoscale. AFM uses a flexible cantilever that scans the surface three dimensionally and deflects when there is a surface feature. The size of the surface feature that causes the deflection in the cantilever corresponds to a change in the laser reflection on the detectors (Figure 3-4). The reflection of the change in laser beam position is recorded against the cantilever height. Three modes of AFM can be conducted on the samples, (i) contact mode, (ii) non-contact mode and (iii) tapping mode. Contact mode and non-contact mode makes the

cantilever to repulse or attract to the sample surface, respectively. During the tapping mode, interaction of sample surface with the cantilever, oscillates near to or equal to the cantilever's resonance frequency. AFM provides useful information about the film surface topography, such as roughness, cracks and grain boundaries of the film surface. [98]

In this PhD, tapping mode AFM were used to study the topographical surface features of the metal oxide films at ambient conditions. During the measurements, the cantilever (spring constant: 40 N m^{-1} and tip radius <10 nm) scans the surface of the sample with a scan rate of 1 Hz.

3.7.2 Scanning electron microscopy

Electron microscopes use an electron gun to analyze the morphology of the samples. Scanning electron microscope (SEM) has a much higher magnification than the optical microscope which uses visible light sources that limits image resolution at high magnification. Two types of electrons are emitted once a sample is hit with a focused electron beam in a vacuum chamber. The secondary electron (emitted after elastic interactions between the beam and the sample), provides information about surface features, and the backscattered electron (emitted after inelastic interactions between the beam and the sample) provides information about the atomic number of the samples. If the number of electrons that strike the sample surface and the number of electrons that are emitted from the sample surface are not same, the surface accumulates charges. This effect significantly affects the image resolution, and happens only with a non-conducting substrate, such as semiconductor and insulator. To prevent this issue, a very thin conducting layer can be deposited on the samples to avoid the charging effect. In conventional SEM, vacuum is created in the measurement chamber to reduce scattering and focus the electron beam on the samples, however, a vacuum environment is destructive for biological samples and wet samples. In ESEM (Environmental scanning electron microscopy), a small amount of water vapor is sprayed in the sample chamber. Water molecules present in the chamber interact with some of incident beam of electrons from the electron gun, secondary electrons and backscattered electrons from the sample and transforms into the positive ions. The secondary and backscattered electrons are collected in the detector by applying a positive bias to the detector. The positively charged ions are pushed towards the negatively charged sample to remove the charge buildup on the sample. In addition,

ESEM can analyze insulating and semiconducting samples directly, without depositing a thin conducting layer.[99, 100]

In this PhD study, we analyzed the surface morphology of the metal oxide films using field emission scanning electron microscopy (JEOL FEG-SEM) and the environmental scanning electron microscopy (Quattro, Thermo Fisher).

3.7.3 X-ray diffraction

Structural properties of the thin films are characterized using X-ray diffraction (XRD). During XRD measurements, the high energy X-rays (high energy electromagnetic radiation, with a low wavelength) are focused on the samples using an X-ray source. If the wavelength of the X-ray is equal to the distance between the atoms in the film, diffraction occurs. The diffraction signal is recorded and analyzed using a detector and then output into an X-ray diffraction pattern. The diffraction peaks are observed with respect to the crystal structure of the samples.[101]

In this PhD work, we characterized the crystal structure of the metal oxide films using X-ray diffractometer (Malvern PanAlytical Empyrean 3 and Bruker D8) with CuKα source, λ = 1.54178 Å.

3.7.4 Stylus Profilometry

The stylus profilometer is used to measure the thickness of the thin films. In this setup, the stylus tip is in contact with the surface of the sample. During the measurement, the stylus moves on the surface and is deflected with respect to the height of the sample. The deflected tip height is measured using sensors. The average surface height (between the thin-film side and the substrate side) is recorded with respect to the lateral position of the sample.

In this PhD work, we used the Dektak 150 (Veeco, USA) stylus profilometer (Tip radius: 12.5 µm, force: 10 mg) to measure the thickness of the metal oxide films.

3.7.5 Cyclic voltammetry

Cyclic voltammetry is a technique for analyzing the electrochemical redox properties of the sample. Generally, the measurement is in a 3-electrode configuration (working, counter and

reference electrode). The sample of interest is placed as a working electrode, a reference electrode is used to measure the potential difference between the changing potential at the working electrode and the constant potential of the reference electrode, measured using potentiostat. The counter electrode is placed to complete the circuit so that the current flows between working and counter electrode. This current is recorded with the potentiostat. All the electrodes are immersed in an electrolyte solution during the measurements. Cyclic voltammetry experiments can also work in two electrode configuration, adapted from the 3-electrode system, in which the counter electrode also acts as a reference electrode by maintaining constant potential. In cyclic voltammetry, the potential between the working and reference electrode is linearly scanned between the known potential window of the sample, in forward and reverse directions at a defined scan rate and for a desired number of cycles. During the forward and reverse scan, the electrochemically active material in the working electrode undergoes oxidation (loss of electrons) and reduction (gain of electrons). The processes are recorded as current versus voltage plot.[102, 103]

We carried out cyclic voltammetry in transistor configuration, in which the active channel material between source and drain operates as a working electrode, ion-gating medium as the electrolyte and the activated carbon on carbon paper as a counter and quasi-reference electrode. The activated carbon electrode is used as a quasi-reference electrode due to its high capacitance (specific capacitance ~ 100 F/g), and stable potential during cyclic voltammetry. Cyclic voltammetry is a common tool to understand the doping mechanisms, e.g. electrostatic or electrochemical, of IGTs. Also, the safe operation voltage of the transistor can be determined from the cyclic voltammogram.[60, 104]

In this work, we used versaSTAT4 (Princeton Applied Research) potentiostat to run the cyclic voltammetry of the active channel material in transistor configuration. The reference electrode lead and counter electrode lead of the potentiostat is short-circuited to connect the activated carbon gate electrode. The source and drain terminal of the device is short circuited to connect the working electrode lead of the potentiostat.

3.8 Device characterization

3.8.1 Electrical characteristics

IGTs contains three terminals namely source, drain and gate. The electrical conductivity of the semiconductor between source and drain is modulated by applying voltage to the gate electrode. In IGTs, the ion-gating medium is present between the gate electrode and the semiconductor. The drain and gate voltage are applied in IGTs with respect to the source voltage. The source terminal is grounded (V_s = 0 V) during the transistor measurement. When the gate voltage is applied in IGTs, the polarity of the voltage controls the type of ions in the ion-gating medium, and the magnitude of voltage controls the density of ions in the ion-gating medium. If a density of ions accumulates, it enhances or depletes the electronic charges in the semiconductor. The voltage between source and drain electrodes allows the electronic charges to move in the semiconductor channel. The drain electrode is extracting the electronic charges from the semiconductor and the source electrode replenishes electronic charges in the semiconductor. Contact resistance is not a key issue in ion-gated transistors, since the formation of electrical double layers at metal/semiconductor interfaces, due to the presence of the ionic gating medium, is expected to facilitate charge carrier injection.[105]

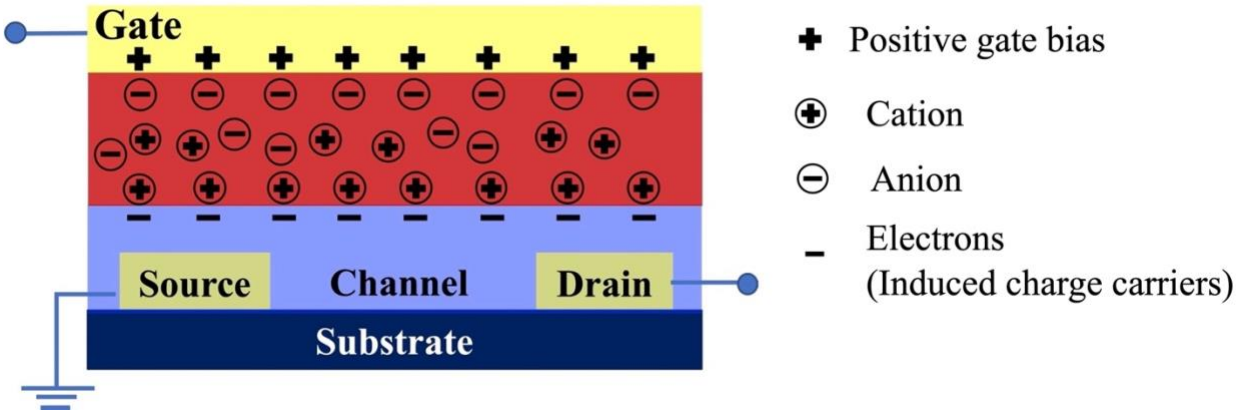

Figure 3-5 Schematic representation of n-type IGTs under positive bias.

We have studied n-type channel materials in this PhD work. The positive voltages were applied to the gate and drain electrodes. When the gate voltage is positively biased, the positive ions pile up in the semiconductor and negative ions at the gate electrode. The accumulation of

positive ions in the semiconductor will increase the electronic charge carriers (electrons) in the semiconductor (Figure 3-5). The ionic-electronic modulation leads to a change of channel conductivity, which in turn modulates the source and drain current. The accumulation of sub-nanometer dimensions of ions at the gate and semiconductor causes a strong electric field at the semiconductor/electrolyte and gate electrode/electrolyte interface, enabling low voltage operation due to increased capacitance.[69] Transistor characteristics of IGTs are measured using a semiconductor parameter analyzer equipped with a micromanipulator. Output and transfer characteristics are measured for the IGTs, all performed below 2 V. For the output characteristics, the drain-source voltage is swept at a defined scan rate, while keeping the gate-source voltage constant. For the transfer characteristics, the gate-source voltage is swept at a defined scan rate while keeping the drain source voltage constant. In both characteristics, drain-source current and gate-source current are recorded. During all measurements, the parameter analyzer (Keysight B1500A) is controlled using the EasyEXPERT software. The reported figures of merit of the transistors in this thesis are the average of three devices.

CHAPTER 4 ARTICLE 1: ION-GATED TRANSISTORS BASED ON POROUS AND COMPACT TiO_2 FILMS: EFFECT OF Li IONS IN THE GATING MEDIUM

Arunprabaharan Subramanian[1], Ben George[1], Sanyasi Rao Bobbara[1], Irina Valitova[1], Irene Ruggeri[1,2], Francesca Borghi[3], Alessandro Podestà[3], Paolo Milani[3], Francesca Soavi[2], Clara Santato[4] and Fabio Cicoira[1*]

[1] Department of Chemical Engineering, Polytechnique Montréal, H3T 1J4, Canada.

[2] Dipartimento di Chimica "Giacomo Ciamician", Università di Bologna, Via Selmi 2, Bologna, 40126, Italy.

[3] CIMaINa and Dipartimento di Fisica "Aldo Pontremoli", Università degli Studi di Milano, via Celoria 16, Milano, 20133, Italy.

[4] Department of Engineering Physics, Polytechnique Montréal, H3T 1J4, Canada.

Has been published in AIP Advances

* Corresponding author: fabio.cicoira@polymtl.ca

KEYWORDS: Ion-gated transistors, Metal oxides, Titanium dioxide, Ionic liquids, Thin films

4.1 Abstract

Ion-gated transistors (IGTs) are attractive for chemo- and bio-sensing, wearable electronics and bioelectronics, because of their ability to act as ion/electron converters and their low operating voltage (e.g. below 1 V). Metal oxides are of special interest as transistor channel materials in IGTs due to their high mobility, chemical stability, and ease of processing in air at relatively low temperatures (< 350˚C). Titanium dioxide is an abundant material that can be used as a channel material in *n*-type IGTs. In this work, we investigated the role of the morphology of the TiO_2 channel (porous versus compact films) and the size of the cations in the gating media ([EMIM][TFSI] and [Li][TFSI] dissolved in [EMIM][TFSI]) to obtain the electrical characteristics of IGTs. We found that both the film morphology and the type of gating medium highly affect the electrical response of the devices.

4.2 Introduction

Metal oxide semiconductors are exploited in a variety of applications, such as sensing, energy conversion and storage, and display technologies.[26, 106-108] They are widely studied as active channel materials for thin-film transistors (TFTs) and ion-gated transistors (IGTs) due to their abundance, chemical stability, transparency, and ease of processing at low temperatures in ambient conditions.[109, 110] Amorphous indium-gallium-zinc-oxide (a-IGZO) is currently used in *n*-type TFT backplanes of flat panel and organic light-emitting diode (OLED) displays, due to its high electrical conductivity, film uniformity, transparency, as well as mechanical and chemical stability.[12, 107, 111-114] Indium-based oxides also show excellent performance as channel material for IGTs (charge carrier mobility up to ~ 120 $cm^2\ V^{-1}s^{-1}$).[115] However, as the availability of indium in the Earth's crust is limited, there is an increasing interest in indium-free metal oxides, such as ZnO, SnO_2, Cu_xO, NiO, and TiO_2, both for TFTs and IGTs.[49, 52, 53, 60, 72, 109, 116-126] Among indium-free metal oxides, TiO_2 (*n*-type) is sought for its availability, cost-effective processability, high chemical stability, and biocompatibility.[127, 128] Our groups reported on TiO_2-based IGTs using 1-ethyl-3-methylimidazolium bis(trifluoromethylsulfonyl)imide ([EMIM][TFSI]) as the gating medium and found that patterning of the channel leads to enhanced transistor performance.[52]

IGTs use ion-gating media, such as aqueous saline solutions, polymer electrolytes, ionic liquids, and ion gels. A high specific capacitance (ca. 10-100 $\mu F/cm^2$), which permits operation at low voltages (< 2V), is achieved by the formation of a thin electrical double layer at the semiconductor/gating medium interface. Besides pure electrostatic or electrochemical doping, different mechanisms have been considered to describe the operation of IGTs, such as interface confined electrochemical doping. [58-60, 110, 129-133]

In this work, we explored IGTs based on TiO_2 active layers deposited using thermal evaporation, to produce compact films, and solution casting to produce porous films. Transistors based on compact films show electron mobilities about two orders of magnitude higher than those based on porous ones. In order to gain further insight into the doping mechanism, we employed two gating media: [EMIM][TFSI] and lithium bis(trifluoromethanesulfonyl)imide ([Li][TFSI]) dissolved in [EMIM][TFSI]. The characteristics of transistors based on compact and porous films both depend on the gating media, which points to different working mechanisms. While $[EMIM]^+$ ions (ionic

radius ~ 3.5 Å) are expected to dope TiO_2 by electrostatic and interface-confined electrochemical doping, [52] $[Li]^+$ ions, having a small radius (~ 0.7 Å), are expected to dope TiO_2 electrochemically via lattice intercalation.[134-136]

4.3 Experimental

E-beam evaporation was carried out at a deposition rate of 0.7 Å/s and a pressure of 3×10^{-5} Torr using a Thermionics e-beam evaporator. Solution processed TiO_2 films were obtained by drop casting a suspension containing 2 g of TiO_2 (a mixture of rutile and anatase in xylene, MilliporeSigma, #700339) and 0.4 g of polyvinylidene fluoride (PVDF, MilliporeSigma) binder in 20 ml of dimethylformamide (DMF, Caledon Laboratory Chemicals, purity 98.5%). The suspension was mixed in a planetary mixer (Thinky ARM-310) for 30 minutes at 2000 rpm and then filtered through a 0.2 µm nylon filter. Finally, it was drop casted on the substrates, which were first heated at 60°C for 30 minutes to remove excess solvent, and subsequently annealed at 450°C in a tube furnace for 1 hour in ambient air.[52] The thickness of the films, measured using a profilometer (Dektak 150), were ~ 60 nm for evaporated films and ~ 3 µm for drop-casted films. A high thickness was required for the drop-casted films in order to achieve a complete coverage of the portion of the substrate containing the devices (Figure S1).

Scanning electron microscopy (SEM) was performed using a JEOL FEG-SEM, JSM 7600F. X-ray diffraction (XRD) was performed with a Bruker D8 diffractometer using a (CuKα) beam, at every $2\theta = 0.01$. Atomic Force Microscopy (AFM) was performed by a Multimode Nanoscope (Bruker) in tapping mode, in air, using Bruker NCHV probes, with resonance frequency between 270 and 400 KHz, k=40 N/m and nominal tip radius 8 nm.

Ion-gated transistors were fabricated according to a procedure described in previous publications. [52, 121] The TiO_2 films were deposited, as described above, on SiO_2/Si substrates pre-patterned with Ti/Au (5nm/40nm) source-drain electrodes (W/L=4000µm/10µm) by vacuum sublimation and drop casting. As gating media, we used 1-ethyl-3-methylimidazolium bis(trifluoromethylsulfonyl)imide [EMIM][TFSI] (IoLiTec GmbH) and a mixture of 10 mL [EMIM][TFSI] and 0.86 g [Li][TFSI] (MilliporeSigma), both saturating a Durapore® PVDF 0.22 µm membrane. Activated carbon (PICACTIF SUPERCAP BP10) on carbon paper (Spectracarb 2050) was used as the gate electrode. The high surface area (~1000–2000 $m^2\ g^{-1}$) of this electrode

is amenable to high current modulation, while its inertness towards undesired electrochemical reactions is advantageous for device stability.[52, 104]

Transistor characteristics were measured in a N_2-purged glove box (O_2 and H_2O <3 ppm) with a semiconductor parameter analyzer (Agilent B1500A). We prepared four types of transistors, based on evaporated and solution-processed TiO_2 channels and two different gating media, i.e. [EMIM][TFSI] and 0.3 M [Li][TFSI] in [EMIM][TFSI]. The transistor characterization was performed at a sweep rate of 50 mV/s. Cyclic voltammetry was performed using a Princeton Applied Research VERSASTAT 4 potentiostat (See Figure S2 for the device configuration during cyclic voltammetry). Device characterization was performed in the following order: cyclic voltammetry (three cycles were performed, the third cycle is reported), output characteristics, transfer characteristics in linear regime (three cycles were performed, the second cycle is reported), transfer characteristics in saturation regime (three cycles were performed, the second cycle is reported).

4.4 Results and Discussion

SEM and AFM images reveal that evaporated films are compact, with a root mean square (RMS) roughness of 1.0 ± 0.1 nm (Figure 4-1 a and Figure S3a and b), while solution-processed ones are porous with a RMS roughness of 117 ± 5 nm (Figure 4-1 b and Figure S3c and d). According to XRD patterns, TiO_2 evaporated films primarily consist of the anatase phase (Figure 4-1 c), while solution-processed ones consist of a mixture of anatase and rutile phases (Figure 4-1 d).[52]

Figure 4-2 shows the output and transfer characteristics of evaporated TiO_2 transistors gated with [EMIM][TFSI] (Figure 4-2 a-c) and [Li][TFSI]+[EMIM][TFSI] (Figure 4-2d-f). All the devices show *n*-type behavior and function below 1.5 V. Gating with [Li][TFSI]+[EMIM][TFSI] produces an increase in the transistor current of about a factor of 2. The transfer curves (Figure 4-2 b and Figure 4-2 e) show hysteresis, indicating slow ion transport in TiO_2 films both during doping (forward scan) and dedoping (backward scan) (See Figure S4 for the hysteresis loop area calculation and Table S1 for the values of hysteresis loop area of evaporated TiO_2 IGTs).[60, 137] The threshold voltages, extracted from the linear transfer characteristics, are in the range of 0.4 V-0.5 V for both gating media (Table S2). The saturation (V_{ds} = 1 V) transfer characteristics (Figure 4-2 c and Figure 4-2 f) show that the ON/OFF ratios are rather low (Table S2), due to high OFF currents

(about 10^{-4}-10^{-3} A), which might be attributed to the higher intrinsic conductivity of evaporated TiO_2 films.

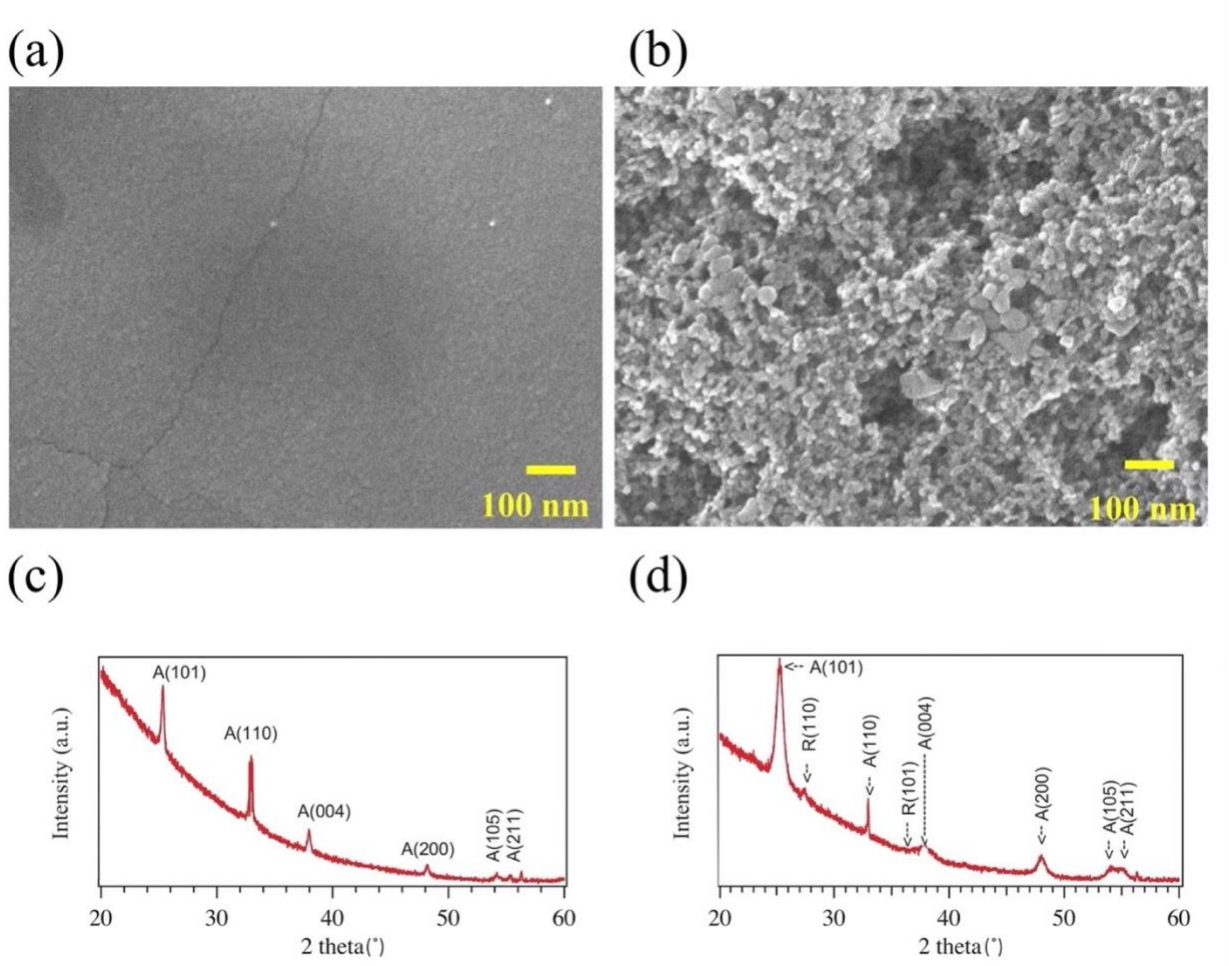

Figure 4-1 SEM images of (a) evaporated and (b) solution-processed TiO_2 films. XRD patterns of (c) evaporated and (d) solution-processed TiO_2 films. A and R indicate the peaks of the anatase (Joint committee on powder diffraction standards (JCPDS) card number: 01-089-4203) and rutile (JCPDS card number: 01-083-2242) phases of TiO_2. Figure 4-1 (d) is reproduced with permission from ACS Appl. Mater. Interfaces 8, 23 (2016). Copyright 2016 American Chemical Society.[52]

Figure 4-3 shows the output and transfer characteristics of solution-processed TiO_2 IGTs using [EMIM][TFSI] (Figure 4-3 a-c) and [Li][TFSI]+[EMIM][TFSI] (Figure 4-3 d-f), acquired at a sweep rate of 50 mV/s. Solution-processed TiO_2 IGTs show a lower drain current than the evaporated ones. Both output and transfer characteristics (Figure 4-3) show that gating with [Li][TFSI]+[EMIM][TFSI] dramatically affects transistor characteristics, producing an increase in

the transistor saturation current of about a factor of 20. The drain current saturation is clearly observed for solution processed devices. Transfer characteristics in the linear regime (Figure 4-3 b and e) show hysteresis for both gating media. The areas of the hysteresis loops in [EMIM][TFSI] gated devices are smaller than those of [Li][TFSI]+[EMIM][TFSI] gated devices, due to the lower drain current and the higher threshold voltage, especially for solution processed devices (Table S3). The areas of the hysteresis loops in evaporated devices are not affected by the gating media, and their values are similar to the [Li][TFSI]+[EMIM][TFSI] gated solution-processed devices (Table S1 and Table S3). The threshold voltages extracted from the linear transfer characteristics were 1.3 V for devices gated with [EMIM][TFSI] and 0.9 V for those gated with [Li] [TFSI] + [EMIM] [TFSI] (Table S4).

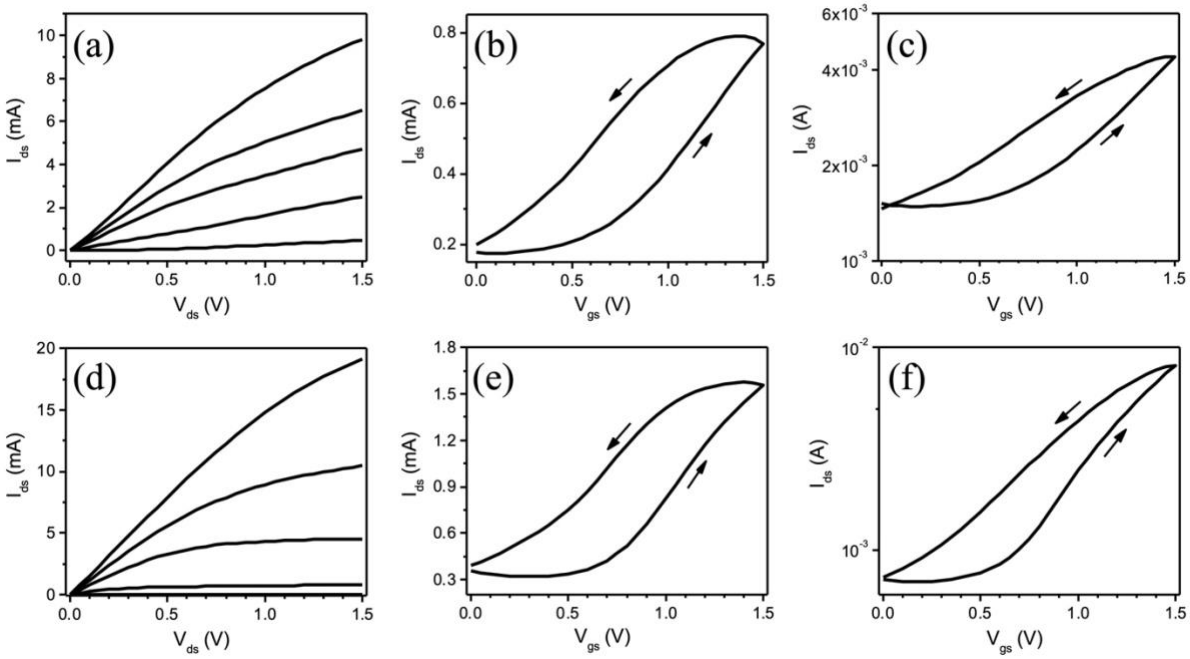

Figure 4-2: Output and transfer characteristics in the linear and saturation regime of transistors based on evaporated TiO_2 films (~ 60 nm thick) gated with [EMIM][TFSI] (a-c), and [Li][TFSI]+[EMIM][TFSI] (d-f) measured with a sweep rate of 50 mV/s. The output characteristics were acquired at V_{gs} = 0, 1, 1.2, 1.3, 1.5 V (a, d) and the transfer characteristics at $V_{ds,\,lin}$ = 100 mV (b, e) and at $V_{ds,\,sat}$ = 1 V (c, f). The transfer characteristics in the saturation (c, f) regime are represented on a logarithmic drain-source current scale.

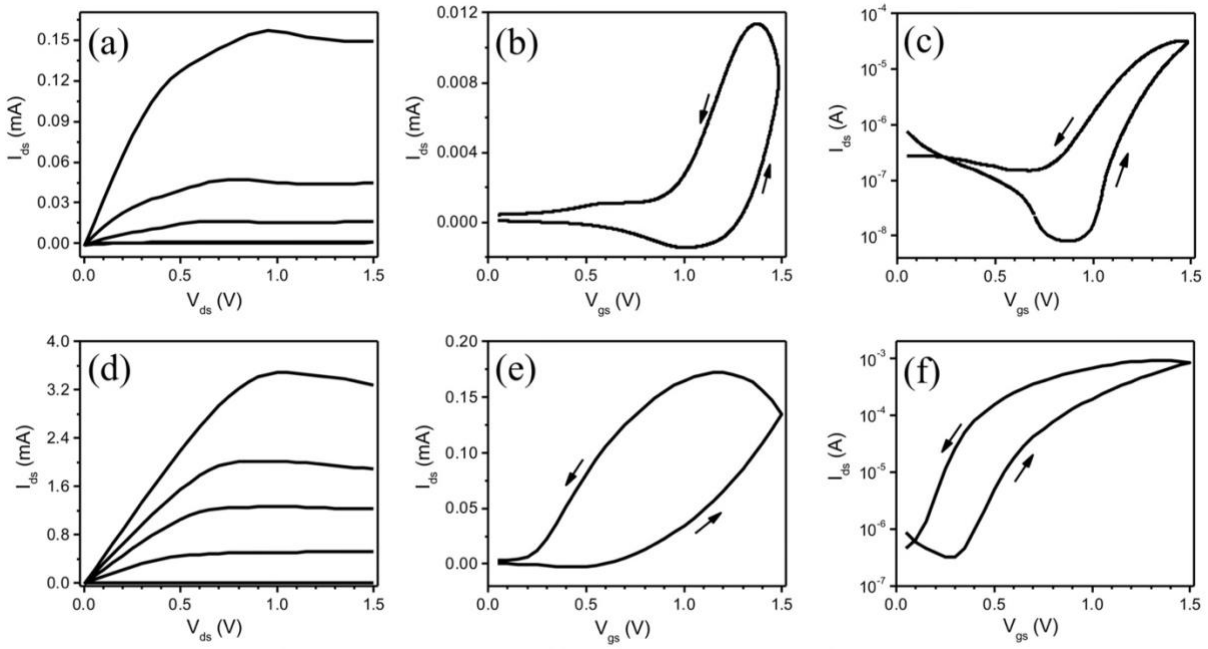

Figure 4-3 Output and transfer characteristics in the linear and saturation regime of transistors based on solution-processed TiO_2 films (~ 3µm thick) gated with [EMIM][TFSI] (a-c), and [Li][TFSI]+[EMIM][TFSI] (d-f) measured with a sweep rate of 50 mV/s. The output characteristics were acquired at V_{gs} = 0, 1, 1.2, 1.3, 1.5 V (a, d) and the transfer characteristics at $V_{ds,\ linear}$ = 100 mV (b, e) and at $V_{ds,\ saturation}$ = 1V (c, f). The transfer characteristics in the saturation (c, f) regime are represented on a logarithmic drain-source current scale.

The ON/OFF ratios, extracted from the saturation regime of transfer characteristics (Figure 4-3 c and Figure 4-3 f), were 40 for the devices gated with [EMIM] [TFSI] and 10^3 for the devices gated with [Li] [TFSI] + [EMIM] [TFSI] (Table S4).

The effect of the gating medium on the transistor current can be explained by a change of doping mechanism: while the large $[EMIM]^+$ ions likely lead to a combination of electrostatic and interface-confined electrochemical doping, [52, 60] the smaller $[Li]^+$ ions ($r_{EMIM}{}^+/r_{Li}{}^+ \sim 5$) might lead to electrochemical doping via intercalation of Li^+ ions in the TiO_2 lattice. [134, 135] The number of Li intercalation events is favored by the porous morphology of the solution processed films, which explains the much larger difference in saturation current and ON/OFF ratio with respect to $[EMIM]^+$ gating. Moreover, the small size of Li^+ ions (~ 0.7 Å)[38] also facilitates a higher packing

density at the gating media/TiO_2 interface, which might lead to more efficient electrostatic and interface-confined electrochemical doping.

The charge carrier mobility was extracted from the transfer characteristics in the linear regime according to the formula, $\mu_{lin} = \frac{L\, I_{d,lin}}{W\, e\, n\, V_d}$, where L indicates the interelectrode distance (10 µm), W the electrode width (4000 µm), V_d the drain-source voltage (0.1 V), n the charge carrier density, e the elementary charge (1.6×10^{-19} C) and $I_{d,lin}$ the drain-source current at 1.5 V. [52] The charge carrier density is calculated from the linear transfer characteristics, using the formula $n = \frac{Q}{eA} = \frac{\int I_g dV_g}{r_v eA}$ where Q is the doping charge, I_g is the gate-source current in the forward scan (Figure 4-2 b, e and Figure 4-3 b, e), r_v is the sweep rate of the gate voltage, and A is the surface area of the semiconductor in contact with the membrane soaked with the gating media (in our case 0.36±0.04 cm^2).[52] For porous films, we also calculated the mobility using the surface area of the same region measured from Brunauer-Emmett-Teller (BET) analysis (see Supporting Information). [52, 137] The calculated charge carrier densities and mobilities are summarized in Tables S4 and S5. For evaporated TiO_2 IGTs, a charge carrier mobility of ~ 0.5 cm^2/Vs was extracted for both gating media (Table S2). The obtained mobility value is comparable with values reported in previous articles based on metal oxide TFTs and IGTs.[52, 72, 120, 124, 126, 138-141] Solution-processed TiO_2 IGTs showed a lower mobility, with a significant dependence on the gating media. For devices gated with [EMIM][TFSI], we obtained charge carrier density of $\sim 2 \times 10^{15}$ cm^{-2} leading to charge carrier mobility of 5×10^{-4} $cm^2\, V^{-1}s^{-1}$, while for those gated with [Li][TFSI]+[EMIM][TFSI], we obtained charge carrier density of $\sim 6 \times 10^{15}$ cm^{-2} leading to charge carrier mobility of $\sim 4 \times 10^{-3}$ $cm^2\, V^{-1}s^{-1}$. Solution-processed devices show a large spread in the charge carrier density and mobility values, likely due to the less reproducible film deposition technique.[142]

Figure 4-4 shows the cyclic voltammetry (CV) of the evaporated and solution-processed TiO_2 based IGTs with [EMIM][TFSI] and [Li][TFSI]+[EMIM][TFSI], performed in a two-electrode configuration, with the TiO_2 channel acting as the working electrode and the activated carbon gate (specific capacitance of ~ 100 F/g) acting simultaneously as the counter and quasi-reference electrode.[104]

The currents obtained with solution-processed TiO_2 are higher than those measured with evaporated TiO_2 films due to the higher thickness. The cyclic voltammetries show wide cathodic

and anodic waves related to the reversible reduction-oxidation process of TiO_2. The cathodic signal represents the n-doping of TiO_2 and the anodic one represents the dedoping process. For evaporated films, redox processes are evident below -0.7 V for both gating media (Figure 4-4 a and b). The CVs also indicate an irreversible cathodic process occurring below -1.3 V, which is more evident for [Li][TFSI]+[EMIM][TFSI] gating. For solution-processed TiO_2, the absence of defined peaks is indicative of pseudocapacitive behavior at potentials lower than -0.7 V for devices gated with [EMIM][TFSI] (Figure 4-4 c) and lower than -0.5 V for devices gated with [Li][TFSI]+[EMIM][TFSI] (Figure 4-4 d).[52] In the case of solution-processed TiO_2 gated with [Li][TFSI]+[EMIM][TFSI], additional cathodic and anodic peaks are observed at -0.6 V and -0.25 V (Figure 4-4 d).

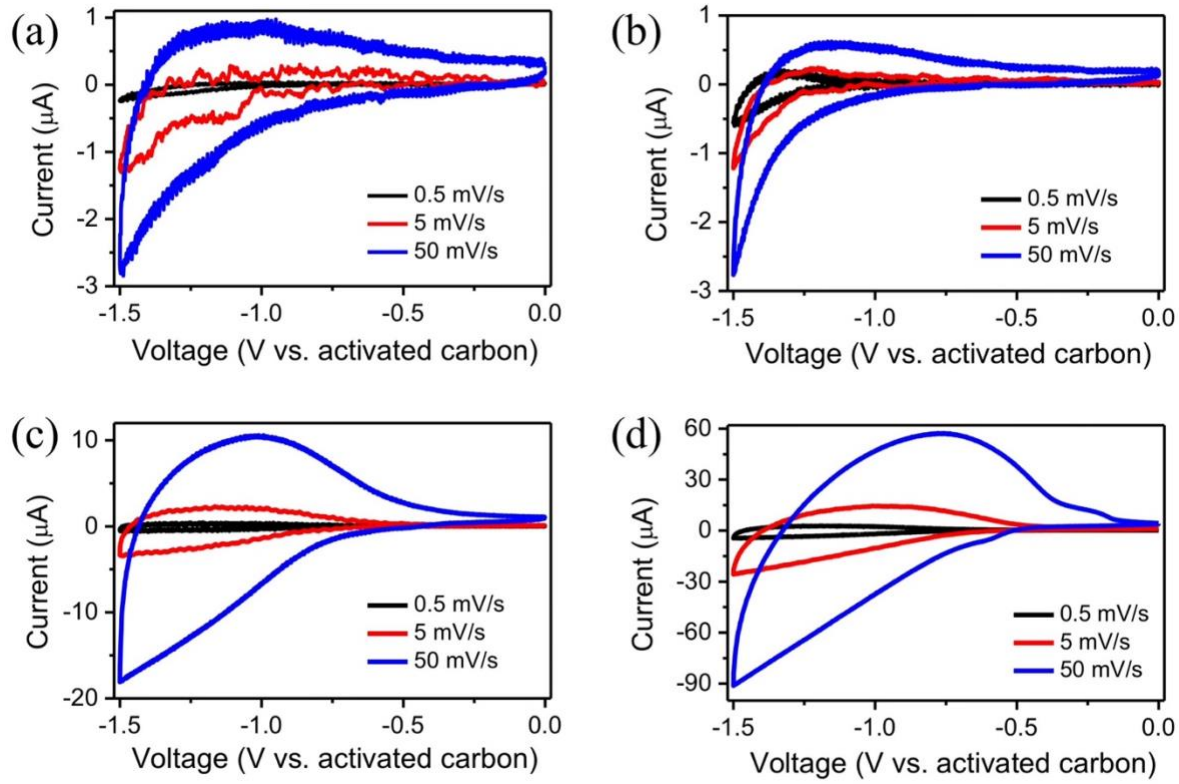

Figure 4-4 Cyclic voltammetry of transistors based on evaporated TiO_2 films gated with [EMIM][TFSI] (a) and [Li][TFSI]+[EMIM][TFSI] (b), and solution processed TiO_2 films gated with [EMIM][TFSI] (c) and [Li][TFSI]+[EMIM][TFSI] (d), at 0.5 mV/s, 5 mV/s, and 50 mV/s respectively.

From the area encompassed by the CV loop, it can be discerned that the solution-processed TiO_2 based IGTs (Figure 4-4 c and d) have higher charge storage capacity than their evaporated TiO_2 counterparts (Figure 4-4 a and b). Pseudocapacitance values of all the devices, calculated by the slope of doping charge *vs.* voltage plots, are summarized in Table S6 and S7 (for porous solution-processed TiO_2 films, we also included values calculated using the BET surface area). The porous films have higher pseudocapacitance than do compact films; hence, the former can store more charge. All devices show a high pseudocapacitance at low sweep rates. $[Li]^+$ based gating media lead to a higher pseudocapacitance than do the pure $[EMIM]^+$ based gating media.

4.5 Conclusions

In summary, we investigated the electrical and electrochemical properties of *n*-type IGTs based on evaporated (predominantly anatase) and solution-processed (mixture of rutile and anatase) polycrystalline TiO_2 films as channel materials, doped by [EMIM][TFSI] and [Li][TFSI] dissolved in [EMIM][TFSI].[143] The transistor characteristics of evaporated films are not significantly affected by the presence of Li^+ in the gating medium. For solution-processed films, the presence of Li^+ in the gating medium leads to a significant increase of the electron mobility. We hypothesize that the presence of Li^+ facilitates charge transport at grain boundaries in the solution processed films. The evaporated TiO_2 films show a higher mobility of 0.5 $cm^2V^{-1}s^{-1}$ compared to solution-processed films. The charge carrier density is not dramatically affected by the presence of Li^+ in [EMIM][TSFI], as we could have expected considering the different ion size (~ 0.7 Å for Li^+ vs 3.5 Å for [EMIM]). This points to the complex arrangements of the ions in the electrical double layer, responsible for the doping of the transistor channel. Work is in progress to shed light on such complexity (originated from the number of ionic interactions, from electrostatic to van der Waals) by Atomic Force Microscopy Force-Distance profiling performed in highly viscous ionic liquids.[144]

4.6 Acknowledgments

The authors are grateful to Yves Drolet for technical assistance. Funding for this project was provided by NSERC (Discovery grants, F. C. and C. S.) and the Québec Ministry of Economy Science and Innovation (project PSR-SIIRI-810). I.V. and A.S. are grateful to FRQNT for financial

support through a doctoral scholarship, A.S. is grateful to the Trottier Energy Institute for a doctoral scholarship and B.G. is grateful to FRQNT for a Master's scholarship. F.S. acknowledges financial support from Alma Mater Studiorum Università di Bologna (Researcher Mobility Program, Italian-Canadian cooperation agreement). This work is supported by CMC Microsystems through the MNT program. This work also benefited from the financial support of FRQNT through a grant awarded to RQMP.

Supplementary Material

See supplementary material for: Schematic representation of the coverage of TiO_2 film on the substrate, device configuration during the electrical and electrochemical characterizations, AFM images of the TiO_2 films, explanation of the hysteresis loop area calculations, values of hysteresis loop area, charge carrier density, mobility, ON/OFF ratio, threshold voltage of IGTs, and the pseudocapacitance values of the TiO_2 films.

CHAPTER 5 ARTICLE 2: COMBINING AQUEOUS SOLUTION PROCESSING AND PRINTING FOR FABRICATION OF FLEXIBLE AND SUSTAINABLE TIN DIOXIDE ION-GATED TRANSISTORS

We report flexible ion-gated transistors based on crystalline SnO2 nanorods deposited via a sustainable aqueous growth technique (~ 95 ˚C) on polyethylene terephthalate (PET). The devices operate at low voltage (ca. 1 V) using either an ionic liquid or an aqueous electrolyte as the ion gating medium. Top contact electrodes are patterned via photolithography or printing.

Arunprabaharan Subramanian,[1] Mona Azimi,[1] Clara Santato,[2] and Fabio Cicoira[1*]

[1] Department of Chemical Engineering, Polytechnique Montréal, H3T 1J4, Montreal, Canada.

[2] Department of Engineering Physics, Polytechnique Montréal, H3T 1J4, Montreal, Canada.

Has been published : Advanced Materials Technologies

* Corresponding author: fabio.cicoira@polymtl.ca

5.1 Abstract

Ion-gated transistors (IGTs) are extensively used in chemo- and bio-sensors as well as intelligent sensors, i.e., with neuromorphic computing functionality exploiting their ion to electron convertibility. Metal oxides are attractive as active channel materials in IGTs because of their low-temperature solution processability, ambient stability and tunable optoelectronic properties. SnO_2 is a low-cost material widely used in thin-film transistors, gas sensors and transparent electrodes. In this work, we prepared films of crystalline SnO_2 nanorods on flexible substrates using a controlled aqueous growth technique, at 95 ˚C. The top contact source and drain metal contacts were patterned by either photolithography or printing. We studied the transistor behaviour of SnO_2 nanorod films gated with different gating media, such as room-temperature ionic liquids, in inert atmosphere, and aqueous saline solutions, in ambient air. In addition, we studied the transistor

behaviour of SnO_2 IGTs in the original flat and tensile bending state. The earth abundancy of tin oxide, the low energy consumption fabrication process by low-temperature solution processing and printing as well as the use of an aqueous electrolyte for the gating medium make our devices extremely promising for green and sustainable electronics.

5.2 Introduction

Metal oxide semiconductors are widely used in transparent conducting electrodes, solar cells, batteries, sensors, flexible display technologies and thin film transistors, due to their tunable physicochemical and optoelectronic properties.[5, 25, 145-147] The metal oxide indium gallium zinc oxide (IGZO), are already commercialized for flat panel display backplanes.[3, 5, 148] However, given the scarcity of indium in the earth's crust, it is critical to develop sustainable indium-free metal oxide semiconductors.[16] Several earth-abundant metal oxides such as ZnO, TiO_2 and SnO_2 have been used as active layers in thin film transistors.[25, 145] Typically, to obtain high-performance crystalline films, these oxides are processed at high temperatures (> 350 ˚C), which are not compatible with flexible electronics.[25, 149-151] Additionally, the brittle nature of crystalline metal oxides limits their applications in flexible electronics.[149]

SnO_2 is a promising metal oxide for electronics applications due to its abundancy, electrical conductivity and optical transparency, which make it interesting for thin-film transistors, gas sensors and transparent electrodes. [152-155] SnO_2 films can be processed via several techniques, such as sputtering, evaporation, pulsed laser deposition and various solution processing methods.[156] Among these, a single step, low temperature process in aqueous solution would meet the requirements for sustainable and cost-effective flexible electronics.[25, 90, 157]

Field effect transistors (FETs) based on SnO_2 films, deposited using physical and chemical methods, exhibited a high field-effect mobility (> 100 cm^2/Vs) at an operating voltage below 5 V.[38-42] Sb-doped SnO_2 showed a mobility of ~ 550 cm^2/Vs, when the material was deposited by vapor-liquid-solid growth, [41] and ~ 158 cm^2/Vs, when radio frequency magnetron sputtering was used.[42] The high mobility of SnO_2 is due to the large overlap of the spherical Sn 5s orbitals in the SnO_2 electronic structure.[38, 158, 159]

The charge carrier density (electrons) in SnO_2 can be tuned by creating oxygen vacancies (i.e. deviation of SnO_2 stoichiometry), by unintentional (i.e impurities during the growth of SnO_2) and intentional doping (i.e. metallic dopants such as Ta, Sb on SnO_2). [160, 161] By tuning the charge carrier density, the transistor mode of operation can be switched from enhancement to depletion mode. Ohta et al., fabricated FETs based SnO_2 films grown by pulsed laser deposition (400 ˚C) and investigated the electron transport properties at different thicknesses. The film thickness was found to affect the crystallinity and charge carrier concentration, as well as the performance and operation mode of the transistors. [43, 44]

Jang et al., deposited SnO_2 films by UV-ozone assisted sol-gel (300 ˚C), which were used as active layers in FETs on flexible polyimide substrates.[162] Lim et al., fabricated flexible SnO_2 FETs on polyethersulfone substrate by direct current reactive magnetron sputtering at room temperature, which did not show significant change in electrical characteristics under tensile (inward) and compressive (outward) bending.[45] Shin et al., prepared SnO_2 nanowires by chemical vapor deposition at 750 ˚C and transferred them to a stretchable substrate (i.e., poly dimethyl siloxane) by sliding transfer at room temperature. FETs based on these nanowires could withstand 40 % strain without any noticeable change in their electrical characteristics.[163] Liu et al., fabricated SnO_2 nanowires by vapor-liquid-solid growth at 900 ˚C, transferred them to a paper substrate at room temperature, and demonstrated successful FETs operation at low voltages (~ 1 V). [164]

Metal oxide ion gated transistors (IGTs) employ semiconducting metal oxides as the active channel materials, and ionic liquids, ion-gels or aqueous solutions as the ion-gating medium.[64, 76, 88, 115, 165-168] IGTs using aqueous media can be used for environmental monitoring, chemical and biological sensing and physiological monitoring. Deionized water can be used as an ion-gating medium, due to its self-ionization into equimolar concentrations of protons and hydroxyl ions (10^{-7} mol/L of H^+ and 10^{-7} mol/L of OH^-),[169, 170] and to the presence of ions resulting from atmospheric CO_2 dissolution.[171] Low voltage operation is enabled in IGTs due to the high capacitance of the electrical double layer formed at the interface of the oxide semiconductor and ion-gating medium.[121] The operating mechanism of IGTs relies on electrostatic (surface doping) and electrochemical doping (volumetric doping) and depends on the permeability of the semiconductor versus the mobile ions present in the gating medium.[59] Grell et al. used spray pyrolyzed SnO_2 films (processing temperature of 400 ˚C) as active layers in IGTs gated by aqueous electrolytes, which

were used for the detection of Cs^{+},[172] Pb^{2+},[86] Cu^{2+},[86] F^{-}[173] and benzyl alcohol[174] in potable water, with limits of detection ranging from µM to pM. Wei et al. fabricated SnO_2 films by solution-processing method with a processing temperature of 150 ˚C and demonstrated a flexible synaptic transistor with 40 % retention of its initial postsynaptic current value after 10000 bending cycles.[46] Our research group fabricated solution-processed SnO_2 films with a processing temperature of 350 ˚C and demonstrated ionic liquid-based IGTs on flexible substrates, which were stable up to a moderate bending.[121]

In this work we synthesized SnO_2 films on thin, flexible polyethylene terephthalate (PET) substrates using an environmentally sustainable aqueous growth at the maximum processing temperature of 95 ˚C. The controlled aqueous growth is a suitable technique to deposit SnO_2 nanorods on crystalline or amorphous substrates using an acidic growth solution at low temperatures (95 ˚C). We fabricated IGTs based on such films by patterning top contact source-drain electrodes both by photolithography (Au) and printing (Ag). The bottom-contact configuration was not compatible with the SnO_2 growth method used in this experiment, as prepatterned electrodes peeled off during the growth of SnO_2 due to the high acidity of the solution (pH~ 0.5). The transistors were operated at low voltage (~ 1 V) using as ion gating medium an ionic liquid in inert atmosphere and an aqueous saline solution in ambient air. We demonstrated that the performance of SnO_2 IGTs on PET does not show significant variation under bending. Our devices, based on earth abundant and low-cost materials processed on lightweight substrates at low temperature, pave the way to a simple and innovative approach towards sustainable electronics.

5.3 Experimental

5.3.1 Materials

Tin chloride pentahydrate, urea, fuming HCl, sodium chloride crystals, activated carbon (Norit, chemically activated), polyvinylidene fluoride (PVDF), N-methyl pyrrolidone, Nafion and hydrophobic PVDF membrane filters (125 µm thick, pore size ~ 220 nm) were purchased from Millipore Sigma. Hydrophilic biodegradable cellulose filters (220 µm thick, pore size ~ 20 µm) were purchased from Whatman plc. PET sheets (Antistatic coating on both sides, thickness ~ 175 µm) were purchased from Policrom Inc., USA. Soda-lime glass slides (Corning 2947, plain micro

slides, thickness ~ 1mm) were purchased from Corning, USA. Silicone elastomer kit (SYLGARD 184) with elastomer base and curing agent was purchased from Dow Corning Corporation, USA. Ionic liquid, 1-ethyl-3-methylimidazolium bis(trifluoromethylsulfonyl)imide ([EMIM][TFSI]) was purchased from IoLiTec-Ionic Liquids Technologies GmbH, Germany. Carbon paper (Spectracarb 2050A) was purchased from Fuel Cell Store, USA. The conductive silver ink (metallic silver, ethyl diglycol acetate, and mineral salts) was purchased from Voltera Inc., Canada.

5.3.2 Device Fabrication

The glass and PET substrates (~10 cm^2) were ultrasonically cleaned using sequential baths of 1 M HCl aqueous solution, ethanol, acetone and DI water followed by UV-Ozone exposure for 15 minutes. The cleaned substrates were placed in a glass bottle (DURAN GL-45) with an autoclavable polypropylene screw cap containing 100 mL aqueous solution of 5 mL fuming HCl, 0.97 mM tin chloride pentahydrate and 150 mM urea, and heated at 95 ˚C for 2 days.[90] The arrays of SnO_2 nanorods were obtained on both glass and PET substrates. After the deposition, the substrates were washed with deionized (DI) water to remove salt residues and dried using a N_2 gun. In order to study the effect of Sn precursor concentration on morphology, crystallinity, and optical properties of resulting films, we carried out the growth process at the tin chloride pentahydrate concentrations of 0.48 mM, 1.94 mM and 2.91 mM, while keeping all other parameters constant.

A top-gate top-contact configuration was employed for the fabrication of ion-gated transistors. We patterned top contact source and drain electrodes on SnO_2 by photolithography (Au) and printing (Ag). The Ti/Au (5nm/40 nm) source and drain electrodes (W/L = 4000 μm/10 μm) on SnO_2 (on glass and PET) were patterned using photolithography followed by electron-beam evaporation, and a lift-off process. Initially, a positive tone photoresist (AZ MIR 900) was spin-coated on SnO_2 and then exposed to UV radiation (i-line, i.e. 365 nm) through a photomask using a mask aligner (Karl Suss MA6). Subsequently, the exposed photoresist was developed using the AZ726 developer. A 5 nm thick Ti adhesion layer and a 40 nm thick Au layer were deposited using an electron beam evaporation system (Thermionics). Afterwards, lift off was performed by immersion in the remover 1165. For SnO_2/PET substrate, the substrate was attached to the PDMS coated glass to ensure flatness during the photolithography. Ag source and drain electrodes (W/L = 4000 μm/110 μm) on

SnO_2/PET (see Figure S1) were printed using a Voltera V-One PCB (printed circuit board) printer equipped with a conductive silver ink cartridge (Nozzle size = 150 µm).

For ionic liquid gating, a PVDF membrane filter (9×4 mm) soaked with [EMIM] [TFSI] was placed on the top of the patterned electrodes. Prior to use, [EMIM] [TFSI] was purified at 60 ˚C for overnight under vacuum (~10^{-5} Torr).[121]

For aqueous electrolyte gating, we confined the aqueous gating medium, i.e. 0.1 M NaCl, using a PDMS (polydimethylsiloxane) well or a cellulose (9×4 mm) filter soaked with 0.1 M aqueous NaCl solution and placed on the top of the patterned electrodes. To complete the device fabrication, an activated carbon gate electrode was placed on top of cellulose filter. To confine the gating medium using a PDMS well, a rectangular well was prepared from PDMS (size of inner well ~ 2×6×6 mm), attached to the substrate and filled with 0.1 M NaCl aqueous solution using a micropipette.

In both cases, gating was achieved with an activated carbon electrode, was placed on top of the filter or immersed in the solution. The process flow for device fabrication is shown in Figure S2. The activated carbon gate electrodes for ionic liquid gating medium were prepared using a carbon ink containing activated carbon (28mg mL^{-1}) and PVDF (1.4 mg mL^{-1}) in N-methyl pyrrolidone. Those for aqueous gating medium were prepared using a carbon ink containing activated carbon (28mg mL^{-1}) and Nafion (1.4 mg mL^{-1}) in isopropyl alcohol. The carbon ink was drop-casted on the carbon paper (Spectracarb 2050), which was subsequently heated at 60˚C for 5 h to remove solvent traces.[137]

5.3.3 Characterization

The morphological characteristics of the SnO_2 films were studied using an environmental scanning electron microscope (Quattro, Thermo Fisher). The width of the nanorods was calculating using a free image-processing software ImageJ (version 1.53a). The structural characteristics of the SnO_2 films were analyzed with a Malvern PanAlytical Empyrean 3 diffractometer using a CuKα (λ= 1.54178 Å) beam. The optical characteristics of the SnO_2 films were analyzed using Lambda 9 spectrophotometer. The characterization of IGTs was carried out using an electrical probe station equipped with a micromanipulator and a semiconductor parameter analyzer (Keysight B1500A). The electrochemical characterization (cyclic voltammetry) of SnO_2 films was performed in

transistor configuration using a VERSASTAT 4 potentiostat (Princeton Applied Research). The tensile bending experiments were carried out by attaching the device to a curved surface with a curvature radius of ~20 mm and ~10 mm. We measured the electrical characteristics of the device before bending (original flat state) and in the bent state to determine whether bending affected the device performance.

The measurements of the ionic liquid gated transistors were carried out in a N_2 glove box (O_2 and H_2O < 5 ppm), with a scan rate of 10, 50 and 100 mV/s, while those of aqueous electrolyte gated transistors were carried out in ambient conditions. Due to the fast evaporation of water in the 0.1M NaCl aqueous solution-soaked cellulose filter at ambient conditions, we performed the transistor and electrochemical measurements only at the scan rates of 50 mV and 100 mV/s.

5.3.4 Charge carrier mobility and charge carrier density calculations

The charge carrier mobility was calculated from the linear transfer characteristics (V_{ds} = 0.1 V), using the formula

$$\mu_{lin} = \frac{L\, I_{ds,lin}}{W\, e\, n\, V_{ds}}$$

where L is the interelectrode distance, W is the electrode width, $I_{ds,lin}$ is the drain-source current, e is the elementary charge (1.6×10^{-19} C), n is the charge carrier density and V_{ds} is the drain-source voltage. The charge carrier density (n) was obtained from the linear transfer characteristics, using the formula.[52, 175, 176]

$$n = \frac{Q}{eA} = \frac{\int I_{gs} dV_{gs}}{r_v e A}$$

where Q is the doping charge, I_{gs} is the gate-source current in the forward scan of the linear transfer characteristics, r_v is the scan rate of the gate-source voltage, and A is the geometric surface area of the semiconductor in contact with the gating media (~ 0.3 cm^2 for ionic liquid gated IGTs and aqueous electrolyte gated IGTs with cellulose filter; 0.06 cm^2 for the aqueous electrolyte gated IGTs with PDMS well). The reported mobility values are the averaged of three devices and the error corresponds to the standard deviation.

5.4 Results and Discussion

Structure and morphology of the SnO_2 films obtained from aqueous growth at 95 °C

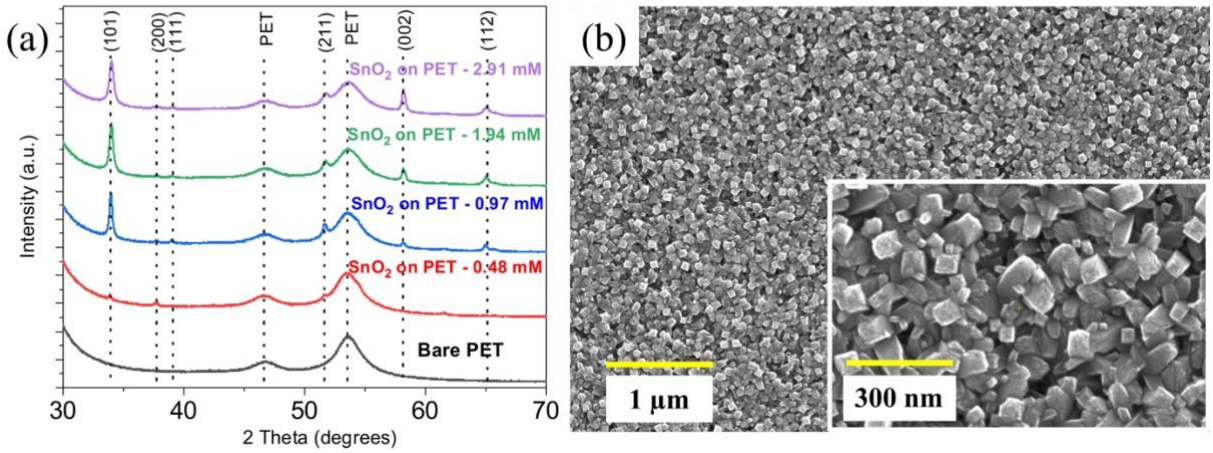

Figure 5-1 XRD patterns of SnO_2 films deposited on PET (b) SEM images of a SnO_2 film deposited on PET using 0.97 mM Sn precursor.

We studied the structural, morphological and optical properties of SnO_2 films prior to the transistor assembly. Figure 5-1 a shows the XRD patterns of SnO_2-coated PET substrates prepared with different concentrations of the Sn precursor (0.48 mM, 0.97 mM, 1.94 mM and 2.91 mM of $SnCl_4 \cdot 5H_2O$). The diffraction peak intensity increases with increasing precursor concentration.[177] The XRD pattern reveals the characteristic pattern of cassiterite, i.e., rutile SnO_2.[90] For all concentrations of the Sn precursor, we observed a diffraction peak at ~2θ = 34˚(magnified view shown in Figure S3 a), corresponding to the (101) plane, whose intensity significantly decreases when the Sn precursor concentration decreases down to 0.48 mM, due to the lower amount of SnO_2 and, possibly, also to the lower degree of crystallinity of the films. Due to the broad peak originated by the PET substrate, the peak of the (110) plane of SnO_2 (~2θ = 26.5˚) is not visible in the pattern (magnified view in Figure S3 b). The peaks at ~2θ =38˚ and ~2θ =39˚ correspond to the (200) and (111) plane of SnO_2. The diffraction peaks observed at ~2θ 52˚, 58˚ and 65˚ corresponds to the (211), (002) and (112) plane, respectively. SnO_2 films on PET substrates exhibits higher crystallinity as compared to films on glass substrates. (Figure S4).

The SEM images (Figure 5-1b) show the presence of nanorods with square cross-sections. The inset shows the magnified top-view of the SnO_2 nanorods. A relatively uniform distribution of nanorods was observed on PET substrates. The width of the nanorods ranges from ~55 nm to ~65 nm (calculated using the average width of 20 nanorods in Figure 5-1 b. Optical transmittance spectra of SnO_2 on PET (Figure S5 a) and glass substrate (Figure S5 b) show decrease in transmittance when the concentration of Sn precursor is increased from 0.48 mM to 2.91 mM. Overall, a higher transmittance is observed for films on PET, which represents an advantage for fabrication of transparent flexible devices.

Cyclic voltammetry to gain insight on charge transfer processes in SnO_2 films

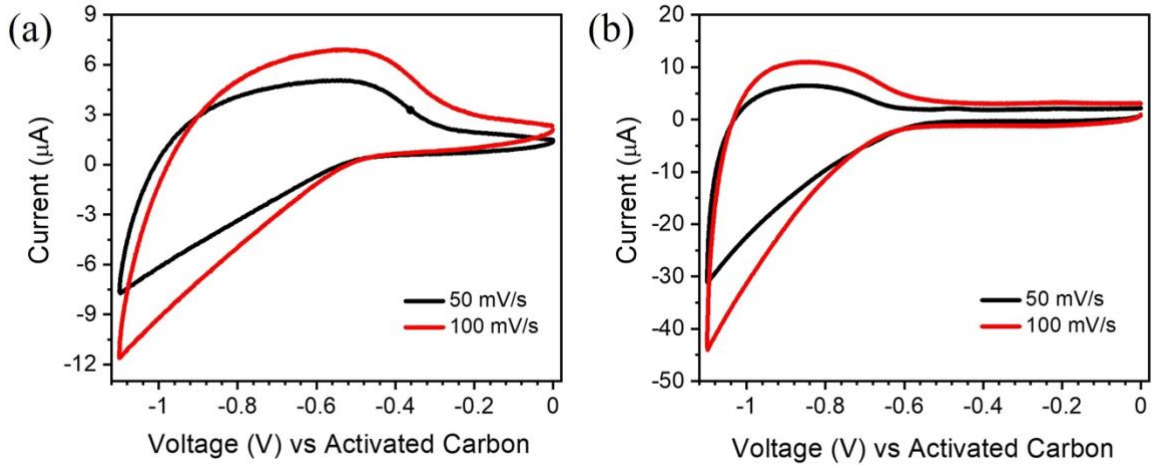

Figure 5-2 Cyclic voltammograms of SnO_2 films (with Au source/drain electrodes) on PET substrates gated with (a) [EMIM][TFSI] and (b) 0.1 M NaCl aqueous solution (cellulose filter).

Cyclic voltammograms (CVs) of the SnO_2 films (with Au source/drain electrodes) gated with [EMIM][TFSI] and 0.1 M NaCl aqueous solution are shown in Figure 5-2. CVs are measured in IGT configuration, with the SnO_2 film between the Au source and drain electrodes functioning as the working electrode and the activated carbon gate (specific capacitance ~ 100 F/g) functioning as the counter and quasi-reference electrode. The cathodic and anodic processes observed in the CV correspond to the doping and dedoping of the SnO_2 films. An increase in cathodic current is detected when the potential is swept negatively from -0.5 V to -1.1 V for both the devices. A significantly broader anodic wave is observed for the [EMIM] [TFSI] gated devices (Figure 5-2 a) compared to the 0.1 M NaCl aqueous solution gated devices (Figure 5-2 b). The broadening of the

anodic wave in the cyclic voltammogram is likely due to slower de-doping by the larger $[EMIM]^+$ cations. A well-defined anodic wave in the aqueous electrolyte-based systems is likely due to the faster de-doping by the smaller Na^+ ions.

Flexible SnO_2 transistors with Au top contacts gated by ionic liquid and aqueous NaCl

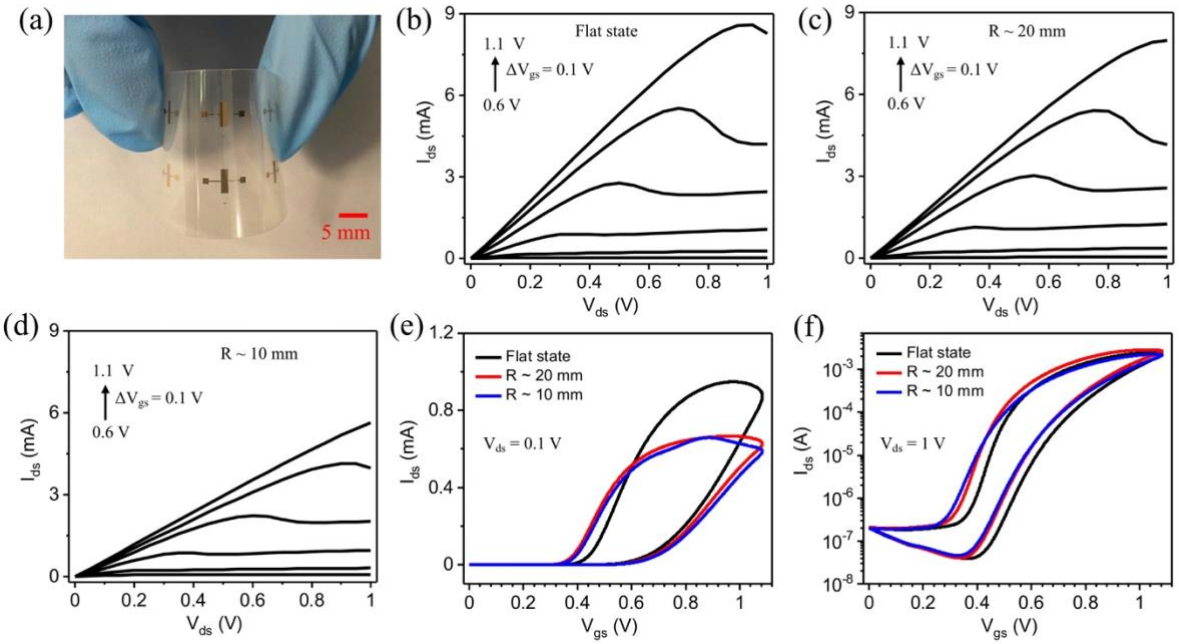

Figure 5-3 (a) Photograph of Au electrodes patterned on a SnO_2 film deposited on a PET substrate. Output characteristics of the [EMIM][TFSI]-gated IGTs based on SnO_2 films with Au source/drain electrodes on PET substrates measured in a N_2 glove box under flat state (b), curvature radius ~ 20 mm (c) and curvature radius ~ 10mm (d). The output characteristics were measured at V_{gs} = 0.6, 0.7, 0.8, 0.9, 1.0, 1.1 V. Transfer characteristics measured under flat and bending state in the linear (e) and saturation (f) regime. The linear and saturation transfer characteristics are represented on linear and logarithmic drain–source current (absolute values) scale versus linear gate-source voltage. The scan rate of is 50 mV/s.

Figure 5-3 a shows the photograph of Au-patterned electrodes on SnO_2 deposited on PET substrates. Figure 5-3 b-f shows the output and transfer characteristics of SnO_2 films gated with the ionic liquid [EMIM][TFSI], measured in a N_2 glove box. The devices were characterized in the flat state (Figure 5-3 b) and under bending on surfaces with curvature radii of ~20 mm (Figure 5-3

c) and ~10 mm (Figure 5-3 d). Compared to the unbent device, we observed no significant variation for a bending radius of R~20 mm (Figure 5-3 b-c), while a ~30% decrease of the drain current (at V_{ds} = 1 V) was observed for the bending radius R~10 mm (Figure 5-3 b and d). A significant hysteresis was observed in the linear transfer curve, due to slow ionic transport during the doping/dedoping of the channel (Figure 5-3 e). The ON/OFF ratio, extracted from the saturation transfer characteristics (Figure 5-3 (f)), was as high as ~10^5 for devices in the flat state and in the bent state (20 mm and 10 mm curvature radius). Also, there were no significant changes in transistor characteristics after 100 bending cycles with the curvature radius of R ~ 10 mm (Figure S6). The performances of our flexible transistor measurements are comparable with those of flexible SnO_2 FETs and IGTs reported in the literature.[45, 121] The electrical characteristics of the IGTs at different scan rates (10 and 100 mV/s) do not show significant differences (Figure S7 and S8), likely because the rate of doping/dedoping of SnO_2 films is not affected by the scan rate within the investigated range of rates. Transfer curves measured with 10 repetitive cycles in linear and saturation region show good operational stability (Figure S9), with no significant change in device characteristics. The transient response indicates stable OFF and ON currents for 1000 seconds (24 pulses) (Figure S10).

Figure 5-4 shows the output and transfer characteristics of SnO_2 IGTs (with Au source/drain electrodes) gated with 0.1 M NaCl aqueous solution measured in ambient conditions. A clearer drain current saturation (Figure 5-4 a) was observed for these devices at low voltages as compared to the ionic liquid-gated ones. A higher voltage is required to completely dope the SnO_2 with the larger $[EMIM]^+$ ions (~ 3.5 Å) to attain the saturation current. For aqueous solution-gated devices, almost no hysteresis is observed in both linear and saturation regime (Figure 5-4 b-c), unlike ionic liquid-gated devices. This is likely due to the faster doping/de-doping of smaller Na^+ ions (ion size ~ 1.02 Å) during the forward/backward scan. The ON/OFF ratio, extracted from the saturation transfer characteristics is ~ 10^4 (Figure 5-4 c). The output and transfer characteristics with a scan rate of 100 mV/s (Figure S11) do not show significant differences with respect to 50 mV/s.

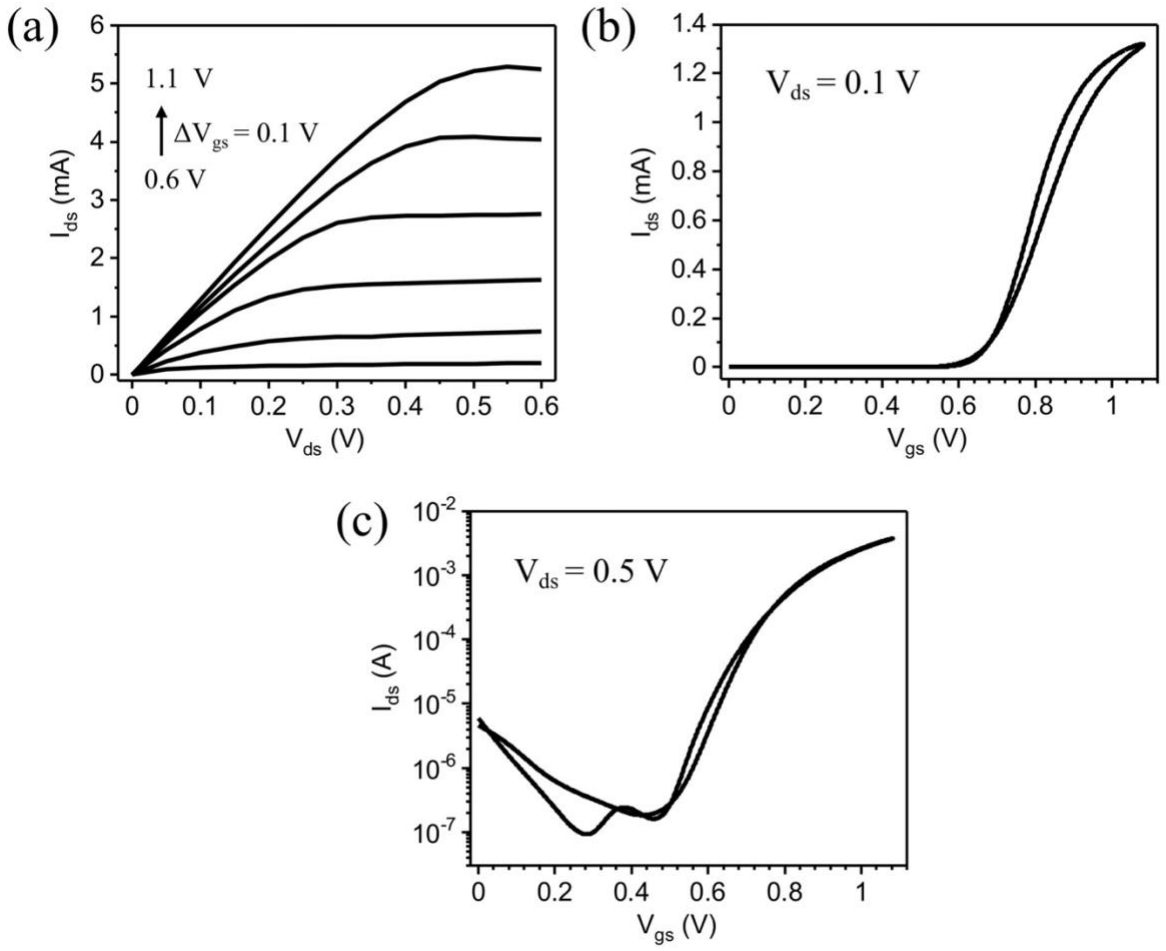

Figure 5-4 (a) Output and (b,c) transfer characteristics of the 0.1 M NaCl aqueous solution gated IGTs based on SnO2 films with Au source/drain electrodes on PET substrates measured in ambient conditions. Cellulose filter soaked with 0.1 M aqueous NaCl solution acted as an ion-gating medium. The output characteristics were measured at Vgs = 0.6, 0.7, 0.8, 0.9, 1.0, 1.1 V with a scan rate of 50 mV/s. The transfer characteristics were measured in (b) linear (Vds = 0.1 V) and (c) saturation (Vds = 0.5 V) region with a scan rate of 50 mV/s. The linear and saturation transfer characteristics are represented on linear and logarithmic drain–source current (absolute values) scale versus linear gate-source voltage.

A charge carrier density of ~5×10^{14} cm^{-2} and a mobility of ~0.15 cm^2/Vs were extracted for the SnO_2 IGTs gated with [EMIM][TFSI] under the original flat state. These values were not significantly affected by bending at either radii. A charge carrier density of ~1×10^{15} cm^{-2} and mobility of ~0.1 cm^2/Vs were obtained for the SnO_2 IGTs gated with 0.1 M $NaCl_{(aq)}$. Overall,

similar charge carrier densities and mobilities were obtained for the two gating media. The mobility values of photolithographically patterned Au electrodes based SnO_2 IGTs are comparable with the values of SnO_2 based FETs and IGTs reported in the literature. [121, 178, 179]

For comparative purposes, we assembled similar devices on glass substrates, for both ionic liquid and aqueous gating (Figure S12 and S13). With respect to PET substrates, we observed significantly lower transistor currents, likely due to less uniform film morphology on glass.

SnO_2 transistors with printed top Ag contacts, gated by aqueous NaCl

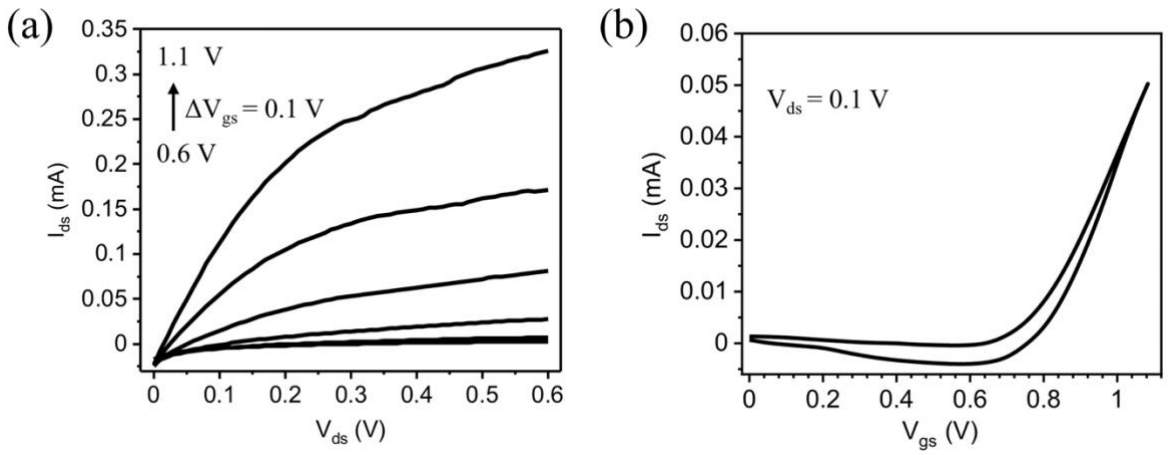

Figure 5-5 (a) Output and (b) transfer characteristics of the 0.1 M NaCl aqueous solution gated IGTs based on SnO_2 films with printed Ag source/drain electrodes (L/W = 110 µm/4000 µm) on PET substrates measured in ambient conditions. The PDMS well filled with 0.1 M NaCl aqueous solution acted as the gating medium. The output characteristics were measured at V_{gs} = 0.6, 0.7, 0.8, 0.9, 1.0, 1.1 V and the transfer characteristics at V_{ds} = 0.1 V with a scan rate of 50 mV/s. The transfer characteristics is represented on a logarithmic drain–source current (absolute values) scale versus linear gate-source voltage.

Figure 5-5 shows the output and transfer characteristics of SnO_2 films (with Ag printed top, source/drain electrodes) gated with 0.1 M NaCl aqueous solution and measured in ambient conditions. Although these devices do not show state-of-the-art- performance, this straightforward, direct writing and low-energy consumption fabrication method is of high interest for sustainable electronics. The drain-source leakage current observed (Figure 5-5 a) in the printed Ag electrodes

at low drain-source voltage (~ -25 µA) is likely due to the unpatterned channel material, the exposure of the silver contacts to the electrolyte and the large channel length (~ 110 µm). The ON/OFF ratio, extracted from the saturation transfer characteristics is ~ 10^3 (Figure S14). A charge carrier density of ~ 5.0 ×10^{16} cm^{-2} and a mobility of ~1.0 ×10^{-3} cm^2/Vs were extracted. The output and transfer characteristics at different scan rates (10 and 100 mV/s) showed no significant change in the transistor characteristics (Figure S15). We believe that the device performance is affected by the limited stability of printed Ag electrodes, especially when in contact with the electrolyte under bias. Work is in progress to protect the Ag electrodes with a printed protective layer to avoid exposure to the ion-gating medium to improve the stability.[180]

5.5 Conclusions and Perspectives

We successfully fabricated low-temperature crystalline SnO_2 nanorod-based IGTs making use of an ionic liquid and an aqueous saline solution as the gating media. The aqueous electrolyte-gated transistors employed biodegradable cellulose soaked with the aqueous electrolyte as the gating medium; for these transistors, the electron mobility was ~ 0.1 cm^2/Vs. The low temperature processing of earth-abundant tin dioxide on flexible substrates paves the way for next generation flexible, wearable and sustainable electronics. Currently, work is in progress to fabricate films of SnO_2 nanorods on silicone rubber substrates enabling them to be used for stretchable electronic applications. We also demonstrated a clean room-free fabrication of source-drain metal top contacts for our SnO_2 IGTs using a PCB printer. This printer enables the facile fabrication of metal electrodes for the production of sustainable electronics. The printed Ag source and drain top metal contact-based SnO_2 IGTs, although showing lower performance compared to their counterparts making use of photolithographically patterned Au contacts, pave the way for a low cost and environmentally sustainable fabrication method or the electrodes. Our devices can be useful for environmentally sustainable devices used in water quality monitoring, pH sensors, humidity sensors and non-invasive glucose detection, i.e., monitoring blood glucose levels using sweat, saliva, and tears.

5.6 Acknowledgements

The Natural Science and Engineering Council Canada (NSERC) is acknowledged for Discovery Grants awarded to FC and CS. Equipment and infrastructure used for this research were acquired and maintained by the Canada Foundation for Innovation and Quebec Strategic Networks (CQMF-QCAM, RQMP, and GCM), respectively. AS and MA are grateful to the Trottier Energy Institute for a doctoral scholarship. AS is grateful to FRQNT for a doctoral scholarship.

CHAPTER 6 ARTICLE 3: SOLUTION- PROCESSED TITANIUM DIOXIDE ION-GATED TRANSISTORS (IGTS) AND PH SENSORS USING IONIC LIQUID AND AQUEOUS SALINE SOLUTION

Article 3 has been submitted to Frontiers In Electronics on 11th November 2021 (submission number: 813535). The supplementary information of the article is provided in Appendix C.

Arunprabaharan Subramanian[1], Mona Azimi[1], Cheng Yee Leong[2], Siew Ling Lee[2], Clara Santato[3], Fabio Cicoira[1*]

[1] Department of Chemical Engineering, Polytechnique Montréal, Montreal, Quebec, Canada

[2]Department of Chemistry, University of Technology Malaysia, Johor Bahru, Johor, Malaysia

[3]Department of Engineering Physics, Polytechnique Montréal, Montreal, Quebec, Canada

Has been published : Frontiers in Electronics

*Correspondence:Corresponding Author fabio.cicoira@polymtl.ca

6.1 Abstract

Titanium dioxide (TiO_2) is an abundant metal oxide, widely used in the food industry, cosmetics, medicine, water treatment, and electronic devices. TiO_2 is of interest for next-generation indium-free thin-film transistors and ion-gated transistors due to its tunable optoelectronic properties, ambient stability, and solution processability. In this work, we fabricated TiO_2 films using a wet chemical approach and demonstrated their transistor behavior once immersed in room temperature ionic liquids and aqueous electrolytes. In addition, we demonstrated the pH sensing behavior of the TiO_2 IGTs with a pH sensitivity of ~ 48 mV/pH. Furthermore, we demonstrated a low temperature (120 ˚C), solution processed TiO_2-based IGTs on flexible PET substrates, and showed that the IGTs were stable under moderate tensile bending.

6.2 Introduction

Oxide semiconductors are commonly used in display technologies, energy conversion as well as chemo- and bio-sensing, due to their remarkable physicochemical properties, tunable optoelectronic properties and mixed ion-electron conductivities.[5, 8, 77, 181-183] They are cost-effective, transparent to visible light, stable in ambient conditions and solution-processable at low temperatures in ambient air.[25, 184] Oxide semiconductors are extensively studied as active channels material for field-effect transistors (FETs) and ion-gated transistors (IGTs),[4, 147, 185] where charge carrier mobility, ON/OFF current ratio, operating voltage and switching speed are key parameters for determining device performance. Amorphous indium gallium zinc oxide (IGZO), showing a mobility above 10 cm^2/Vs, is already used in organic light emitting diode (OLED) display backplanes.[4, 9, 34, 186] However, due to the scarcity of indium in the earth's crust, several alternative oxide semiconductors are being explored.[187] For instance, in addition to display technologies, the earth-abundant materials ZnO, SnO_2 and TiO_2 are investigated for sensor applications.[77, 79, 188, 189] To develop sensors for physiological (e.g. point-of-care testing) and environmental monitoring (e.g. water quality monitoring), the semiconductors need to be stable in ambient conditions.[181] TiO_2 is known for its abundancy, non-toxicity, tunable optoelectronic properties and high stability under ambient conditions and biocompatibility.[47] Depending on the type of synthesis, thermal treatment temperature, and type of gating media, FETs and IGTs based of TiO_2 channels exhibit charge carrier mobility ranging from 0.05 to 10 cm^2/Vs.[48-54]

Various film processing routes lead to different morphologies, crystal structures and chemical compositions of TiO_2, resulting in different electrical properties.[190] TiO_2 can be processed via a variety of sustainable wet chemical approaches, such as spin-coating, dip-coating, spray-coating and printing. [30] However, the high processing temperature (> 250 ˚C) and brittle nature of metal oxide films limit their applicability in flexible and stretchable electronics. [150, 191, 192]

Metal oxide-based IGTs employ semiconducting metal oxides as active channel materials and ionic liquids, ion-gels or aqueous saline solutions as the ion-gating medium.[57-59, 89, 185] Due to its autoionization, deionized (DI) water can also be used as gating medium.[170] IGTs operate at low voltages, due to the formation of an electrical double layer at the oxide semiconductor/ion-gating medium interface. [59, 193] Current modulation in IGTs can be explained by electrostatic (surface

doping) and electrochemical (volumetric doping) doping. Surface doping is achieved by the migration of ions from the gating medium towards the surface of the semiconductor and subsequent formation of a high-capacitance electrical double layer, whereas volumetric doping is achieved when ions from the gating medium pass through the permeable surface into the bulk of the semiconductor. [58, 59, 69, 194, 195] Horita *et al.* fabricated anatase TiO_2-based IGTs using ionic liquids, ion-gels and polyvinyl alcohol and investigated the transistor performance by the dependence of mobile ions in the ion-gating media.[53] We recently demonstrated that characteristics of IGTs based on porous and compact TiO_2 films gated by pure 1-ethyl-3-methylimidazolium bis(trifluoromethylsulfonyl)imide ([EMIM][TFSI]), and Li^+ ions in [EMIM] [TFSI] were significantly affected by the film morphology and the type of gating medium. [88]

IGTs can be used as chemical sensors and biosensors due to their ability to function as ion/electron converters.[69, 196] In IGT sensors, the analyte, i.e. substance to be detected, can be included in the gating medium, leading to a change of the electronic signal proportional to its concentration.[181, 196, 197] In IGTs, the analyte is in direct contact with semiconductor, while in the case of ion-sensitive field-effect transistor (ISFETs), it is in direct contact with the gate dielectric. The low operating voltage of oxide-based IGTs makes possible the detection of biomolecules that feature undesired redox reactions at high voltages. In addition, surface functionalization of the oxide semiconductor permits functionalization with specific chemical/biological species. As an example, the surface functionalization of ZnO with the glucose oxidase enzyme enabled the specific quantitative detection of *d*-glucose in IGT configuration.[76] The detection of coronavirus and cancer biomarkers were recently reported using oxide IGTs. [82, 84, 198]

Oxide-based IGTs can be used as pH sensors, exploiting the threshold voltage shift induced by changes in the pH of the gating medium. [166, 199, 200] Previous reports based on TiO_2 extended-gate ISFETs showed a maximum pH sensitivity of 60 mV/pH.[201-204] These devices are composed of a FET (transducing unit), a sensing unit and control gate electrode. The sensing unit and the control gate are placed in the environment containing the analyte solution and are remotely connected to the gate terminal of the FET which is placed outside the analyte. [204]

In this work, we synthesized TiO_2 films using a sustainable wet chemical method employing green alcohol solvents (isopropanol and ethanol). We demonstrated the successful operation of TiO_2 IGTs at low voltages in an ionic liquid and an aqueous saline solution. TiO_2 IGTs were also

used as pH sensors with a pH sensitivity of ~ 48 mV/pH. Due to the *n*-type nature of the TiO_2 film, the increase of $[H]^+$ (decrease of pH) makes the IGTs turn on at lower voltages. Conversely, the IGTs turn on at higher voltages at higher pH levels. In addition, we fabricated TiO_2 films on flexible PET substrates at the maximum processing temperature of 120 °C and showed that their performance was not severely affected under tensile bending state.

6.3 Experimental

6.3.1 Film Deposition

The solution for TiO_2 sol-gel synthesis on rigid substrates (route I) was prepared by stirring a mixture of containing 1.7 mL of titanium butoxide (Alfa Aesar, 99%), 65 µL of concentrated HNO_3 (Thermo Fisher Scientific, 70%), 90 µL of deionized water (Milli-Q water purification system, resistivity of 18.2 MΩ.cm) and 19.1 mL of isopropyl alcohol (HoneyWell, 99.9%) for 6 h at room temperature.[205, 206] This solution was spin-coated on Au/Ti (40 nm/5 nm) pre-patterned SiO_2/*p*-Si (200 nm/500 µm) substrates (Wafer Pro, USA) at 2000 rpm for 40 s. The films were heated initially at 100 ˚C for 15 minutes to evaporate the solvents and subsequently in a tubular furnace in ambient air (Thermolyne 21100) at 450 ± 10 ˚C for 1h .[206]

TiO_2 films on flexible PET substrates were obtained with a different method (route II), which only required a thermal treatment at 120 ˚C. A TiO_2 suspension was prepared by stirring a mizture of 10 g of Aeroxide TiO_2 P25 nanoparticles (Photocatalytic standard, particle size ~ 21 nm, Millipore Sigma), 107 mL of ethanol (Commercial Alcohols Inc., Canada), 1.4 mL of deionized water and 3.7 mL of titanium tetraisopropoxide (inorganic binder) (Millipore Sigma) overnight at room temperature. This suspension was spin-coated on Au/Ti (40 nm/5 nm) pre-patterned polyethylene terephthalate (PET) substrates (175 µm thick, antistatic coating on both sides, purchased from Policrom Inc., USA) at 4000 rpm for 40 s. The films were heated at 120 ˚C for 90 minutes in ambient air. [207]

6.3.2 Film Characterization

The topographical characteristics of the TiO_2 films were analyzed using tapping-mode atomic force microscopy (AFM) performed with a Digital Instruments Dimension 3100 and JPK NanoWizard

3 equipped with a silicon cantilever (Spring constant: 40 N/m, tip radius: < 10 µm and resonance frequency: 300 kHz). The thicknesses of the TiO_2 films (~55 nm for route I films and ~1.1 µm for route II films) were measured using a profilometer (Dektak 150, Veeco, USA). The morphological characteristics of the TiO_2 films were analyzed using JEOL JSM-7600F and Hitachi SU8020 field emission scanning electron microscopes (FESEM). The crystal structures of the TiO_2 films were analyzed using X-ray diffraction (XRD) with Bruker D8 and Rigaku SmartLab using CuKα source. The x-rays were scanned (1˚/minute) from 2θ = 10˚ to 2θ= 60˚.

6.3.3 Device Fabrication

Photolithographically patterned Au/Ti (40 nm/5 nm) source and drain electrodes (width/length=4000µm/10µm) on SiO_2/p-Si and PET substrates were prepared based on the procedure described previously.[52, 89, 137] The patterned substrates were ultrasonically cleaned using sequential baths of isopropyl alcohol, acetone and isopropyl alcohol and exposure to UV-ozone for 15 minutes, prior to the deposition of the TiO_2 films.[88]

For ionic liquid gating, a PVDF (polyvinylidene fluoride, 220 nm pore size, Millipore Sigma) membrane soaked with [EMIM] [TFSI] (IoLiTec Ionic Liquids Technologies GmbH, Germany) was placed on the top of the TiO_2 layer and served as the ion-gating media. Activated carbon on carbon paper was used as the gate electrode and placed on top of the ion-gating medium to complete the fabrication of the ionic liquid-gated transistor.[88, 89]

For aqueous electrolyte gating/pH sensing, a polydimethylsiloxane (PDMS) well (size of inner well ~ 2×6×6 mm) was attached to the substrates to confine the NaCl or the buffer solutions.[137] The saline solution was prepared using NaCl (Sigma Aldrich, 0.1 M) in deionized water. The device fabrication was completed by injecting 0.1 M NaCl aqueous solution in the PDMS well and immersing the activated carbon gate electrode in it.[89] For pH sensors, the NaCl solution was replaced by different pH buffer solutions (pH of 1.68, 4.01, 7.00, 10.01 and 12.46, Orion pH buffer solutions, Thermo Scientific).

The carbon ink used in the activated carbon gate electrode for the ionic liquid-gated transistors was prepared using activated carbon (Norit CA1, Sigma-Aldrich, 28mg mL^{-1}) and PVDF (Sigma Aldrich, 1.4 mg mL^{-1}) in N-methyl pyrrolidone (Sigma Aldrich). The carbon ink

used in the activated carbon gate electrode for the aqueous electrolyte-gated transistors was prepared using activated carbon (Norit CA1, Sigma-Aldrich, 28mg mL^{-1}) and Nafion (Sigma Aldrich, 1.4 mg mL^{-1}) in isopropyl alcohol. The activated carbon gate electrodes were obtained by drop-casting the carbon ink on the carbon paper (Spectracarb 2050A, Fuel cell store, USA) followed by heating at 60˚C for 5 h.[52, 137, 208]

6.3.4 Device Characterization

The transistor characterization of IGTs was performed using an electrical probe station equipped with a micropositioner (Signatone Corporation, USA) and a semiconductor parameter analyzer (Keysight B1500A). The electrochemical characterization of TiO_2 films was carried out using a potentiostat (VERSASTAT 4, Princeton Applied Research). The electrical and electrochemical characteristics of the ionic liquid gated transistors were measured in a N_2 glove box (H_2O < 5 ppm and O_2 < 5 ppm). The electrical and electrochemical characteristics of the aqueous electrolyte-gated transistors were measured in ambient conditions.[89]

6.3.5 Charge carrier density and mobility calculations

The charge carrier mobility was extracted from the linear transfer characteristics, using the formula

$$\mu_{lin} = \frac{L\, I_{ds,lin}}{W\, e\, n\, V_{ds}},$$

where L is the interelectrode distance (10 µm), $I_{ds,lin}$ is the drain-source current, W is the electrode width (4000 µm), e is the elementary charge (1.6×10^{-19} C), V_{ds} is the drain-source voltage and n is the charge carrier density. The charge carrier density (n) was calculated from the linear transfer characteristics, using the formula

$$n = \frac{Q}{eA} = \frac{\int I_{gs} dV_{gs}}{r_v eA}$$

Where Q is the doping charge, I_{gs} is the gate-source current in the forward scan of the linear transfer characteristics, r_v is the scan rate of the gate-source voltage (V_{gs}), and A is the geometric area of the TiO_2 films in contact with the ion-gating media (0.36 cm^2 for ionic liquid based IGTs and 0.12 cm^2 for the aqueous electrolyte-gated IGTs). [89]

6.3.6 pH sensitivity calculations

The pH sensitivity of IGTs was calculated using gate-source voltage shift with respect to the drain-source current (10^{-5} A) in the forward scan of linear transfer characteristics (V_{ds} = 0.1 V). The gate-source voltage shift (ΔV_{gs}) of IGTs for each pH buffer solution was plotted against the pH value and then the data points were fitted as a straight line by linear regression. The slope (V/pH) of the straight line corresponds to the pH sensitivity.[166, 209]

6.4 Results and discussion

6.4.1 Film characterization

Morphological, topographical, and structural properties of TiO_2 films were studied before transistor assembly. For films on rigid SiO_2/p-Si (route I), SEM images reveal a homogeneous homogenous, uniform, and crack-free morphology (Figure 6-1 a). The rms roughness was found to be 1.0±0.2 nm (Figure 6-1 b). XRD patterns show the presence of the anatase phase (diffraction peak at 2θ ~ 25˚, Figure 6-1 c).[88] An analogous characterization of TiO_2 films on PET (route II) revealed a more granular morphology with a uniform distribution of TiO_2 nanoparticles (Figure 6-1 d). The rms roughness was found to be 85.4±4.2 nm (Figure 6-1 e). Due to the response from the PET substrate at 2θ ~ 25 ˚, the main anatase diffraction peak was not visible in the XRD pattern (Figure 6-1 f). The inset of Figure 6-1f shows the magnified pattern with 2θ ranging from 35˚ to 60˚, indicating the presence of both anatase and rutile phases.

6.4.2 Electrochemical characterization

CV was measured in a transistor configuration, with the TiO_2 active channel functioning as the working electrode and the activated carbon gate (specific capacitance of ~ 100 F/g) functioning as the counter and quasi-reference electrode.[88, 89] The cathodic and anodic signals in cyclic voltammograms indicate the doping and dedoping of the TiO_2 films. Cyclic voltammograms (CVs) of the route I TiO_2 films in [EMIM][TFSI] and 0.1 M NaCl solution, are shown in Figure 6-2 (a, b). The electrochemical reduction of TiO_2 starts around -0.6 V for both [EMIM] [TFSI] and 0.1 M aqueous NaCl gating (Figure 6-2 a and b). The reduction-oxidation signals are displayed by the wide cathodic and anodic waves. Cyclic voltammograms of route II TiO_2 films with [EMIM][TFSI]

show that the electrochemical reduction potential of TiO_2 starts at ~ – 1.1 V, which is more cathodic than for route I TiO_2 films (~ -0.6 V) (Figure 6-2 (c)). This information indicates that the route II TiO_2 films can be safely operated between V_{gs} ~ 1 V and V_{gs} ~ 2 V in transistor configuration. As compared to route I TiO_2, a higher gate voltage is necessary to activate the channel material, likely due to the lower temperature thermal treatment.

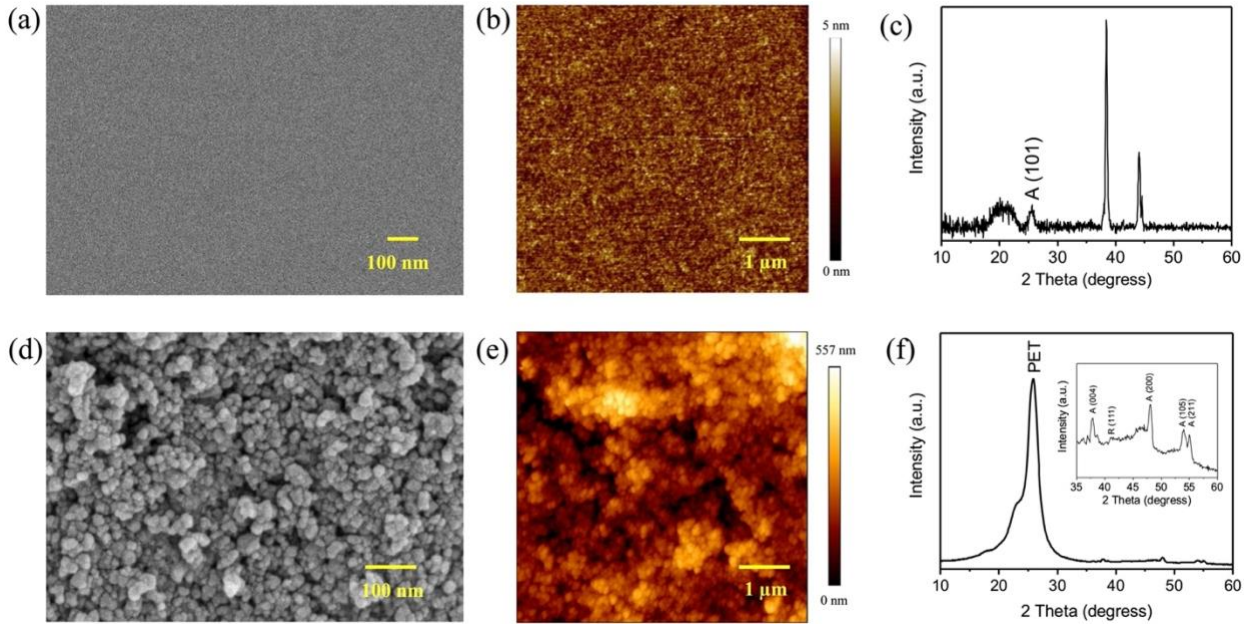

Figure 6-1 (a, d) SEM images, (b, e) AFM images and (c, f) XRD patterns of TiO_2 films on SiO_2/*p*-Si (a-c) and PET (d-f) substrates prepared by route I and route II. A and R indicate anatase and rutile phases of TiO_2.

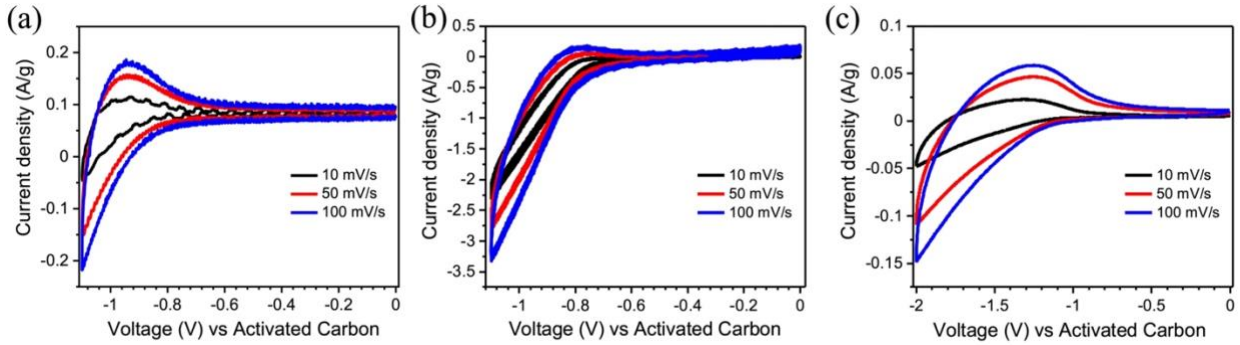

Figure 6-2 Cyclic voltammetry in transistor configuration for route I TiO_2 films gated with [EMIM][TFSI] (a) and 0.1 M NaCl (b), and route II TiO_2 films gated with [EMIM][TFSI] (c). The scan rates are 10 mV/s, 50 mV/s, and 100 mV/s.

6.4.3 Ion-gated transistors based on route I TiO_2 films on SiO_2/p-Si substrates

The output and transfer characteristics of sol-gel TiO_2 films gated with [EMIM][TFSI], measured in a N_2–purged glove box, show *n*-type enhancement mode of operation (Figure 6-3 a, b). The transfer curves reveal an ON/OFF current, extracted between V_{gs} = 0 V and V_{gs} = 1.1 V, of ~ 10^3. The hysteresis in the transfer curve is attributed to the slow ion transport during forward and reverse scans. The output and transfer characteristics of route I TiO_2 films, gated with 0.1 M NaCl, show a higher drain-source current than the [EMIM] [TFSI] counterparts (Figure 6-3 c, d). The transfer curves shows that the ON/OFF current ratio of the transistors, calculated between V_{gs} = 0 V and V_{gs} = 1.1 V, is ~10^4. Compared to the [EMIM][TFSI]-gated devices, $NaCl_{(aq)}$-gated transistors show a clearer drain current saturation as well as a lower hysteresis, likely due to the faster dedoping. The charge carrier density and charge carrier mobility were ~ 1.7×10^{14} cm^{-2} and ~3.5×10^{-2} cm^2/Vs for [EMIM][TFSI] gated devices and ~1.5×10^{16} cm^{-2} and ~4.5×10^{-3} cm^2/Vs for the NaCl gated ones.

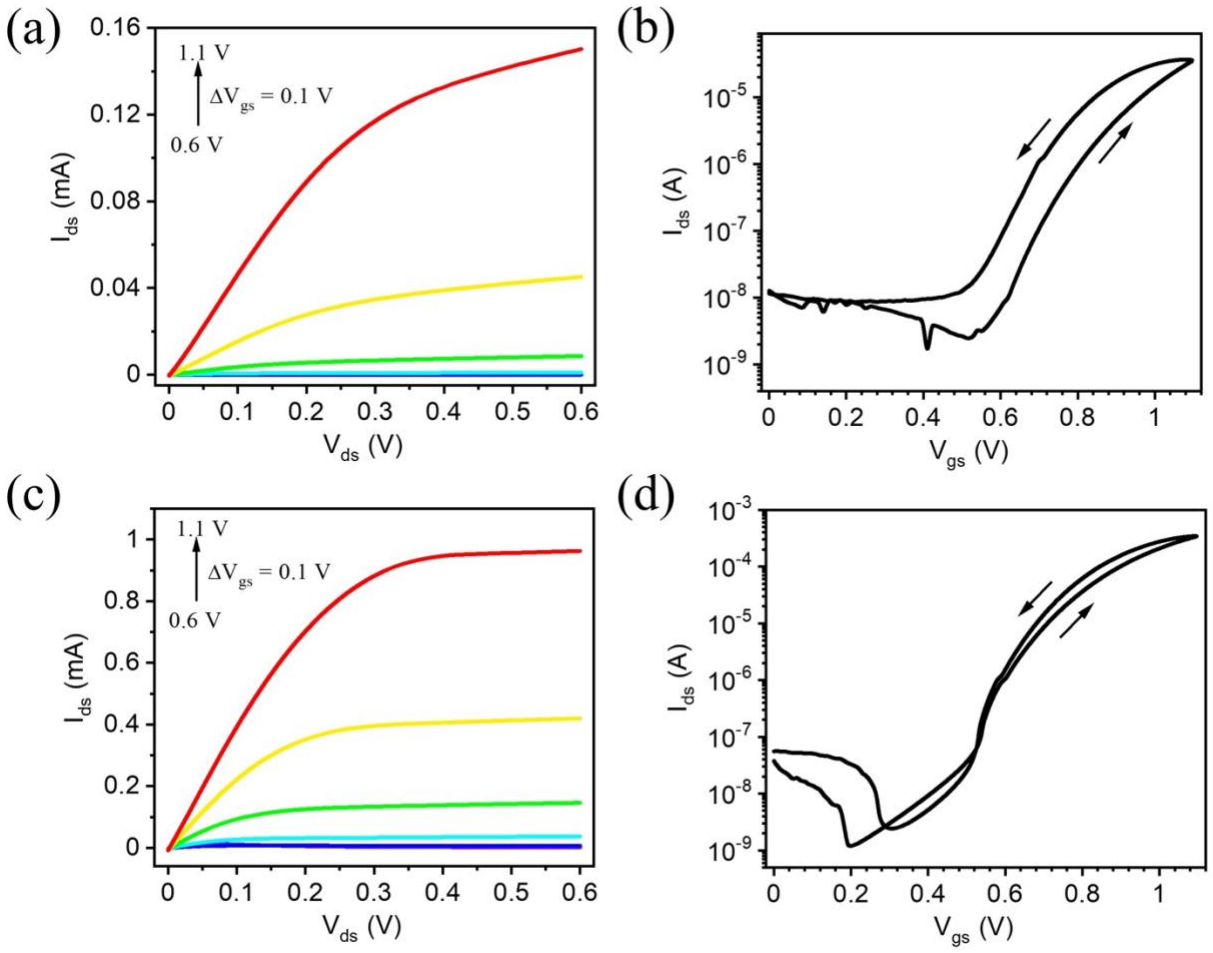

Figure 6-3 (a, c) Output and (b, d) transfer characteristics of route I TiO_2 films on SiO_2/p-Si substrates gated with [EMIM][TFSI], measured in a N_2-purged glove box (a, b) and with 0.1M $NaCl_{(aq)}$ measured in ambient conditions (c, d). The output characteristics were measured at V_{gs} = 0.6, 0.7, 0.8, 0.9, 1.0, 1.1 V and the transfer characteristics at V_{ds} = 0.1 V with a scan rate of 10 mV/s.

6.4.4 pH sensors based on ion-gated TiO_2 films

Low voltage operation in aqueous media, lightweight, low processing temperature and make TiO_2 IGTs suitable for ion-sensing applications. With the aim to demonstrate pH sensing, we used TiO_2 IGTs with pH buffer solutions as the ion-gating media.

Figure 6-4 (a) shows the transfer characteristics (V_{ds} = 0.1 V) of the TiO_2 films gated with pH buffer solutions (pH from 1.68 to 12.48). Two additional set of data extracted from two other

devices are shown in Figure S1. The change of pH of the gating media leads to a shift of the gate voltage at a given reference drain-source current point (e.g., I_{ds} = 10^{-5} A). Being TiO_2 an n-type semiconductor, when a positive voltage is applied to the gate electrode of TiO_2 IGTs, the positive ions in the gating medium migrate and accumulates on the surface of TiO_2 films, leading to an increase in electron density. Therefore, the negative shift in gate voltage observed when lowering the pH of ion-gating media, can be attributed to the increase of the of H_3O^+ concentration. The gate voltage shift at 10^{-5} A plotted against pH (Figure 6-4 b) shows a pH sensitivity of TiO_2 IGTs of ~ 48 mV/pH (average value of 3 devices), which is comparable with the pH sensitivity values of metal oxide IGT based pH sensors.[166, 200, 210]

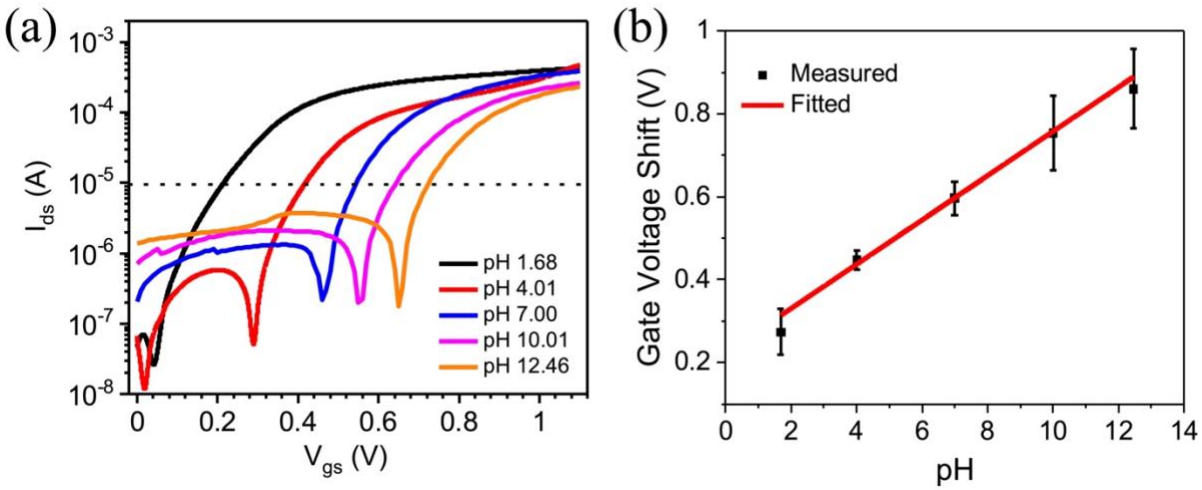

Figure 6-4 (a) Transfer characteristics (Vds = 0.1 V) of route I TiO_2 films on SiO_2/Si substrates gated with pH buffer (pH 1.68, 4.01, 7.00, 10.01 and 12.46) solutions measured in ambient air. The V_{gs} scan rate is 10 mV/s. (b) Gate voltage shift corresponding to the reference drain-source current point (ca 10^{-5} A) versus pH. Each point in Figure 4 (b) corresponds to the average gate voltage shift of 3 devices with respect to pH value. The error bar in the graph indicates the standard deviation of 3 devices.

6.4.5 Ion-gated transistors based on route II TiO_2 films on PET substrates

Transistors processed by route II synthesis on flexible PET substrates, where characterized under flat and bent state using [EMIM][TFSI] as the gating medium. Figure 6-5 shows the output (a-c) and transfer (d, e) characteristics. These transistors required a higher voltage compared to the route

I ones, in agreement with cyclic voltammetry data discussed above (Figure 6-5 c). Route II TiO_2 shows a lower saturation current as compared to the route I TiO_2. The charge carrier density and charge carrier mobility, extracted from the linear transfer characteristics (Figure 6-5 d), were ~ 1.2×10^{15} cm^{-2} and 7.5×10^{-3} cm^2/Vs. The ON/OFF ratio, extracted from the saturation transfer characteristics (Figure 6-5 e), extracted between V_{gs} = 0 V and V_{gs} = 2 V, was ~ 10^2. Transistor characterization under tensile bending radii at R ~ 20 mm (Figure 6-5 b) and at R ~ 10 mm (Figure 6-5 c) shows a slight decrease in I_{ds} and their ON/OFF ratio (Figure 6-5 e) is not severely affected by the bending.

The operating voltage of route II lays beyond the thermodynamical electrochemical stability window of water, therefore preventing their use the aqueous gating medium, as the high voltage may causes unwanted redox processes.

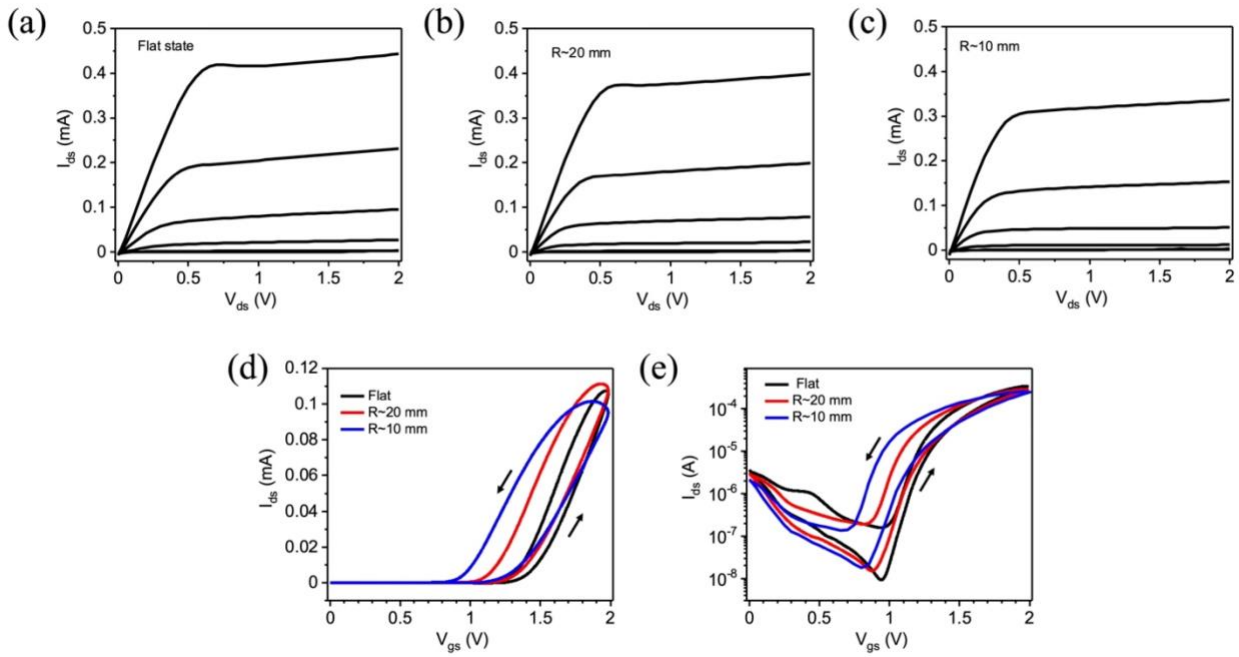

Figure 6-5 (a-c) Output and (d,e) transfer characteristics of route II TiO_2 films on PET substrates gated with [EMIM] [TFSI] measured in a N_2 purged glove box. The output characteristics under (a) flat, (b) bending radius ~20 mm and (c) bending radius ~10 mm measured at V_{gs} = 0, 1.0, 1.25, 1.5, 1.75, 2.0 V. The transfer characteristics under flat and bent state measured in (d) linear (V_{ds} = 0.2 V) and (e) saturation (V_{ds} = 1.75 V) regime. The scan rate is 50 mV/s.

6.5 Conclusions and Perspectives

We fabricated TiO_2 films on rigid and flexible substrates using sustainable wet methods. We demonstrated the transistor behavior of TiO_2 films using room temperature ionic liquid and aqueous saline solution. TiO_2 IGTs were successfully used as pH sensors with a sensitivity of ~ 48 mV/pH. Furthermore, TiO_2 films were deposited on the flexible PET substrates at the maximum processing temperature of 120 ˚C. The transistor behavior of TiO_2 IGTs was not severely affected by the tensile bending radii (R ~ 20 mm and R ~ 10 mm). In view of the flexibility, biocompatibility, and low temperature processability, route II TiO_2 IGTs pave the way to future low-cost flexible electronics.

6.6 Acknowledgements

The Natural Sciences and Engineering Research Council of Canada (NSERC) is acknowledged for a Discovery Grant (F.C.). Equipment and infrastructure used for this research were acquired and maintained by the Canada Foundation for Innovation and Quebec Strategic Networks (CQMF-QCAM, RQMP, CREPEC and GCM), respectively. AS and MA are grateful to the Trottier Energy Institute for a doctoral scholarship. AS is grateful to the FRQNT for a doctoral scholarship. CYL is grateful to the Polytechnique Montréal for a research internship scholarship.

CHAPTER 7 GENERAL DISCUSSION

Metal oxide transistors with ionic-gating operate at low voltages, and have the ability to induce high concentrations of charge carriers in the active channel material. The electrical double layer formed at the interface of the metal oxide/ion-gating medium provides large capacitance that allows low operating voltages.[59, 147] Currently, there are a wide variety of applications of ion-gated transistors (IGTs) in advancing technologies, such as, rollable display backplanes and electrochromic displays, sensors, neuromorphic devices, and memory devices.[58, 69, 211]

In addition to the electrical double layer capacitance, another important driver of IGT performance is electrolyte ion implantation into the channel material, causing electrochemical doping. Whether the working mechanism of IGTs is electrostatic or electrochemical determines the switching speed of transistors. Electrostatic doping, for example, gives an IGT switching speed in the micro-second range, while electrochemical doping gives a switching speed in the milli-second range. Materials able to be implanted with, and subsequently release, ions are useful for devices involving energy storage, electrochromism (coloration ↔ bleach), opto-electronics and electrocatalysis.[195, 212, 213] Also, by using materials and methods to controllably alter the doping mechanism of an IGT, the parameters can be fine-tuned to fit the functionalities needed for a specific application. As an example, an electronic oscillator operates at high frequencies, so the transistors should function through electrostatic doping to achieve high switching speeds.[57] The relatively slow process of ion uptake through the bulk of the semiconducting channel material limits applications for electrochemically driven IGTs in electronic circuits that operate at high frequencies. Electrochemically driven IGTs find their applications in memory devices, such as neuromorphic devices, where ions need to be held in the active channel material for a controlled and specific time.[165]

The first published article is devoted to exploring the doping mechanism of our TiO_2 IGTs. We explored the doping mechanism of IGTs by fabricating TiO_2 channel materials with compact and porous morphologies. The doping mechanism of compact channels was driven by electrostatic doping, while electrochemical doping was more prominent when porous channels were used. In addition, the IGT doping mechanism was investigated by using electrolytes containing ions of different size for the ion-gating medium.

Compact and porous films were prepared using electron-beam evaporation and solution-processing, respectively. We used two electrolytes for the ion-gating media: (i) [EMIM] [TFSI] and (ii) [EMIM] [TFSI] with $[Li]^+$ ions. We hypothesized that the doping caused by large $[EMIM]^+$ ions (ionic radius ~3.5 Å) is likely due to the electrostatic and interface-confined electrochemical doping, while, when $[Li]^+$ ions (ionic radius ~0.7 Å) are added to the [EMIM] [TFSI], the doping is primarily driven by electrochemical doping. The small size of $[Li]^+$ ions may allow it to penetrate the surface of TiO_2 and intercalate into the TiO_2 lattice to form bulk-electrochemical doping. We analyzed the transistor characteristics under four conditions: (i) compact TiO_2 film using [EMIM] [TFSI] gating medium, (ii) compact TiO_2 film using [EMIM] [TFSI] with $[Li]^+$ ions gating medium, (iii) porous TiO_2 film using [EMIM] [TFSI] gating medium and (iv) porous TiO_2 film using [EMIM] [TFSI] with $[Li]^+$ ions gating medium. We observed that transistors with compact TiO_2 films show higher drain current compared to porous films. Additionally, the properties of transistors with compact films were not significantly affected by the addition of $[Li]^+$ ions, while the presence of $[Li]^+$ in the gating medium in contact with porous TiO_2 films, significantly increased the drain current. Porous films have high surface area which leads to higher ion density at the channel surface compared to compact films. In addition, the porous films showed higher electron mobility in the presence of [Li]+ ions, likely due to the $[Li]^+$ ions facilitating the charge transport at the grain boundaries of porous TiO_2. The charge carrier density of the porous films was not significantly changed in the presence of $[Li]^+$ ions possibly due to the complex arrangement of ions in electrical double layer inhibiting the accumulation of a specific charge. Ultimately, we were able to demonstrate that changing the size of ions in the gating medium and the morphology of the channel material affects the doping mechanism and the electrical characteristics of the transistor.

The second article is devoted to the fabrication of SnO_2-based transparent and flexible electronics using sustainable materials. The earth-abundant SnO_2 films were prepared on flexible PET (polyethylene terephthalate) substrates using low temperature (95 ˚C) controlled aqueous growth. The resulting is crystalline with nanorod structured morphology. The SnO_2 films are thin and have >80 % transparency in the visible region. We employed a top-contact architecture for the transistor design, since in the bottom-contact architecture, the highly acidic nature of the SnO_2 growth solution would cause the Au electrodes to peel off. The transistors were assembled using ionic liquid as the gating media, and had an operating voltage below 1 V. We investigated the

electrical characteristics under bending to a curvature radius ~20 mm and ~ 10 mm. We found the transistor characteristics did not significantly change under bending to 10 mm, thus these transistors would be suitable for flexible electronic applications. Interestingly, we observed a hysteresis in the transfer characteristics and hypothesizes the hysteresis was due to the speed difference of ionic transport during doping/de-doping process. In addition, SnO_2 is stable in aqueous environments, so we demonstrated the fabrication of transistors assembled using a cellulose membrane soaked with saline for aqueous electrolyte gating. We observed clearer drain current saturation in the transistor output curve with saline solution gating when compared to ionic liquid gating. A slight hysteresis is observed in the transfer curve likely due to the faster de-doping of small $[Na]^+$ ions. Also, we demonstrated fabrication of Ag source and drain electrodes using PCB printer that was accomplished without a clean room. Afterwards, we assembled the transistor using saline solution-soaked cellulose. Printing electrodes and using saline solution makes these transistors promising for sustainable electronics, however, the performance we observed was below state of art performance for transistors.

The third article is devoted for developing pH sensing transistors and flexible electronics. TiO_2 films were fabricated using solution-processing and "green" solvents. First, we measured the electrical characteristics of the TiO_2 IGTs using ionic liquid and an aqueous electrolyte. We obtained high ON/OFF ratios for both ion-gating mediums (~10^3 for the ionic liquid, ~10^4 for the saline solution). We obtained flatter saturation in the drain current for the saline solution gated transistor when compared to the ionic-liquid gated transistors. The hysteresis observed for the saline solution-gated transistor is smaller than the ionic-liquid gated transistors, due to the faster de-doping of $[Na]^+$ ions.

We chose to use our TiO_2 IGT as a pH sensor because of its stability in ambient and aqueous environments, and the difference in electrical response between transistors using ionic liquid and an aqueous electrolyte. We measured the electrical characteristics of IGTs when exposed to a pH buffer solution. We observed that the turn-on voltage of the transistors highly depends on the ion-concentration in the electrolyte. TiO_2 is an n-type semiconductor, and the presence of $[H_3O]^+$ ions in the pH buffer modulates the charge carrier density on the channel. TiO_2 IGTs turn-on at lower voltages due to the presence of the high concentration of $[H_3O]^+$ ions in the solution increasing the charge carrier accumulation at the channel. The gate voltage, with respect to the reference drain

current, is shifted with respect to the pH of the solution. The slope of the gate-source voltage shift versus the pH plot, demonstrates the level of pH sensitivity of the transistors.

By employing a low temperature process for fabricating TiO_2 films using a TiO_2 suspension in solution, we assembled flexible IGTs by depositing TiO_2 solution on PET substrates. The transistors were analyzed under mechanical bending, and no significant changes were observed with respect to bending. The solution processed TiO_2 films prepared at low temperatures on PET substrates demonstrate transistors with moderate performance under bending.

In general, the fabrication method we described for these IGTs is able to produce transistors with high performance. In the future, we may be able to replace transistors made with indium-based materials with earth-abundant material IGTs for display and sensing technologies. These results will impact future methods for indium-free metal oxides in the next generation flexible transparent display (including electrochromic displays) and sensor applications. Our pH sensors are a good demonstration of a miniaturized sensor design and could replace benchtop glass electrode-based pH Sensors. The vision of this PhD research project, and the above discussed methods for building ion-gated metal oxide transistors will pave the way to advance ion-gating with metal oxides for the next generation IGTs.

CHAPTER 8 CONCLUSION AND RECOMMENDATIONS

We have demonstrated indium-free metal oxides for ion-gated transistors in this PhD work. All the transistors presented are designed toward the operation in biologically relevant conditions, and as an alternative to the transistors based on critical, indium-based materials. In addition, each transistor design functions in n-type enhancement mode, operates below 2 V and uses ion-gating and high capacitance activated carbon as the gate electrode. The electrical performance of the prepared transistors is shown in Table 8-1.

Table 8-1 Electrical performance of IGTs

Channel material (metal oxides)	**Processing method of channel material**	**Substrates**	**Maximum processing temperature**	**Source and drain electrode**	**Ion-gating medium**	**Mobility of IGTs (cm^2/Vs)**	**ON/OFF ratio**
SnO_2	Controlled aqueous growth *(Tin chloride)*	**PET**	**95 ˚C**	Gold	Ionic liquid	**~ 0.15**	~ 10^5
				Gold	Saline solution	**~ 0.11**	~ 10^4
				Silver	Saline solution	**~ 0.001**	~ 10^2
TiO_2	Electron beam evaporation *(TiO_2 pellets)*	SiO_2/Si	450 ˚C	Gold	Ionic liquid	**~ 0.5**	~ 5
				Gold	Li^+/Ionic liquid	**~ 0.6**	~ 10
	Solution-processing *(TiO_2 nanoparticle in xylene)*	SiO_2/Si	450 ˚C	Gold	Ionic liquid	**~ 0.0005**	~ 10^2
				Gold	Li^+/Ionic liquid	**~ 0.004**	~ 10^3
	Solution-processing (Titanium butoxide)	SiO_2/Si	450 ˚C	Gold	Ionic liquid	**~ 0.035**	~ 10^3
				Gold	Saline solution	**~ 0.0045**	~ 10^4
	Solution-processing *(TiO_2 P25 nanoparticle)*	**PET**	**120 ˚C**	Gold	Ionic liquid	**~ 0.0075**	~ 10^2

We investigated the doping mechanism of IGTs made with porous and compact TiO_2 channel material morphology, and by changing the size of ions in the ion-gating medium. We fabricated transparent and crystalline SnO_2 films on flexible substrates using wet chemical

synthesis and studied their electrical characteristics in IGT configuration under bending. Finally, by considering the stable aqueous environment operation of TiO_2 active channel films, we demonstrated the pH sensing behaviour using TiO_2 IGTs.

The compact and porous TiO_2 films were fabricated using evaporation and solution-processing methods. We employed two different ion-gating media, (i) pure ionic liquid and (ii) $[Li]^+$ ions in the ionic liquid. Compact TiO_2 films gated with pure ionic liquid show higher drain current, but the effect of additional $[Li]^+$ ions in the gating medium, doesn't significantly affect the electrical characteristics of compact evaporated films. Porous films gated with pure ionic liquid shows lower electrical performance as compared to compact films, but the performance is improved by the additional $[Li]^+$ ions in the gating medium. We found that the presence of $[Li]^+$ ions in the gating medium didn't significantly improve the charge carrier concentration. This effect is due to the complexity of ion arrangement at the electrical double layer, originating from the ionic interactions between ions. Currently, work is in progress to perform the cyclic voltammetry at a sufficiently low scan rate (10 to 100 μV/s) to gain insight into the $[Li]^+$ intercalation events on the TiO_2 surface. In the future, it would be beneficial to perform atomic force microscopy force–distance profiling to understand the ion arrangement at the electrical double layer. The IGTs (with ionic liquid) are stable in the wide operating temperature, so it would be interesting to study the effect of temperature on their response time.

We fabricated SnO_2 films on the PET substrates through controlled aqueous growth. We investigated the electrical characteristics of SnO_2 films in IGT configuration using ionic liquid and saline solution. The IGTs with ionic liquid and saline solution showed a mobility of 0.1 cm^2/Vs. The transistors under bending (curvature radius ~ 20 mm and ~ 10 mm) show no significant change in electrical characteristics when compared to unbent transistors, thus are attractive candidates for transparent and flexible electronics. We demonstrated clean-room free fabrication of source/drain metal contacts using a PCB printer. Printed source and drain electrodes, operating in aqueous electrolyte environments, makes our transistors sustainable. We believe that the device performance is affected by the limited stability of printed Ag electrodes, especially when in contact with the electrolyte under bias. Currently, work is in progress to protect the Ag electrodes with a printed protective layer to avoid exposure to the ion-gating medium to improve the stability. In the

future, it would be beneficial to fabricate SnO_2 films on silicone elastomer substrates to make suitable for the stretchable electronics.

We fabricated TiO_2 films by a sustainable (using green alcohol solvents) wet chemical approach using metal alkoxide and metal oxide nanoparticles. Initially, we processed the metal alkoxide based TiO_2 films on rigid substrate due to its high temperature processability. We compared the electrical characteristics of IGTs in ionic liquid and saline solution. The transistors gated with saline solution exhibits clearer saturation with higher drain-current. By considering the aqueous environment stable nature of TiO_2 IGTs, we employed TiO_2 IGTs for detecting pH of the analyte solution. We showed the pH sensitivity of TiO_2 IGT ~ 48 mV/pH. Later, by using the TiO_2 suspension (using TiO_2 nanoparticle), we deposited TiO_2 film on PET substrates at low temperatures (~120 ˚C) and demonstrated its electrical characteristics using ionic liquid as the gating media. The electrical characteristics under bending did not show any significant change making them useful for low cost, flexible, sustainable electronics.

Overall, our results demonstrate indium-free metal oxides for ion-gating transistors suitable for application in electronics such as, electrochromic displays, transparent displays, and sensors. Our first article provides fundamental insights into the TiO_2 channel interaction with ions in the gating media. This study may be useful in designing an electrochromic switch (bleach ↔ colored) display and smart windows, since TiO_2 is an electrochromic material. Our second article provides valuable insights for flexible display applications. By depositing transparent conducting metal oxide contacts (source, drain and gate) on the transparent and flexible SnO_2 deposited on PET substrates, and using solid electrolytes (avoids the leakage problem of the liquid electrolyte), it will be possible to make fully transparent and flexible SnO_2 based displays. Also, the demonstration of transistor operation under aqueous electrolytes paves the way for the biosensing applications. Our third article paves the way towards the realization of fully printed transistors, since the TiO_2 suspension can be printable on biodegradable substrates (paper substrate). Also, the conductive polymer (PEDOT:PSS) contacts and polyvinyl alcohol (PVA) gel gating medium can be printed on the paper substrate to fabricate fully printed transistors. This transistor design may be employed in disposable medical sensors.

REFERENCES

1. Ross, I. M., The foundation of the silicon age. *Bell Labs technical journal* **1997,** *2* (4), 3-14.

2. Thompson, S. E.; Parthasarathy, S., Moore's law: the future of Si microelectronics. *Materials today* **2006,** *9* (6), 20-25.

3. Hosono, H., How we made the IGZO transistor. *Nature Electronics* **2018,** *1* (7), 428-428.

4. Wager, J. F., Oxide TFTs: A progress report. *Information Display* **2016,** *32* (1), 16-21.

5. Wager, J. F., TFT Technology: Advancements and Opportunities for Improvement. *Information Display* **2020,** *36* (2), 9-13.

6. Martinez, J.; Piqueras, J., On the mobility of polycrystalline semiconductors. *Solid-State Electronics* **1980,** *23* (4), 297-303.

7. Ramirez, A. P., Oxide electronics emerge. *Science* **2007,** *315* (5817), 1377-1378.

8. Shi, J.; Zhang, J.; Yang, L.; Qu, M.; Qi, D.-C.; Zhang, K. H., Wide bandgap oxide semiconductors: from materials physics to optoelectronic devices. *Advanced Materials* **2021**, 2006230.

9. Nomura, K.; Ohta, H.; Takagi, A.; Kamiya, T.; Hirano, M.; Hosono, H., Room-temperature fabrication of transparent flexible thin-film transistors using amorphous oxide semiconductors. *nature* **2004,** *432* (7016), 488-492.

10. Zhu, Y.; He, Y.; Jiang, S.; Zhu, L.; Chen, C.; Wan, Q., Indium–gallium–zinc–oxide thin-film transistors: Materials, devices, and applications. *Journal of Semiconductors* **2021,** *42* (3), 031101.

11. Salvatore, G. A.; Münzenrieder, N.; Kinkeldei, T.; Petti, L.; Zysset, C.; Strebel, I.; Büthe, L.; Tröster, G., Wafer-scale design of lightweight and transparent electronics that wraps around hairs. *Nature communications* **2014,** *5* (1), 1-8.

12. Cantarella, G.; Vogt, C.; Hopf, R.; Münzenrieder, N.; Andrianakis, P.; Petti, L.; Daus, A.; Knobelspies, S.; Büthe, L.; Tröster, G., Buckled thin-film transistors and circuits on soft elastomers for stretchable electronics. *ACS applied materials & interfaces* **2017,** *9* (34), 28750-28757.

13. Münzenrieder, N.; Cantarella, G.; Vogt, C.; Petti, L.; Büthe, L.; Salvatore, G. A.; Fang, Y.; Andri, R.; Lam, Y.; Libanori, R., Stretchable and conformable oxide thin-film electronics. *Advanced Electronic Materials* **2015,** *1* (3), 1400038.

14. Rech, M., Rare earth elements and the European Union. In *The Political Economy of Rare Earth Elements*, Springer: 2015; pp 62-84.

15. Fortunato, E. M.; Pereira, L. M.; Barquinha, P. M.; Botelho do Rego, A. M.; Gonçalves, G.; Vilà, A.; Morante, J. R.; Martins, R. F., High mobility indium free amorphous oxide thin film transistors. *Applied Physics Letters* **2008,** *92* (22), 222103.

16. Ramarajan, R.; Joseph, D. P.; Thangaraju, K.; Kovendhan, M., Indium-Free Alternative Transparent Conducting Electrodes: An Overview and Recent Developments. *Metal and Metal Oxides for Energy and Electronics* **2021**, 149-183.

17. Liu, A.; Guo, Z.; Liu, G.; Zhu, C.; Zhu, H.; Shin, B.; Fortunato, E.; Martins, R.; Shan, F., Redox Chloride Elimination Reaction: Facile Solution Route for Indium-Free, Low-Voltage, and High-Performance Transistors. *Advanced Electronic Materials* **2017,** *3* (3), 1600513.

18. Edgar, L. J., Method and apparatus for controlling electric currents. Google Patents: 1930.

19. William, S., Circuit element utilizing semiconductive material. Google Patents: 1951.

20. Dawon, K., Electric field controlled semiconductor device. Google Patents: 1963.

21. Brattain, W.; Garrett, C., Experiments on the interface between germanium and an electrolyte. *Bell System Technical Journal* **1955,** *34* (1), 129-176.

22. Weimer, P. K., The TFT a new thin-film transistor. *Proceedings of the IRE* **1962,** *50* (6), 1462-1469.

23. Alferov, Z.; Kroemer, H.; Kilby, J., Nobel Prize in Physics 2000. 2000.

24. Apple. *https://www.apple.com/ca/apple-events/september-2021/?useASL=true* **2021**.

25. Park, J. W.; Kang, B. H.; Kim, H. J., A review of low-temperature solution-processed metal oxide thin-film transistors for flexible electronics. *Advanced Functional Materials* **2020,** *30* (20), 1904632.

26. Fortunato, E.; Barquinha, P.; Martins, R., Oxide semiconductor thin-film transistors: a review of recent advances. *Adv. Mater.* **2012,** *24* (22), 2945-2986.

27. Valitova, I. Electrolyte Gated Metal Oxide Transistors. Ecole Polytechnique, Montreal (Canada), 2017.

28. Jo, G.; Maeng, J.; Kim, T.-W.; Hong, W.-K.; Choi, B.-S.; Lee, T., Channel-length and gate-bias dependence of contact resistance and mobility for In 2 O 3 nanowire field effect transistors. *Journal of Applied Physics* **2007,** *102* (8), 084508.

29. Schroder, D. K., *Semiconductor material and device characterization*. John Wiley & Sons: 2015.

30. Thomas, S. R.; Pattanasattayavong, P.; Anthopoulos, T. D., Solution-processable metal oxide semiconductors for thin-film transistor applications. *Chemical Society Reviews* **2013,** *42* (16), 6910-6923.

31. Petti, L.; Münzenrieder, N.; Vogt, C.; Faber, H.; Büthe, L.; Cantarella, G.; Bottacchi, F.; Anthopoulos, T. D.; Tröster, G., Metal oxide semiconductor thin-film transistors for flexible electronics. *Applied Physics Reviews* **2016,** *3* (2), 021303.

32. Banger, K.; Yamashita, Y.; Mori, K.; Peterson, R.; Leedham, T.; Rickard, J.; Sirringhaus, H., Low-temperature, high-performance solution-processed metal oxide thin-film transistors formed by a 'sol–gel on chip'process. *Nature materials* **2011,** *10* (1), 45-50.

33. Petti, L., Metal Oxide Semiconductor Thin-Film Transistors for Flexible Electronics. *ETH Zurich* **2016,** *PhD Thesis*.

34. Song, J.; Huang, X.; Han, C.; Yu, Y.; Su, Y.; Lai, P., Recent Developments of Flexible InGaZnO Thin-Film Transistors. *physica status solidi (a)* **2021,** *218* (7), 2000527.

35. Garlapati, S. K.; Divya, M.; Breitung, B.; Kruk, R.; Hahn, H.; Dasgupta, S., Printed electronics based on inorganic semiconductors: From processes and materials to devices. *Advanced Materials* **2018,** *30* (40), 1707600.

36. Wang, B.; Thukral, A.; Xie, Z.; Liu, L.; Zhang, X.; Huang, W.; Yu, X.; Yu, C.; Marks, T. J.; Facchetti, A., Flexible and stretchable metal oxide nanofiber networks for multimodal and monolithically integrated wearable electronics. *Nature communications* **2020,** *11* (1), 1-11.

37. Liang, K.; Ren, H.; Li, D.; Wang, Y.; Tang, Y.; Zhao, M.; Wang, H.; Li, W.; Zhu, B., Fully-printed flexible n-type tin oxide thin-film transistors and logic circuits. *Journal of Materials Chemistry C* **2021**.

38. Shih, C. W.; Chin, A.; Lu, C. F.; Su, W. F., Remarkably high mobility ultra-thin-film metal-oxide transistor with strongly overlapped orbitals. *Scientific reports* **2016,** *6* (1), 1-6.

39. Huang, G.; Duan, L.; Dong, G.; Zhang, D.; Qiu, Y., High-mobility solution-processed tin oxide thin-film transistors with high-κ alumina dielectric working in enhancement mode. *ACS applied materials & interfaces* **2014,** *6* (23), 20786-20794.

40. Avis, C.; Billah, M. M.; Kim, Y. G.; Siddik, A. B.; Jang, J., Analysis of the Solution-Processed a-SnOX and HfO2 Interface for Applications in Thin-Film Transistors. *ACS Applied Electronic Materials* **2021**.

41. Wan, Q.; Dattoli, E.; Lu, W., Doping-Dependent Electrical Characteristics of SnO2 Nanowires. *small* **2008,** *4* (4), 451-454.

42. Sun, J.; Lu, A.; Wang, L.; Hu, Y.; Wan, Q., High-mobility transparent thin-film transistors with an Sb-doped SnO2 nanocrystal channel fabricated at room temperature. *Nanotechnology* **2009,** *20* (33), 335204.

43. Liang, D.-D.; Chen, B.; Cho, H. J.; Ohta, H., Thickness Optimization toward High-Performance Bottom-Gated Transparent Tin Dioxide Thin-Film Transistors. *ACS Applied Electronic Materials* **2020,** *2* (10), 3454-3458.

44. Liang, D.; Chen, B.-j.; Feng, B.; Ikuhara, Y.; Cho, H. J.; Ohta, H., Optimization of Two-Dimensional Channel Thickness in Nanometer-Thick SnO2-Based Top-Gated Thin-Film Transistors Using Electric Field Thermopower Modulation: Implications for Flat-Panel Displays. *ACS Applied Nano Materials* **2020**.

45. Lim, D.; Jeon, Y.; Kim, M.; Kim, Y.; Kim, S., Electrical characteristics of SnO2 thin-film transistors fabricated on bendable substrates using reactive magnetron sputtering. *Journal of Nanoscience and Nanotechnology* **2016,** *16* (11), 11697-11700.

46. Wei, H.; Ni, Y.; Sun, L.; Yu, H.; Gong, J.; Du, Y.; Ma, M.; Han, H.; Xu, W., Flexible electro-optical neuromorphic transistors with tunable synaptic plasticity and nociceptive behavior. *Nano Energy* **2021,** *81*, 105648.

47. Chen, X.; Selloni, A., Introduction: titanium dioxide (TiO2) nanomaterials. ACS Publications: 2014.

48. Zhong, N.; Cao, J. J.; Shima, H.; Akinaga, H., Effect of Annealing Temperature on $\hbox {TiO} _ {2} $-Based Thin-Film-Transistor Performance. *IEEE electron device letters* **2012,** *33* (7), 1009-1011.

49. Chong, H. Y.; Kim, T. W., Electrical characteristics of thin-film transistors fabricated utilizing a UV/ozone-treated TiO 2 channel layer. *Journal of electronic materials* **2013,** *42* (3), 398-402.

50. Yajima, T.; Oike, G.; Nishimura, T.; Toriumi, A., Independent control of phases and defects in TiO2 thin films for functional transistor channels. *physica status solidi (a)* **2016,** *213* (8), 2196-2202.

51. Zhang, J.; Zhang, Y.; Cui, P.; Lin, G.; Ni, C.; Zeng, Y., One-Volt TiO_2 Thin Film Transistors With Low-Temperature Process. *IEEE Electron Device Letters* **2021,** *42* (4), 521-524.

52. Valitova, I.; Kumar, P.; Meng, X.; Soavi, F.; Santato, C.; Cicoira, F., Photolithographically patterned TiO2 films for electrolyte-gated transistors. *ACS Appl. Mater. Interfaces* **2016,** *8* (23), 14855-14862.

53. Horita, R.; Ohtani, K.; Kai, T.; Murao, Y.; Nishida, H.; Toya, T.; Seo, K.; Sakai, M.; Okuda, T., Transport Properties of Anatase–TiO2 Polycrystalline-Thin-Film Field-Effect Transistors with Electrolyte Gate Layers. *Japanese Journal of Applied Physics* **2013,** *52* (11R), 115803.

54. Tiwale, N.; Subramanian, A.; Dai, Z.; Sikder, S.; Sadowski, J. T.; Nam, C.-Y., Large mobility modulation in ultrathin amorphous titanium oxide transistors. *Communications Materials* **2020,** *1* (1), 1-8.

55. Ribes, G.; Mitard, J.; Denais, M.; Bruyere, S.; Monsieur, F.; Parthasarathy, C.; Vincent, E.; Ghibaudo, G., Review on high-k dielectrics reliability issues. *IEEE Transactions on Device and materials Reliability* **2005,** *5* (1), 5-19.

56. Lin, H.; Ye, P.; Wilk, G., Leakage current and breakdown electric-field studies on ultrathin atomic-layer-deposited Al 2 O 3 on GaAs. *Applied physics letters* **2005,** *87* (18), 182904.

57. Huang, W.; Chen, J.; Wang, G.; Yao, Y.; Zhuang, X.; Pankow, R. M.; Cheng, Y.; Marks, T. J.; Facchetti, A., Dielectric materials for electrolyte gated transistor applications. *Journal of Materials Chemistry C* **2021,** *9* (30), 9348-9376.

58. Kim, S. H.; Hong, K.; Xie, W.; Lee, K. H.; Zhang, S.; Lodge, T. P.; Frisbie, C. D., Electrolyte-gated transistors for organic and printed electronics. *Advanced Materials* **2013,** *25* (13), 1822-1846.

59. Bisri, S. Z.; Shimizu, S.; Nakano, M.; Iwasa, Y., Endeavor of iontronics: from fundamentals to applications of ion-controlled electronics. *Advanced Materials* **2017,** *29* (25), 1607054.

60. Meng, X.; Quenneville, F.; Venne, F. d. r.; Di Mauro, E.; Işık, D.; Barbosa, M.; Drolet, Y.; Natile, M. M.; Rochefort, D.; Soavi, F., Electrolyte-gated WO3 transistors: electrochemistry, structure, and device performance. *The Journal of Physical Chemistry C* **2015,** *119* (37), 21732-21738.

61. Rivnay, J.; Inal, S.; Salleo, A.; Owens, R. M.; Berggren, M.; Malliaras, G. G., Organic electrochemical transistors. *Nature Reviews Materials* **2018,** *3* (2), 1-14.

62. Rawlings, D.; Thomas, E. M.; Segalman, R. A.; Chabinyc, M. L., Controlling the doping mechanism in poly (3-hexylthiophene) thin-film transistors with polymeric ionic liquid dielectrics. *Chemistry of Materials* **2019,** *31* (21), 8820-8829.

63. Thiemann, S.; Sachnov, S.; Porscha, S.; Wasserscheid, P.; Zaumseil, J., Ionic liquids for electrolyte-gating of ZnO field-effect transistors. *The Journal of Physical Chemistry C* **2012,** *116* (25), 13536-13544.

64. Hong, K.; Kim, S. H.; Lee, K. H.; Frisbie, C. D., Printed, sub-2V ZnO electrolyte gated transistors and inverters on plastic. *Advanced Materials* **2013,** *25* (25), 3413-3418.

65. Park, S.; Lee, S.; Kim, C.-H.; Lee, I.; Lee, W.-J.; Kim, S.; Lee, B.-G.; Jang, J.-H.; Yoon, M.-H., Sub-0.5 V highly stable aqueous salt gated metal oxide electronics. *Scientific reports* **2015,** *5*, 13088.

66. Nasr, B.; Wang, D.; Kruk, R.; Rösner, H.; Hahn, H.; Dasgupta, S., High-speed, low-voltage, and environmentally stable operation of electrochemically gated zinc oxide nanowire field-effect transistors. *Advanced Functional Materials* **2013,** *23* (14), 1750-1758.

67. Herlogsson, L.; Crispin, X.; Robinson, N. D.; Sandberg, M.; Hagel, O. J.; Gustafsson, G.; Berggren, M., Low-voltage polymer field-effect transistors gated via a proton conductor. *Advanced Materials* **2007,** *19* (1), 97-101.

68. Zhang, B.; Liu, Y.; Agarwal, S.; Yeh, M.-L.; Katz, H. E., Structure, sodium ion role, and practical issues for β-alumina as a high-k solution-processed gate layer for transparent and low-voltage electronics. *ACS applied materials & interfaces* **2011,** *3* (11), 4254-4261.

69. Torricelli, F.; Adrahtas, D. Z.; Bao, Z.; Berggren, M.; Biscarini, F.; Bonfiglio, A.; Bortolotti, C. A.; Frisbie, C. D.; Macchia, E.; Malliaras, G. G., Electrolyte-gated transistors for enhanced performance bioelectronics. *Nature Reviews Methods Primers* **2021,** *1* (1), 1-24.

70. Baby, T. T.; Garlapati, S. K.; Dehm, S.; Häming, M.; Kruk, R.; Hahn, H.; Dasgupta, S., A general route toward complete room temperature processing of printed and high performance oxide electronics. *ACS nano* **2015,** *9* (3), 3075-3083.

71. Garlapati, S. K.; Gebauer, J. S.; Dehm, S.; Bruns, M.; Winterer, M.; Hahn, H.; Dasgupta, S., Room-temperature processing of printed oxide FETs using ultraviolet photonic curing. *Advanced Electronic Materials* **2017,** *3* (9), 1600476.

72. Zare Bidoky, F.; Tang, B.; Ma, R.; Jochem, K. S.; Hyun, W. J.; Song, D.; Koester, S. J.; Lodge, T. P.; Frisbie, C. D., Sub-3 V ZnO Electrolyte-Gated Transistors and Circuits with Screen-Printed and Photo-Crosslinked Ion Gel Gate Dielectrics: New Routes to Improved Performance. *Advanced Functional Materials* **2019**, 1902028.

73. Liu, N.; Chen, R.; Wan, Q., Recent Advances in Electric-Double-Layer Transistors for Bio-Chemical Sensing Applications. *Sensors* **2019,** *19* (15), 3425.

74. Yarali, E.; Koutsiaki, C.; Faber, H.; Tetzner, K.; Yengel, E.; Patsalas, P.; Kalfagiannis, N.; Koutsogeorgis, D. C.; Anthopoulos, T. D., Recent Progress in Photonic Processing of Metal-Oxide Transistors. *Advanced Functional Materials* **2020,** *30* (20), 1906022.

75. Bretos, I.; Diodati, S.; Jimenez, R.; Tajoli, F.; Ricote, J.; Bragaggia, G.; Franca, M.; Calzada, M. L.; Gross, S., Low-temperature solution crystallization of nanostructured oxides and thin films. *Chemistry–A European Journal* **2020**.

76. Bandiello, E.; Sessolo, M.; Bolink, H. J., Aqueous electrolyte-gated ZnO transistors for environmental and biological sensing. *Journal of Materials Chemistry C* **2014,** *2* (48), 10277-10281.

77. Manjakkal, L.; Szwagierczak, D.; Dahiya, R., Metal oxides based electrochemical pH sensors: Current progress and future perspectives. *Progress in Materials Science* **2020,** *109*, 100635.

78. Limo, M. J.; Sola-Rabada, A.; Boix, E.; Thota, V.; Westcott, Z. C.; Puddu, V.; Perry, C. C., Interactions between metal oxides and biomolecules: from fundamental understanding to applications. *Chemical reviews* **2018,** *118* (22), 11118-11193.

79. Nunes, D.; Pimentel, A.; Gonçalves, A.; Pereira, S.; Branquinho, R.; Barquinha, P.; Fortunato, E.; Martins, R., Metal oxide nanostructures for sensor applications. *Semiconductor Science and Technology* **2019,** *34* (4), 043001.

80. Ghoneim, M.; Nguyen, A.; Dereje, N.; Huang, J.; Moore, G.; Murzynowski, P.; Dagdeviren, C., Recent progress in electrochemical pH-sensing materials and configurations for biomedical applications. *Chemical reviews* **2019,** *119* (8), 5248-5297.

81. Bollinger, A. T.; Dubuis, G.; Leng, X.; He, X.; Božović, I., Electrolyte-Gated Oxides. *Journal of Superconductivity and Novel Magnetism* **2020,** *33* (1), 223-228.

82. Ishikawa, F. N.; Chang, H.-K.; Curreli, M.; Liao, H.-I.; Olson, C. A.; Chen, P.-C.; Zhang, R.; Roberts, R. W.; Sun, R.; Cote, R. J., Label-free, electrical detection of the SARS virus N-protein with nanowire biosensors utilizing antibody mimics as capture probes. *ACS nano* **2009,** *3* (5), 1219-1224.

83. Rim, Y. S.; Bae, S.-H.; Chen, H.; Yang, J. L.; Kim, J.; Andrews, A. M.; Weiss, P. S.; Yang, Y.; Tseng, H.-R., Printable ultrathin metal oxide semiconductor-based conformal biosensors. *ACS nano* **2015,** *9* (12), 12174-12181.

84. Chang, H.-K.; Ishikawa, F. N.; Zhang, R.; Datar, R.; Cote, R. J.; Thompson, M. E.; Zhou, C., Rapid, label-free, electrical whole blood bioassay based on nanobiosensor systems. *ACS nano* **2011,** *5* (12), 9883-9891.

85. Liu, Q.; Liu, Y.; Wu, F.; Cao, X.; Li, Z.; Alharbi, M.; Abbas, A. N.; Amer, M. R.; Zhou, C., Highly sensitive and wearable In2O3 nanoribbon transistor biosensors with integrated on-chip gate for glucose monitoring in body fluids. *ACS nano* **2018,** *12* (2), 1170-1178.

86. Alqahtani, Z.; Alghamdi, N.; Grell, M., Monitoring the lead-and-copper rule with a water-gated field effect transistor. *Journal of water and health* **2020,** *18* (2), 159-171.

87. Alghamdi, N.; Alqahtani, Z.; Zhou, C.; Sano, N.; Conte, M.; Grell, M., Sensing aromatic pollutants in water with catalyst-sensitized water-gated transistor.

88. Subramanian, A.; George, B.; Bobbara, S. R.; Valitova, I.; Ruggeri, I.; Borghi, F.; Podestà, A.; Milani, P.; Soavi, F.; Santato, C., Ion-gated transistors based on porous and compact TiO2 films: Effect of Li ions in the gating medium. *AIP Advances* **2020,** *10* (6), 065314.

89. Subramanian, A.; Azimi, M.; Santato, C.; Cicoira, F., Combining Aqueous Solution Processing and Printing for Fabrication of Flexible and Sustainable Tin Dioxide Ion-Gated Transistors. *Advanced Materials Technologies* **2021**, 2100843.

90. Vayssieres, L.; Graetzel, M., Highly ordered SnO2 nanorod arrays from controlled aqueous growth. *Angewandte Chemie International Edition* **2004,** *43* (28), 3666-3670.

91. Vayssieres, L.; Beermann, N.; Lindquist, S.-E.; Hagfeldt, A., Controlled aqueous chemical growth of oriented three-dimensional crystalline nanorod arrays: Application to iron (III) oxides. *Chemistry of materials* **2001,** *13* (2), 233-235.

92. Liu, C.; Tian, Q.; Liao, L., 4 - Sol–gel precursor inks and films. In *Solution Processed Metal Oxide Thin Films for Electronic Applications*, Cui, Z.; Korotcenkov, G., Eds. Elsevier: 2020; pp 41-61.

93. Arunprabaharan Subramanian, M. A., Cheng Yee Leong, Siew Ling Lee, Clara Santato, Fabio Cicoira, Solution-processed titanium dioxide ion-gated transistors (IGTs) and pH sensors using ionic liquid and aqueous saline solution. *Frontiers In Electronics* **2021,** *Submission ID: 813535*.

94. Luo, Q., 5 - Nanoparticles inks. In *Solution Processed Metal Oxide Thin Films for Electronic Applications*, Cui, Z.; Korotcenkov, G., Eds. Elsevier: 2020; pp 63-82.

95. Bormashenko, E.; Bormashenko, Y.; Frenkel, M., Formation of Hierarchical Porous Films with Breath-Figures Self-Assembly Performed on Oil-Lubricated Substrates. *Materials* **2019,** *12* (18), 3051.

96. Kandjani, S. A.; Mirershadi, S.; Nikniaz, A., Inorganic–organic perovskite solar cells. *Solar Cells-New Approaches and Reviews* **2015,** *10*, 58970.

97. Bashir, A.; Awan, T. I.; Tehseen, A.; Tahir, M. B.; Ijaz, M., Chapter 3 - Interfaces and surfaces. In *Chemistry of Nanomaterials*, Awan, T. I.; Bashir, A.; Tehseen, A., Eds. Elsevier: 2020; pp 51-87.

98. Ashkenaz, D. E.; Paige Hall, W.; Haynes, C. L.; Hicks, E. M.; McFarland, A. D.; Sherry, L. J.; Stuart, D. A.; Wheeler, K. E.; Yonzon, C. R.; Zhao, J., Coffee cup atomic force microscopy. *Journal of Chemical Education* **2010,** *87* (3), 306-307.

99. Cazaux, J., Recent developments and new strategies in scanning electron microscopy. *Journal of microscopy* **2005,** *217* (1), 16-35.

100. Danilatos, G. D., Foundations of Environmental Scanning Electron Microscopy. In *Advances in Electronics and Electron Physics*, Hawkes, P. W., Ed. Academic Press: 1988; Vol. 71, pp 109-250.

101. Ermrich, M.; Opper, D., XRD for the analyst. *Getting acquainted with the principles. Second. Panalytical* **2013**.

102. Elgrishi, N.; Rountree, K. J.; McCarthy, B. D.; Rountree, E. S.; Eisenhart, T. T.; Dempsey, J. L., A practical beginner's guide to cyclic voltammetry. *Journal of chemical education* **2018,** *95* (2), 197-206.

103. Colburn, A. W.; Levey, K. J.; O'Hare, D.; Macpherson, J. V., Lifting the lid on the potentiostat: a beginner's guide to understanding electrochemical circuitry and practical operation. *Physical Chemistry Chemical Physics* **2021,** *23* (14), 8100-8117.

104. Sayago, J.; Soavi, F.; Sivalingam, Y.; Cicoira, F.; Santato, C., Low voltage electrolyte-gated organic transistors making use of high surface area activated carbon gate electrodes. *Journal of Materials Chemistry C* **2014,** *2* (28), 5690-5694.

105. Braga, D.; Ha, M.; Xie, W.; Frisbie, C. D., Ultralow contact resistance in electrolyte-gated organic thin film transistors. *Applied Physics Letters* **2010,** *97* (19), 245.

106. Yu, X.; Marks, T. J.; Facchetti, A., Metal oxides for optoelectronic applications. *Nature materials* **2016,** *15* (4), 383.

107. Xu, W.; Li, H.; Xu, J.-B.; Wang, L., Recent advances of solution-processed metal oxide thin-film transistors. *ACS applied materials & interfaces* **2018,** *10* (31), 25878-25901.

108. Tachikawa, T.; Majima, T., Metal oxide mesocrystals with tailored structures and properties for energy conversion and storage applications. *NPG Asia Materials* **2014,** *6* (5), e100-e100.

109. Park, J. W.; Kang, B. H.; Kim, H. J., A Review of Low-Temperature Solution-Processed Metal Oxide Thin-Film Transistors for Flexible Electronics. *Adv. Funct. Mater.* **2019**, 1904632.

110. Leighton, C., Electrolyte-based ionic control of functional oxides. *Nature materials* **2019,** *18* (1), 13.

111. Sheng, J.; Hong, T.; Lee, H.-M.; Kim, K.; Sasase, M.; Kim, J.; Hosono, H.; Park, J.-S., Amorphous IGZO TFT with High Mobility of~ 70 cm2/Vs via Vertical Dimension Control using PEALD. *ACS Appl. Mater. Interfaces* **2019**.

112. Cantarella, G.; Münzenrieder, N.; Petti, L.; Vogt, C.; Büthe, L.; Salvatore, G.; Daus, A.; Tröster, G., Flexible In–Ga–Zn–O thin-film transistors on elastomeric substrate bent to 2.3% strain. *IEEE Electron Device Letters* **2015,** *36* (8), 781-783.

113. Cantarella, G.; Costanza, V.; Ferrero, A.; Hopf, R.; Vogt, C.; Varga, M.; Petti, L.; Münzenrieder, N.; Büthe, L.; Salvatore, G., Design of engineered elastomeric substrate for stretchable active devices and sensors. *Adv. Funct. Mater.* **2018,** *28* (30), 1705132.

114. Nomura, K.; Ohta, H.; Takagi, A.; Kamiya, T.; Hirano, M.; Hosono, H., Room-temperature fabrication of transparent flexible thin-film transistors using amorphous oxide semiconductors. *Nature* **2004,** *432* (7016), 488.

115. Garlapati, S. K.; Mishra, N.; Dehm, S.; Hahn, R.; Kruk, R.; Hahn, H.; Dasgupta, S., Electrolyte-gated, high mobility inorganic oxide transistors from printed metal halides. *ACS Appl. Mater. Interfaces* **2013,** *5* (22), 11498-11502.

116. Shih, C. W.; Chin, A., Remarkably high mobility thin-film transistor on flexible substrate by novel passivation material. *Scientific reports* **2017,** *7* (1), 1147.

117. Shih, C. W.; Chin, A.; Lu, C. F.; Su, W. F., Remarkably high mobility ultra-thin-film metal-oxide transistor with strongly overlapped orbitals. *Scientific reports* **2016,** *6*, 19023.

118. Kim, S. Y.; Ahn, C. H.; Lee, J. H.; Kwon, Y. H.; Hwang, S.; Lee, J. Y.; Cho, H. K., p-Channel oxide thin film transistors using solution-processed copper oxide. *ACS Appl. Mater. Interfaces* **2013,** *5* (7), 2417-2421.

119. Liu, A.; Zhu, H.; Guo, Z.; Meng, Y.; Liu, G.; Fortunato, E.; Martins, R.; Shan, F., Solution Combustion Synthesis: Low-Temperature Processing for p-Type Cu: NiO Thin Films for Transparent Electronics. *Adv. Mater.* **2017,** *29* (34), 1701599.

120. Shih, W.; Young, S.; Ji, L.; Water, W.; Shiu, H., TiO2-based thin film transistors with amorphous and anatase channel layer. *Journal of The Electrochemical Society* **2011,** *158* (6), H609-H611.

121. Valitova, I.; Natile, M. M.; Soavi, F.; Santato, C.; Cicoira, F., Tin dioxide electrolyte-gated transistors working in depletion and enhancement modes. *ACS applied materials & interfaces* **2017,** *9* (42), 37013-37021.

122. Schladt, T. D.; Graf, T.; Aetukuri, N. B.; Li, M.; Fantini, A.; Jiang, X.; Samant, M. G.; Parkin, S. S., Crystal-facet-dependent metallization in electrolyte-gated rutile TiO2 single crystals. *ACS nano* **2013,** *7* (9), 8074-8081.

123. Han, Y.-L.; Luo, Z.-Z.; Li, C.-J.; Shen, S.-C.; Qu, G.-L.; Xiong, C.-M.; Dou, R.-F.; He, L.; Nie, J.-C., Carrier-mediated Kondo effect and Hall mobility by electrolyte gating in slightly doped anatase TiO 2 films. *PhRvB* **2014,** *90* (20), 205107.

124. Peng, W.-C.; Chen, Y.-C.; He, J.-L.; Ou, S.-L.; Horng, R.-H.; Wuu, D.-S., Tunability of p-and n-channel TiO x thin film transistors. *Scientific reports* **2018,** *8* (1), 9255.

125. Chung, S. M.; Shin, J.-H.; Hong, C.-H.; Cheong, W.-S., Thin Film Transistor Based on TiOx Prepared by DC Magnetron Sputtering. *Journal of nanoscience and nanotechnology* **2012,** *12* (7), 5440-5443.

126. Choi, H.; Shin, J.; Shin, C., Impact of source/drain metal work function on the electrical characteristics of anatase TiO2-based thin film transistors. *ECS Journal of Solid State Science and Technology* **2017,** *6* (7), P379-P382.

127. Tian, J.; Zhao, Z.; Kumar, A.; Boughton, R. I.; Liu, H., Recent progress in design, synthesis, and applications of one-dimensional TiO2 nanostructured surface heterostructures: a review. *Chemical Society Reviews* **2014,** *43* (20), 6920-6937.

128. Weir, A.; Westerhoff, P.; Fabricius, L.; Hristovski, K.; Von Goetz, N., Titanium dioxide nanoparticles in food and personal care products. *Environmental science & technology* **2012,** *46* (4), 2242-2250.

129. Fujimoto, T.; Awaga, K., Electric-double-layer field-effect transistors with ionic liquids. *Physical Chemistry Chemical Physics* **2013,** *15* (23), 8983-9006.

130. Du, H.; Lin, X.; Xu, Z.; Chu, D., Electric double-layer transistors: a review of recent progress. *JMatS* **2015,** *50* (17), 5641-5673.

131. Yuan, H.; Shimotani, H.; Ye, J.; Yoon, S.; Aliah, H.; Tsukazaki, A.; Kawasaki, M.; Iwasa, Y., Electrostatic and electrochemical nature of liquid-gated electric-double-layer transistors based on oxide semiconductors. *Journal of the American Chemical Society* **2010,** *132* (51), 18402-18407.

132. Barbosa, M.; Oliveira, F. M.; Meng, X.; Soavi, F.; Santato, C.; Orlandi, M., Tungsten oxide ion gel-gated transistors: how structural and electrochemical properties affect the doping mechanism. *Journal of Materials Chemistry C* **2018,** *6* (8), 1980-1987.

133. Yuen, J. D.; Dhoot, A. S.; Namdas, E. B.; Coates, N. E.; Heeney, M.; McCulloch, I.; Moses, D.; Heeger, A. J., Electrochemical doping in electrolyte-gated polymer transistors. *Journal of the American Chemical Society* **2007,** *129* (46), 14367-14371.

134. Moitzheim, S.; De Gendt, S.; Vereecken, P., Investigation of the Li-Ion Insertion Mechanism for Amorphous and Anatase TiO2 Thin-Films. *Journal of The Electrochemical Society* **2019,** *166* (2), A1-A9.

135. Lindström, H.; Södergren, S.; Solbrand, A.; Rensmo, H.; Hjelm, J.; Hagfeldt, A.; Lindquist, S.-E., Li+ ion insertion in TiO2 (anatase). 2. Voltammetry on nanoporous films. *The Journal of Physical Chemistry B* **1997,** *101* (39), 7717-7722.

136. Granqvist, C. G., *Handbook of inorganic electrochromic materials*. Elsevier: 1995.

137. Silva, G. V. D. O.; Subramanian, A.; Meng, X.; Zhang, S.; Barbosa, M. S.; Baloukas, B.; Chartrand, D.; Gonzáles, J. C.; Orlandi, M. O.; Soavi, F., Tungsten oxide ion-gated phototransistors using ionic liquid and aqueous gating media. *Journal of Physics D: Applied Physics* **2019,** *52* (30), 305102.

138. Katayama, M.; Ikesaka, S.; Kuwano, J.; Koinuma, H.; Matsumoto, Y., High quality anatase Ti O 2 film: Field-effect transistor based on anatase Ti O 2. *Applied Physics Letters* **2008,** *92* (13), 132107.

139. Park, J.-W.; Yoo, S., New n-Type $\hbox {TiO} _ {2} $ Transparent Active Channel TFTs Fabricated With a Solution Process. *IEEE electron device letters* **2008,** *29* (7), 724-727.

140. Oike, G.; Yajima, T.; Nishimura, T.; Nagashio, K.; Toriumi, A. In *High electron mobility (> 16 cm 2/V sec) FETs with high on/off ratio (> 10 6) and highly conductive films (σ> 10 2 S/cm) by chemical doping in very thin (∼ 20 nm) TiO 2 films on thermally grown SiO 2*, 2013 IEEE International Electron Devices Meeting, IEEE: 2013; pp 11.5. 1-11.5. 4.

141. Choi, K.-H.; Kim, H.-K., Fabrication of transparent TiO2− x channel-based thin film transistors using an oxygen-deficient TiO2− x target. *Electrochem. Solid-State Lett.* **2011,** *14* (8), H314-H317.

142. Eslamian, M.; Zabihi, F., Ultrasonic substrate vibration-assisted drop casting (SVADC) for the fabrication of photovoltaic solar cell arrays and thin-film devices. *Nanoscale research letters* **2015,** *10* (1), 462.

143. Wahl, A.; Augustynski, J., Charge carrier transport in nanostructured anatase TiO2 films assisted by the self-doping of nanoparticles. *The Journal of Physical Chemistry B* **1998,** *102* (40), 7820-7828.

144. Schwellberger Barbosa, M.; Balke, N.; Tsai, W.-Y.; Santato, C.; Orlandi, M. O., On the Structure of the Electrical Double Layer at the Interface between an Ionic Liquid and Tungsten Oxide in Ion-Gated Transistors. *The Journal of Physical Chemistry Letters* **2020**.

145. Jo, J.-W.; Kang, S.-H.; Heo, J. S.; Kim, Y.-H.; Park, S. K., Flexible metal oxide semiconductor devices made by solution methods. *Chemistry–A European Journal* **2020**.

146. Rim, Y. S., Review of metal oxide semiconductors-based thin-film transistors for point-of-care sensor applications. *Journal of Information Display* **2020,** *21* (4), 203-210.

147. Leighton, C., Electrolyte-based ionic control of functional oxides. *Nature Materials* **2019,** *18* (1), 13-18.

148. Troughton, J.; Atkinson, D., Amorphous InGaZnO and metal oxide semiconductor devices: an overview and current status. *Journal of Materials Chemistry C* **2019,** *7* (40), 12388-12414.

149. Baran, D.; Corzo, D.; Blazquez, G. T., Flexible Electronics: Status, Challenges and Opportunities. *Frontiers in Electronics* **2020,** *1*, 2.

150. Asare, J.; Agyei-Tuffour, B.; Amonoo, E. A.; Dodoo-Arhin, D.; Nyankson, E.; Mensah, B.; Oyewole, O. O.; Yaya, A.; Onwona-Agyeman, B., Effects of substrates on the performance of optoelectronic devices: A review. *Cogent Engineering* **2020,** *7* (1), 1829274.

151. Zardetto, V.; Brown, T. M.; Reale, A.; Di Carlo, A., Substrates for flexible electronics: A practical investigation on the electrical, film flexibility, optical, temperature, and solvent resistance properties. *Journal of Polymer Science Part B: Polymer Physics* **2011,** *49* (9), 638-648.

152. Jenifer, K.; Arulkumar, S.; Parthiban, S.; Kwon, J., A Review on the Recent Advancements in Tin Oxide-Based Thin-Film Transistors for Large-Area Electronics. *Journal of Electronic Materials* **2020**, 1-14.

153. Orlandi, M. O., Tin oxide materials. In *Tin Oxide Materials*, Elsevier: 2020; pp 1-9.

154. Scheideler, W.; Subramanian, V., Printed flexible and transparent electronics: enhancing low-temperature processed metal oxides with 0D and 1D nanomaterials. *Nanotechnology* **2019,** *30* (27), 272001.

155. Sharma, A.; Ahmed, A.; Singh, A.; Oruganti, S.; Khosla, A.; Arya, S., Recent Advances in Tin Oxide Nanomaterials as Electrochemical/Chemiresistive Sensors. *Journal of the Electrochemical Society* **2021**.

156. Das, S.; Jayaraman, V., SnO2: A comprehensive review on structures and gas sensors. *Progress in Materials Science* **2014,** *66*, 112-255.

157. Liu, Q.; Qin, M. C.; Ke, W. J.; Zheng, X. L.; Chen, Z.; Qin, P. L.; Xiong, L. B.; Lei, H. W.; Wan, J. W.; Wen, J., Enhanced Stability of Perovskite Solar Cells with Low-Temperature Hydrothermally Grown SnO2 Electron Transport Layers. *Advanced Functional Materials* **2016,** *26* (33), 6069-6075.

158. Zhang, L.; Xu, W.; Liu, W.; Cao, P.; Han, S.; Zhu, D.; Lu, Y., Structural, chemical, optical, and electrical evolution of solution-processed SnO2 films and their applications in thin-film transistors. *Journal of Physics D: Applied Physics* **2020,** *53* (17), 175106.

159. Cao, H.; Liang, L., Tin oxide-based thin-film transistors and their circuits. In *Tin Oxide Materials*, Elsevier: 2020; pp 441-476.

160. Gunkel, F.; Christensen, D. V.; Chen, Y.; Pryds, N., Oxygen vacancies: The (in) visible friend of oxide electronics. *Applied Physics Letters* **2020,** *116* (12), 120505.

161. Dattoli, E. N.; Wan, Q.; Guo, W.; Chen, Y.; Pan, X.; Lu, W., Fully transparent thin-film transistor devices based on SnO2 nanowires. *Nano letters* **2007,** *7* (8), 2463-2469.

162. Jang, B.; Kang, H.; Lee, W.-Y.; Bae, J.-H.; Kang, I.-M.; Kim, K.; Kwon, H.-J.; Jang, J., Enhancement Mode Flexible SnO 2 Thin Film Transistors Via a UV/Ozone-Assisted Sol-Gel Approach. *IEEE Access* **2020,** *8*, 123013-123018.

163. Shin, G.; Yoon, C. H.; Bae, M. Y.; Kim, Y. C.; Hong, S. K.; Rogers, J. A.; Ha, J. S., Stretchable Field-Effect-Transistor Array of Suspended SnO2 Nanowires. *Small* **2011,** *7* (9), 1181-1185.

164. Liu, H.; Tan, R., Fabrication of Flexible In-Plane Gate Nanowire Transistor on a Paper Substrate. *Journal of nanoscience and nanotechnology* **2021,** *21* (9), 4857-4860.

165. Bu, X.; Xu, H.; Shang, D.; Li, Y.; Lv, H.; Liu, Q., Ion-Gated Transistor: An Enabler for Sensing and Computing Integration. *Advanced Intelligent Systems* **2020,** *2* (12), 2000156.

166. Lee, S.; Park, S.; Kim, C.-H.; Yoon, M.-H., Approaching the Nernst Detection Limit in an Electrolyte-Gated Metal Oxide Transistor. *IEEE Electron Device Letters* **2020,** *42* (1), 50-53.

167. Singaraju, S. A.; Baby, T. T.; Neuper, F.; Kruk, R.; Hagmann, J. A.; Hahn, H.; Breitung, B., Development of fully printed electrolyte-gated oxide transistors using graphene passive structures. *ACS Applied Electronic Materials* **2019,** *1* (8), 1538-1544.

168. Yang, J. T.; Ge, C.; Du, J. Y.; Huang, H. Y.; He, M.; Wang, C.; Lu, H. B.; Yang, G. Z.; Jin, K. J., Artificial synapses emulated by an electrolyte-gated tungsten-oxide transistor. *Advanced Materials* **2018,** *30* (34), 1801548.

169. Cramer, T.; Campana, A.; Leonardi, F.; Casalini, S.; Kyndiah, A.; Murgia, M.; Biscarini, F., Water-gated organic field effect transistors–opportunities for biochemical sensing and extracellular signal transduction. *Journal of Materials Chemistry B* **2013,** *1* (31), 3728-3741.

170. Singh, M.; Mulla, M. Y.; Santacroce, M. V.; Magliulo, M.; Di Franco, C.; Manoli, K.; Altamura, D.; Giannini, C.; Cioffi, N.; Palazzo, G., Effect of the gate metal work function on water-gated ZnO thin-film transistor performance. *Journal of Physics D: Applied Physics* **2016,** *49* (27), 275101.

171. Kergoat, L.; Battaglini, N.; Miozzo, L.; Piro, B.; Pham, M.-C.; Yassar, A.; Horowitz, G., Use of poly (3-hexylthiophene)/poly (methyl methacrylate)(P3HT/PMMA) blends to improve the performance of water-gated organic field-effect transistors. *Organic Electronics* **2011,** *12* (7), 1253-1257.

172. Alghamdi, N.; Alqahtani, Z.; Grell, M., Sub-nanomolar detection of cesium with water-gated transistor. *Journal of Applied Physics* **2019,** *126* (6), 064502.

173. Alqahtani, Z.; Alghamdi, N.; Robshaw, T. J.; Dawson, R.; Ogden, M. D.; Buckely, A.; Grell, M., Water-Gated Transistor Using Ion Exchange Resin for Potentiometric Fluoride Sensing. *Micromachines* **2020,** *11* (10), 923.

174. Alghamdi, N.; Alqahtani, Z.; Zhou, C.; Sano, N.; Conte, M.; Grell, M., Sensing aromatic pollutants in water with catalyst-sensitized water-gated transistor. *Chemical Papers* **2020,** *74*, 4169-4180.

175. Paulsen, B. D.; Frisbie, C. D., Dependence of conductivity on charge density and electrochemical potential in polymer semiconductors gated with ionic liquids. *The Journal of Physical Chemistry C* **2012,** *116* (4), 3132-3141.

176. Xia, Y.; Cho, J.; Paulsen, B.; Frisbie, C. D.; Renn, M. J., Correlation of on-state conductance with referenced electrochemical potential in ion gel gated polymer transistors. *Applied Physics Letters* **2009,** *94* (1), 4.

177. Tucic, A.; Marinkovic, Z.; Mancic, L.; Cilense, M.; Miloševic, O., Pyrosol preparation and structural characterization of SnO2 thin films. *Journal of materials processing technology* **2003,** *143*, 41-45.

178. Priyadarshini, D.; Mannam, R.; Rao, M. R.; DasGupta, N., Effect of annealing ambient on SnO2 thin film transistors. *Applied Surface Science* **2017,** *418*, 414-417.

179. Presley, R.; Munsee, C.; Park, C.; Hong, D.; Wager, J.; Keszler, D., Tin oxide transparent thin-film transistors. *Journal of Physics D: Applied Physics* **2004,** *37* (20), 2810.

180. Robin, M.; Portilla, L.; Wei, M.; Gao, T.; Zhao, J.; Shao, S.; Pecunia, V.; Cui, Z., Overcoming electrochemical instabilities of printed silver electrodes in all-printed ion gel gated carbon nanotube thin-film transistors. *ACS applied materials & interfaces* **2019,** *11* (44), 41531-41543.

181. Rim, Y. S., Review of metal oxide semiconductors-based thin-film transistors for point-of-care sensor applications. *Journal of Information Display* **2020**, 1-8.

182. Yoo, H.; Lee, I. S.; Jung, S.; Rho, S. M.; Kang, B. H.; Kim, H. J., A Review of Phototransistors Using Metal Oxide Semiconductors: Research Progress and Future Directions. *Advanced Materials* **2021**, 2006091.

183. Papac, M.; Stevanović, V.; Zakutayev, A.; O'Hayre, R., Triple ionic–electronic conducting oxides for next-generation electrochemical devices. *Nature Materials* **2021,** *20* (3), 301-313.

184. Tiwari, N.; Nirmal, A.; Kulkarni, M. R.; John, R. A.; Mathews, N., Enabling high performance n-type metal oxide semiconductors at low temperatures for thin film transistors. *Inorganic Chemistry Frontiers* **2020,** *7* (9), 1822-1844.

185. Cadilha Marques, G.; Weller, D.; Erozan, A. T.; Feng, X.; Tahoori, M.; Aghassi-Hagmann, J., Progress Report on "From Printed Electrolyte-Gated Metal-Oxide Devices to Circuits". *Advanced Materials* **2019,** *31* (26), 1806483.

186. Ji, D.; Jang, J.; Park, J. H.; Kim, D.; Rim, Y. S.; Hwang, D. K.; Noh, Y.-Y., Recent progress in the development of backplane thin film transistors for information displays. *Journal of Information Display* **2021,** *22* (1), 1-11.

187. Ramarajan, R.; Joseph, D. P.; Thangaraju, K.; Kovendhan, M., Indium-Free Alternative Transparent Conducting Electrodes: An Overview and Recent Developments. *Metal and Metal Oxides for Energy and Electronics* **2020**, 149-183.

188. Sedki, M.; Shen, Y.; Mulchandani, A., Nano-FET-enabled biosensors: Materials perspective and recent advances in North America. *Biosensors and Bioelectronics* **2020**, 112941.

189. Şerban, I.; Enesca, A., Metal oxides-based semiconductors for biosensors applications. *Frontiers in Chemistry* **2020,** *8*, 354.

190. Anitha, V.; Banerjee, A. N.; Joo, S. W., Recent developments in TiO 2 as n-and p-type transparent semiconductors: synthesis, modification, properties, and energy-related applications. *Journal of materials science* **2015,** *50* (23), 7495-7536.

191. Moonen, P. F.; Yakimets, I.; Huskens, J., Fabrication of transistors on flexible substrates: from mass-printing to high-resolution alternative lithography strategies. *Advanced materials* **2012,** *24* (41), 5526-5541.

192. Baeg, K. J.; Lee, J., Flexible electronic systems on plastic substrates and textiles for smart wearable technologies. *Advanced Materials Technologies* **2020,** *5* (7), 2000071.

193. Griffin, J. M., A gateway to understanding confined ions. *Nature Nanotechnology* **2020,** *15* (8), 628-629.

194. Laiho, A.; Herlogsson, L.; Forchheimer, R.; Crispin, X.; Berggren, M., Controlling the dimensionality of charge transport in organic thin-film transistors. *Proceedings of the National Academy of Sciences* **2011,** *108* (37), 15069-15073.

195. Sood, A.; Poletayev, A. D.; Cogswell, D. A.; Csernica, P. M.; Mefford, J. T.; Fraggedakis, D.; Toney, M. F.; Lindenberg, A. M.; Bazant, M. Z.; Chueh, W. C., Electrochemical ion insertion from the atomic to the device scale. *Nature Reviews Materials* **2021**, 1-21.

196. Bu, X.; Xu, H.; Shang, D.; Li, Y.; Lv, H.; Liu, Q., Ion-Gated Transistor: An Enabler for Sensing and Computing Integration. *Advanced Intelligent Systems*, 2000156.

197. Cea, C.; Spyropoulos, G. D.; Jastrzebska-Perfect, P.; Ferrero, J. J.; Gelinas, J. N.; Khodagholy, D., Enhancement-mode ion-based transistor as a comprehensive interface and real-time processing unit for in vivo electrophysiology. *Nature Materials* **2020,** *19* (6), 679-686.

198. AlQahtani, H.; Alswieleh, A.; Al-Khurayyif, I.; AlGarni, S.; Grell, M., Parallel Potentiometric and Capacitive Response in a Water-Gate Thin Film Transistor Biosensor at High Ionic Strength. *Sensors* **2021,** *21* (16), 5618.

199. Kergoat, L.; Herlogsson, L.; Braga, D.; Piro, B.; Pham, M. C.; Crispin, X.; Berggren, M.; Horowitz, G., A water-gate organic field-effect transistor. *Advanced Materials* **2010,** *22* (23), 2565-2569.

200. Bhatt, D.; Kumar, S.; Panda, S., Amorphous IGZO field effect transistor based flexible chemical and biosensors for label free detection. *Flexible and Printed Electronics* **2020,** *5* (1), 014010.

201. Zulkefle, M. A.; Abdul Rahman, R.; Yusof, K. A.; Abdullah, W. F. H.; Rusop, M.; Herman, S. H., Spin Speed and Duration Dependence of TiO2 Thin Films pH Sensing Behavior. *Journal of Sensors* **2016,** *2016*.

202. Yao, P.-C.; Chiang, J.-L.; Lee, M.-C., Application of sol–gel TiO2 film for an extended-gate H+ ion-sensitive field-effect transistor. *Solid State Sciences* **2014,** *28*, 47-54.

203. Yusof, K. A.; Abdul Rahman, R.; Zulkefle, M. A.; Herman, S. H.; Abdullah, W. F. H., EGFET pH sensor performance dependence on sputtered TiO2 sensing membrane deposition temperature. *Journal of Sensors* **2016,** *2016*.

204. Li, J.-Y.; Chang, S.-P.; Chang, S.-J.; Tsai, T.-Y., Sensitivity of EGFET pH sensors with TiO2 nanowires. *ECS Solid State Letters* **2014,** *3* (10), P123.

205. Kajitvichyanukul, P.; Ananpattarachai, J.; Pongpom, S., Sol–gel preparation and properties study of TiO2 thin film for photocatalytic reduction of chromium (VI) in photocatalysis process. *Science and Technology of Advanced Materials* **2005,** *6* (3-4), 352.

206. Parthiban, S.; Anuratha, K.; Arunprabaharan, S.; Abinesh, S.; Lakshminarasimhan, N., Enhanced dye-sensitized solar cell performance using TiO2: Nb blocking layer deposited by soft chemical method. *Ceramics International* **2015,** *41* (1), 205-209.

207. Kim, H.; Hwang, T., Effect of titanium isopropoxide addition in low-temperature cured TiO 2 photoanode for a flexible DSSC. *Journal of sol-gel science and technology* **2014,** *72* (1), 67-73.

208. Tang, H.; Kumar, P.; Zhang, S.; Yi, Z.; Crescenzo, G. D.; Santato, C.; Soavi, F.; Cicoira, F., Conducting polymer transistors making use of activated carbon gate electrodes. *ACS applied materials & interfaces* **2015,** *7* (1), 969-973.

209. Chou, J.-C.; Liao, L. P., Study on pH at the point of zero charge of TiO2 pH ion-sensitive field effect transistor made by the sputtering method. *Thin Solid Films* **2005,** *476* (1), 157-161.

210. Son, H. W.; Park, J. H.; Chae, M.-S.; Kim, B.-H.; Kim, T. G., Bilayer indium gallium zinc oxide electrolyte-gated field-effect transistor for biosensor platform with high reliability. *Sensors and Actuators B: Chemical* **2020,** *312*, 127955.

211. Huang, H.; Ge, C.; Liu, Z.; Zhong, H.; Guo, E.; He, M.; Wang, C.; Yang, G.; Jin, K., Electrolyte-gated transistors for neuromorphic applications. *Journal of Semiconductors* **2021,** *42* (1), 013103.

212. Zhang, H.-T.; Zhang, Z.; Zhou, H.; Tanaka, H.; Fong, D. D.; Ramanathan, S., Beyond electrostatic modification: design and discovery of functional oxide phases via ionic-electronic doping. *Advances in Physics: X* **2019,** *4* (1), 1523686.

213. Shen, H.; Abtahi, A.; Lussem, B. r.; Boudouris, B. W.; Mei, J., Device Engineering in Organic Electrochemical Transistors toward Multifunctional Applications. *ACS Applied Electronic Materials* **2021**.

214. Borghi, F.; Milani, M.; Bettini, L. G.; Podestà, A.; Milani, P., Quantitative characterization of the interfacial morphology and bulk porosity of nanoporous cluster-assembled carbon thin films. *Applied Surface Science* **2019,** *479*, 395-402.

APPENDIX A SUPPLEMENTARY INFORMATION FOR ARTICLE 1: ION-GATED TRANSISTORS BASED ON POROUS AND COMPACT TiO_2 FILMS: EFFECT OF Li IONS IN THE GATING MEDIUM

Arunprabaharan Subramanian[1], Ben George[1], Sanyasi Rao Bobbara[1], Irina Valitova,[1] Irene Ruggeri[1,2], Francesca Borghi[3], Alessandro Podestà[3], Paolo Milani[3], Francesca Soavi[2], Clara Santato[4] and Fabio Cicoira[1]*

[1] Polytechnique Montréal, Department of Chemical Engineering, H3T 1J4, Canada.

[2] Dipartimento di Chimica "Giacomo Ciamician", Università di Bologna, Via Selmi 2, Bologna, 40126, Italy.

[3] CIMaINa and Dipartimento di Fisica "Aldo Pontremoli", Università degli Studi di Milano, via Celoria 16, Milano, 20133, Italy.

[4] Polytechnique Montréal, Department of Engineering Physics, H3T 1J4, Canada.

* Corresponding author: fabio.cicoira@polymtl.ca

BET surface area measurement

Brunauer–Emmett–Teller (BET) measurements were performed employing a surface area analyzer (Micromeritics Gemini, model 2365). According to the method described in previous report,[214] six strips of silicon substrates (5 cm long and 0.5 cm large) are covered by the TiO_2 films deposited by drop-casting. Before each measurement, the samples were degassed under a constant helium flux at 300°C (drop casted TiO_2) for 2 h using a dedicated unit, in order to remove any contaminants which may have been adsorbed on the silicon surface or to the pores of the nanostructured materials. During the adsorption analysis, the values of the relative pressure (P/P_0) ranged from 0.05 to 0.99 for the acquisition of the isotherm plot, while the free space in the test tube was determined by employing a helium gas injection prior measurement. The specific surface area (A_{BET}, expressed in m^2/g) was calculated by considering the relative pressure interval between 0.05 and 0.25, and the associated error was obtained by the propagation of microbalance uncertainty (0.01 $\mu g/cm^2$) and the error of the estimation of the silicon surface area (1%). The total surface area (A_{tot}, expressed in m^2) is the A_{BET} multiplied by the mass of the thin film.

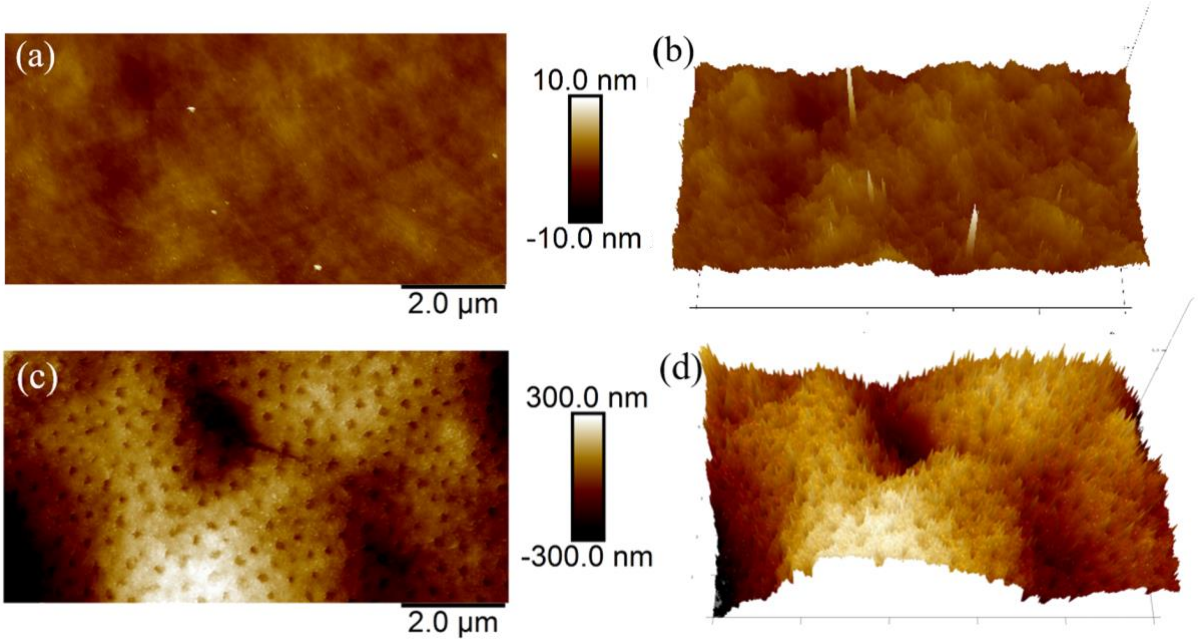

Figure S1. 2D and 3D AFM morphological maps of (a-b) evaporated and (c-d) solution-processed TiO_2 films annealed at 450 ˚C.

Table S1. Hysteresis loop area in linear transfer characteristics of evaporated TiO_2 IGTs.

Gating media	*Area (AV)*
[EMIM][TFSI]	~6×10^{-3}
[Li][TFSI] + [EMIM][TFSI]	~1×10^{-2}

Table S2. Transistor characteristics of evaporated TiO_2 films.

Gating media	$n^{\dagger}$ (cm^{-2})	μ_{lin} $(cm^2V^{-1}s^{-1})$	*ON/OFF ratio*	V_{th} *(V)*
[EMIM][TFSI]	$\sim 2 \times 10^{14}$	$\sim 6 \times 10^{-1}$	3	0.4
[Li] [TFSI] + [EMIM][TFSI]	$\sim 5 \times 10^{14}$	$\sim 5 \times 10^{-1}$	15	0.5

† The values are calculated using geometric surface area.

Table S3. Hysteresis loop area in linear transfer characteristics of solution-processed TiO_2 IGTs.

Gating media	*Area (AV)*
[EMIM][TFSI]	~8×10^{-5}
[Li][TFSI] + [EMIM][TFSI]	~2×10^{-3}

Table S4. Transistor characteristics of solution-processed TiO_2 films.

Gating media	$n^{\dagger}$ (cm^{-2})	μ_{lin} $(cm^2V^{-1}s^{-1})$	*ON/OFF ratio*	V_{th} *(V)*
[EMIM][TFSI]	$\sim 2 \times 10^{15}$	$\sim 5 \times 10^{-4}$	40	1.3
[Li] [TFSI] + [EMIM][TFSI]	$\sim 6 \times 10^{15}$	$\sim 4 \times 10^{-3}$	10^3	0.9

† The values were calculated using geometric surface area.

Table S5. Transistor characteristics of solution-processed TiO_2 films.

Gating media	$n^{\ddagger}$ (cm^{-2})	μ_{lin} $(cm^2V^{-1}s^{-1})$
[EMIM][TFSI]	~5×10^{12}	~2×10^{-1}
[Li][TFSI] + [EMIM][TFSI]	~1×10^{13}	~2

‡The values were calculated using BET surface area.

Table S6. Electrochemical characteristics of evaporated TiO_2 films.

Gating media	*Sweep rate*	*C* † *(mF/cm²)*
[EMIM][TFSI]	*0.5 mV/s*	~1
	5 mV/s	~0.4
	50 mV/s	~0.05
[Li][TFSI] + [EMIM][TFSI]	*0.5 mV/s*	~2.5
	5 mV/s	~0.5
	50 mV/s	~0.1

† The specific capacitance values were calculated using geometric surface area.

Table S7. Electrochemical characteristics of solution-processed TiO_2 films.

Gating media	*Sweep rate*	$C^{\dagger}$ *(mF/cm²)*	$C^{\ddagger}$ *(μF/cm²)*
[EMIM][TFSI]	*0.5 mV/s*	~2	~8
	5 mV/s	~1	~3
	50 mV/s	~0.7	~1
[Li][TFSI] + [EMIM][TFSI]	*0.5 mV/s*	~17	~35
	5 mV/s	~9	~19
	50 mV/s	~5	~9

† Values calculated using geometric surface area.

‡ Values calculated using BET surface area.

APPENDIX B SUPPLEMENTARY INFORMATION FOR ARTICLE 2: COMBINING AQUEOUS SOLUTION PROCESSING AND PRINTING FOR FABRICATION OF FLEXIBLE AND SUSTAINABLE TIN DIOXIDE ION-GATED TRANSISTORS MEDIUM

Arunprabaharan Subramanian,[1] Mona Azimi,[1] Clara Santato,[2] and Fabio Cicoira[1*]

[1] Department of Chemical Engineering, Polytechnique Montréal, H3T 1J4, Montreal, Canada.

[2] Department of Engineering Physics, Polytechnique Montréal, H3T 1J4, Montreal, Canada.

* Corresponding author: fabio.cicoira@polymtl.ca

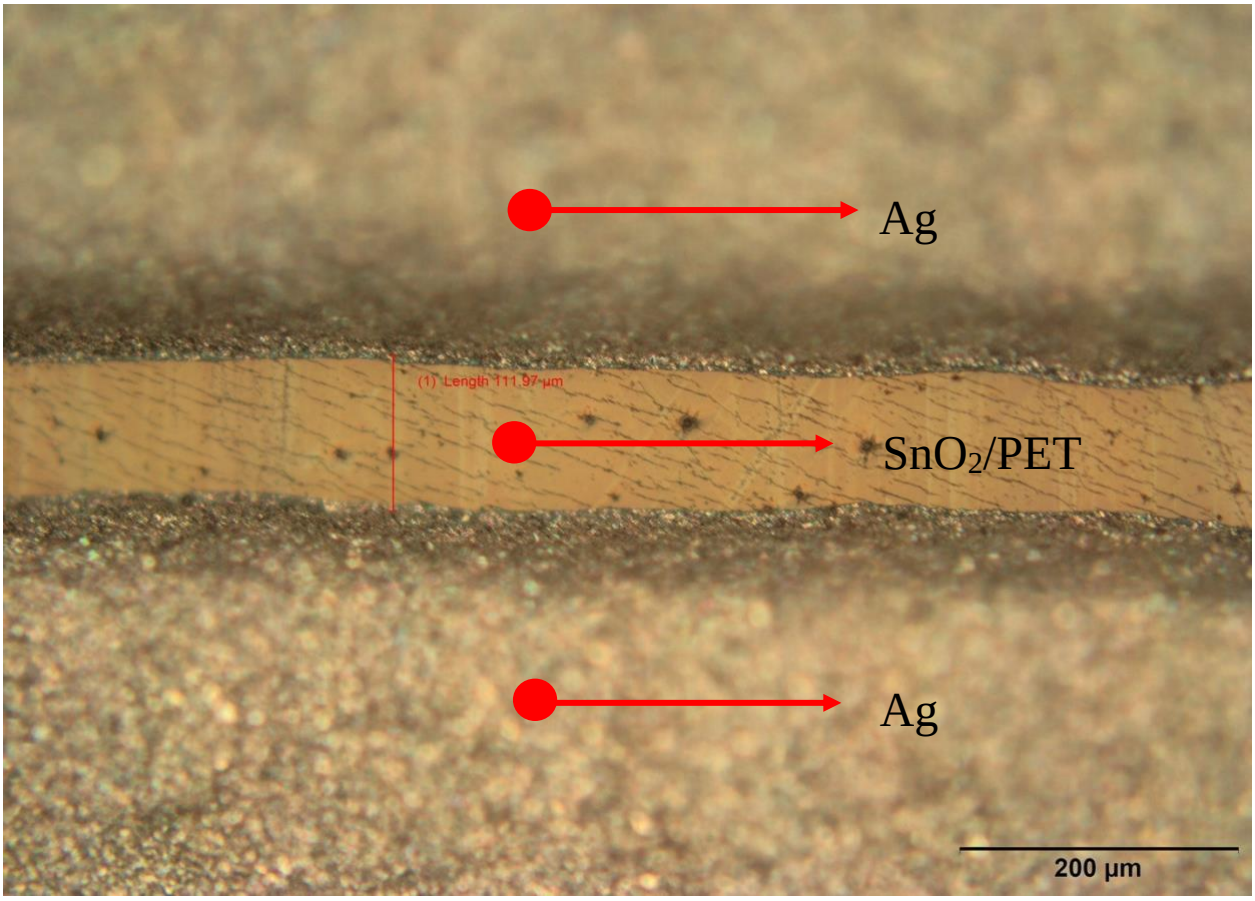

Figure S1. Optical microscope image of silver electrodes printed on SnO_2 films deposited on flexible PET substrates. The channel length is ~ 110 µm.

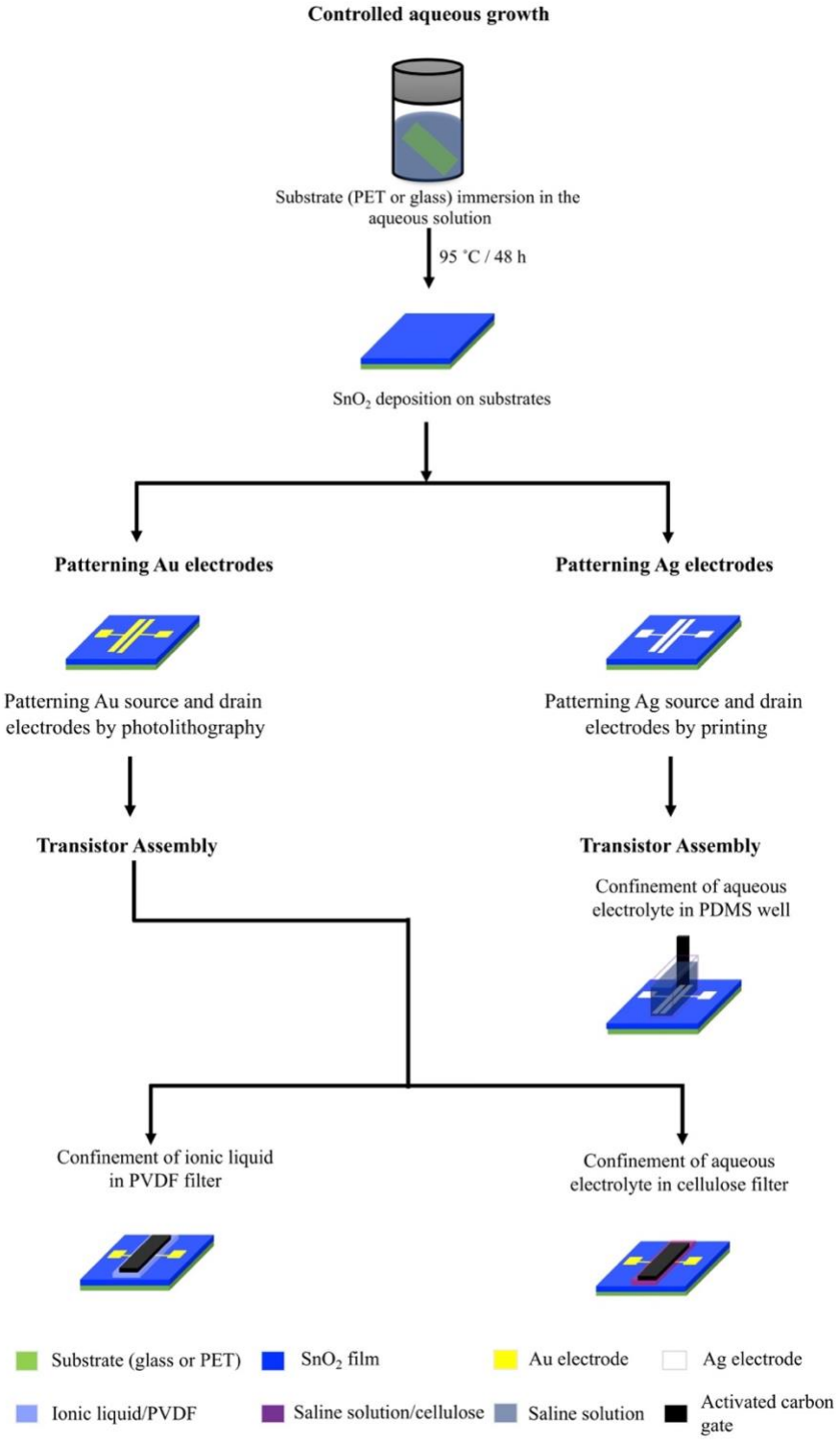

Figure S2. Process flow for the fabrication of the ion-gated transistors investigated in this work.

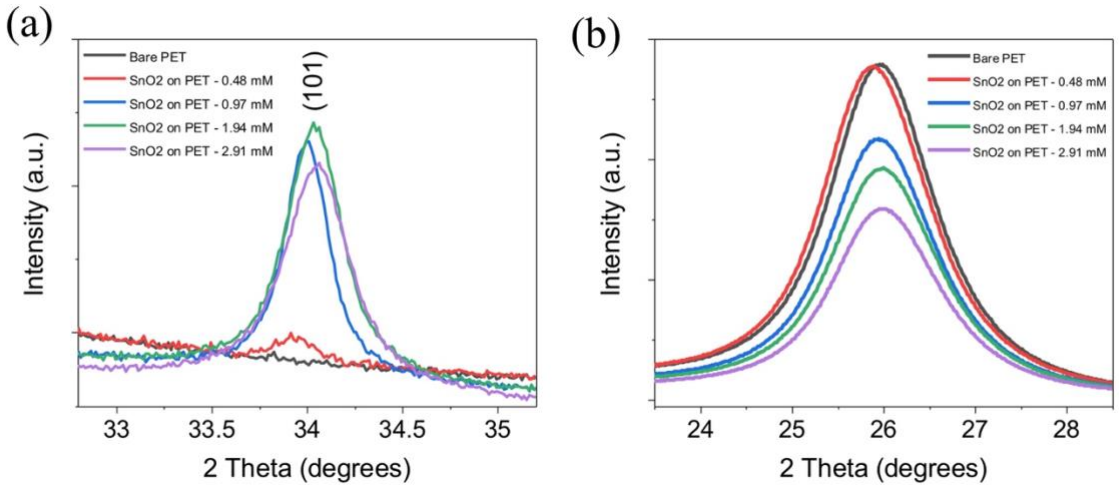

Figure S3. Enlarged view of X-ray diffraction peaks at ~ 2θ = 34 ˚ (a) and ~ 2θ = 26˚ (b).

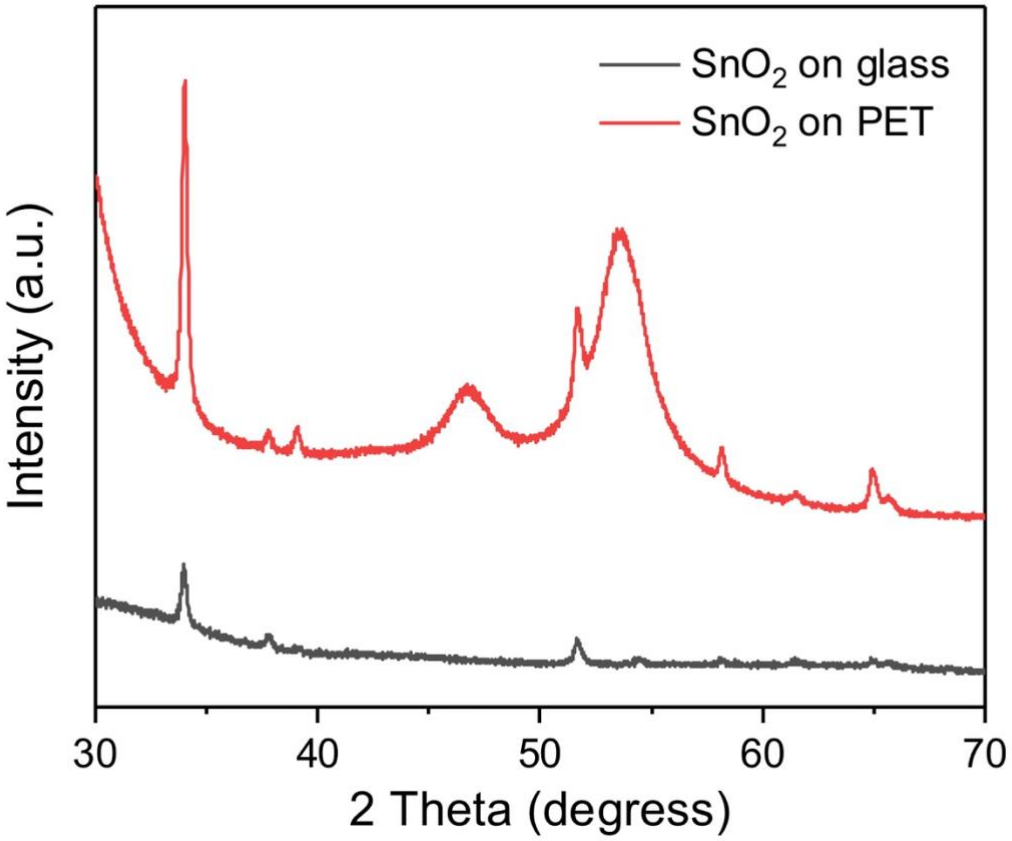

Figure S4. XRD patterns of SnO_2 films prepared with the concentration of 0.97 mM Sn precursor on glass and PET substrates.

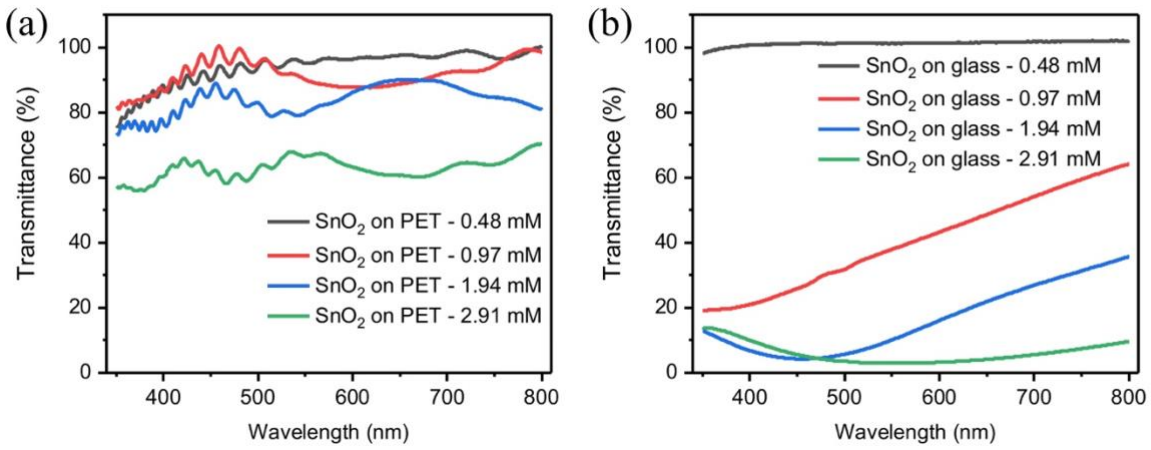

Figure S5. Optical transmittance spectra of the SnO_2 films with different concentrations of Sn precursors on (a) PET substrate and (b) glass substrate.

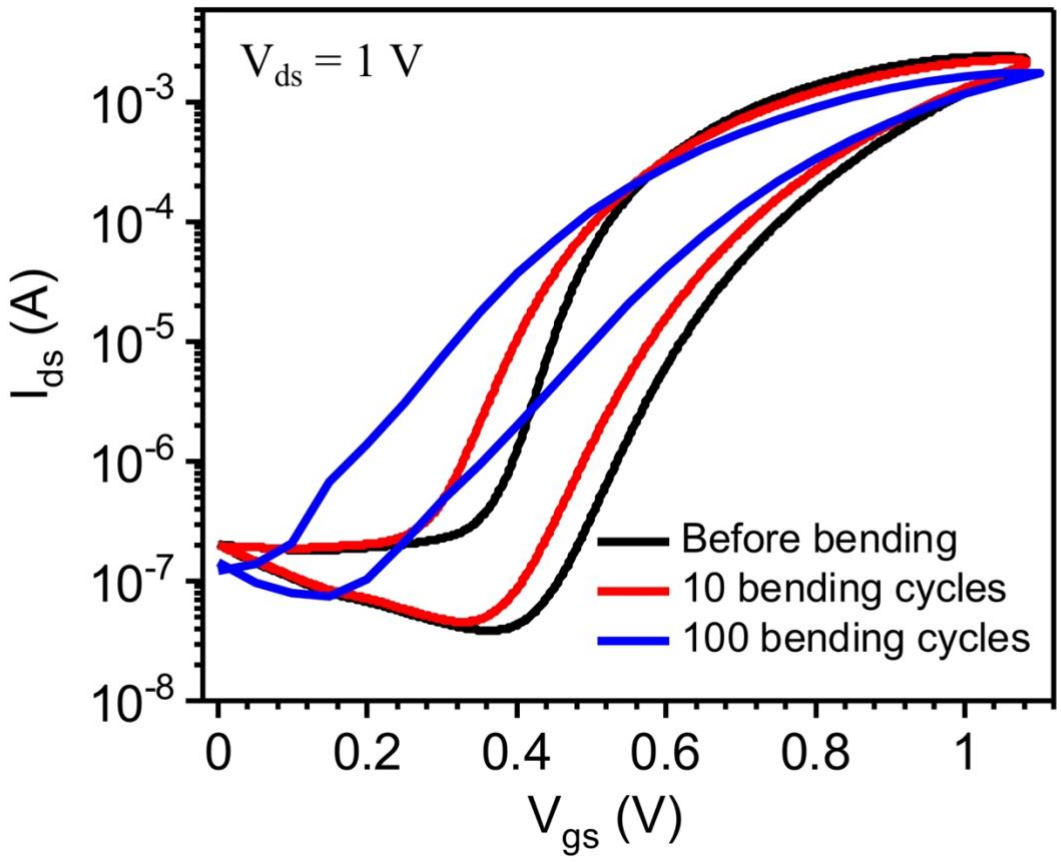

Figure S6. Transfer characteristics of [EMIM][TFSI]-gated IGTs based on SnO_2 films with Au source/drain electrodes on PET substrates measured in N_2 purged glove box before bending and after multiple bending cycles (10 and 100 bending cycles). The transfer characteristics were measured in the saturation regime (V_{ds} = 1 V) with a scan rate of 50 mV/s and represented on logarithmic drain–source current (absolute values) scale versus linear gate-source voltage.

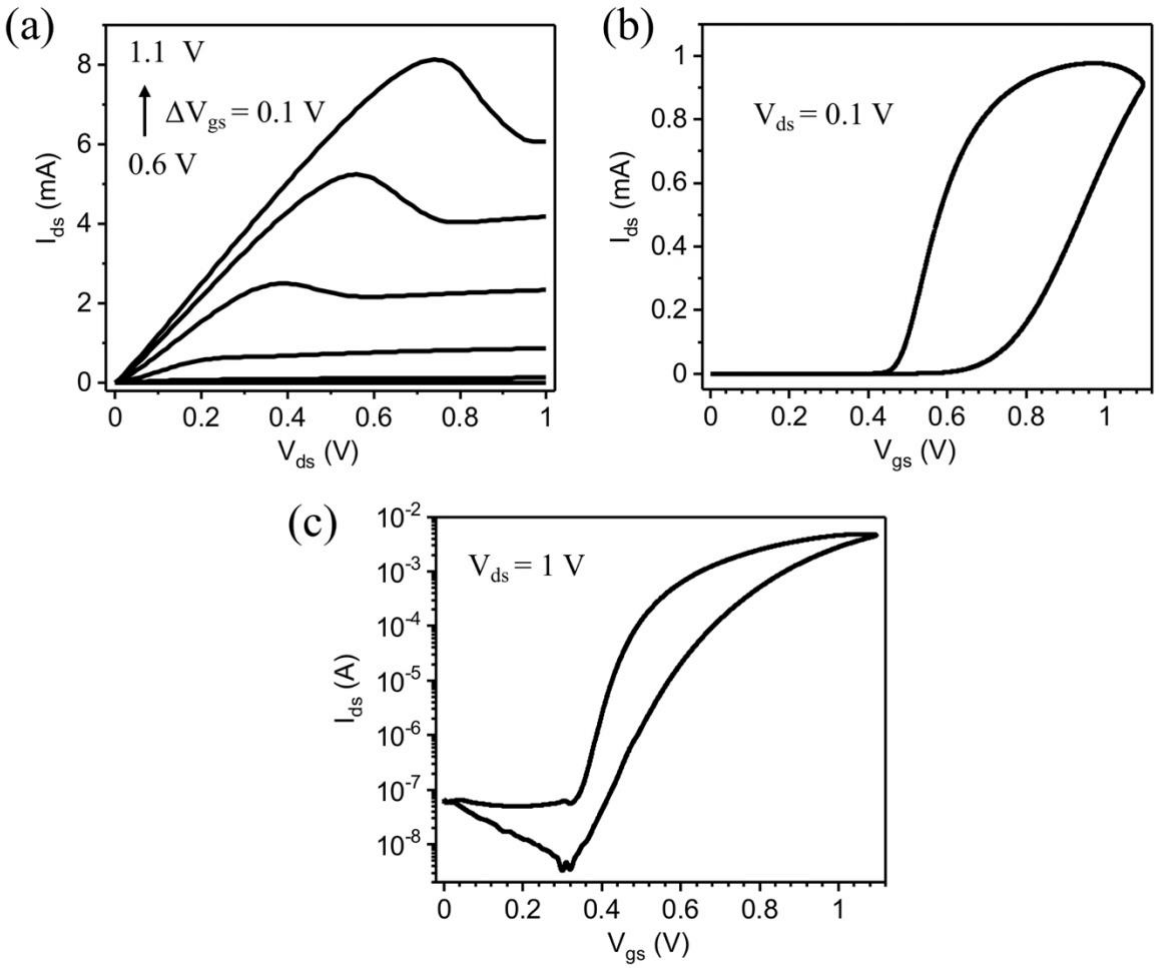

Figure S7. Output (a) and transfer characteristics (b, c) of [EMIM][TFSI]-gated IGTs based on SnO_2 films with Au source/drain electrodes on PET substrates measured in N_2 purged glove box under flat state. The output characteristics (a) were measured at V_{gs} = 0.6, 0.7, 0.8, 0.9, 1.0, 1.1 V with a scan rate of 10 mV/s. The transfer characteristics were measured in the (b) linear (V_{ds} = 0.1 V) and (c) saturation (V_{ds} = 1 V) regime with a scan rate of 10 mV/s. The linear and saturation transfer characteristics are represented on linear and logarithmic drain–source current (absolute values) scale versus linear gate-source voltage.

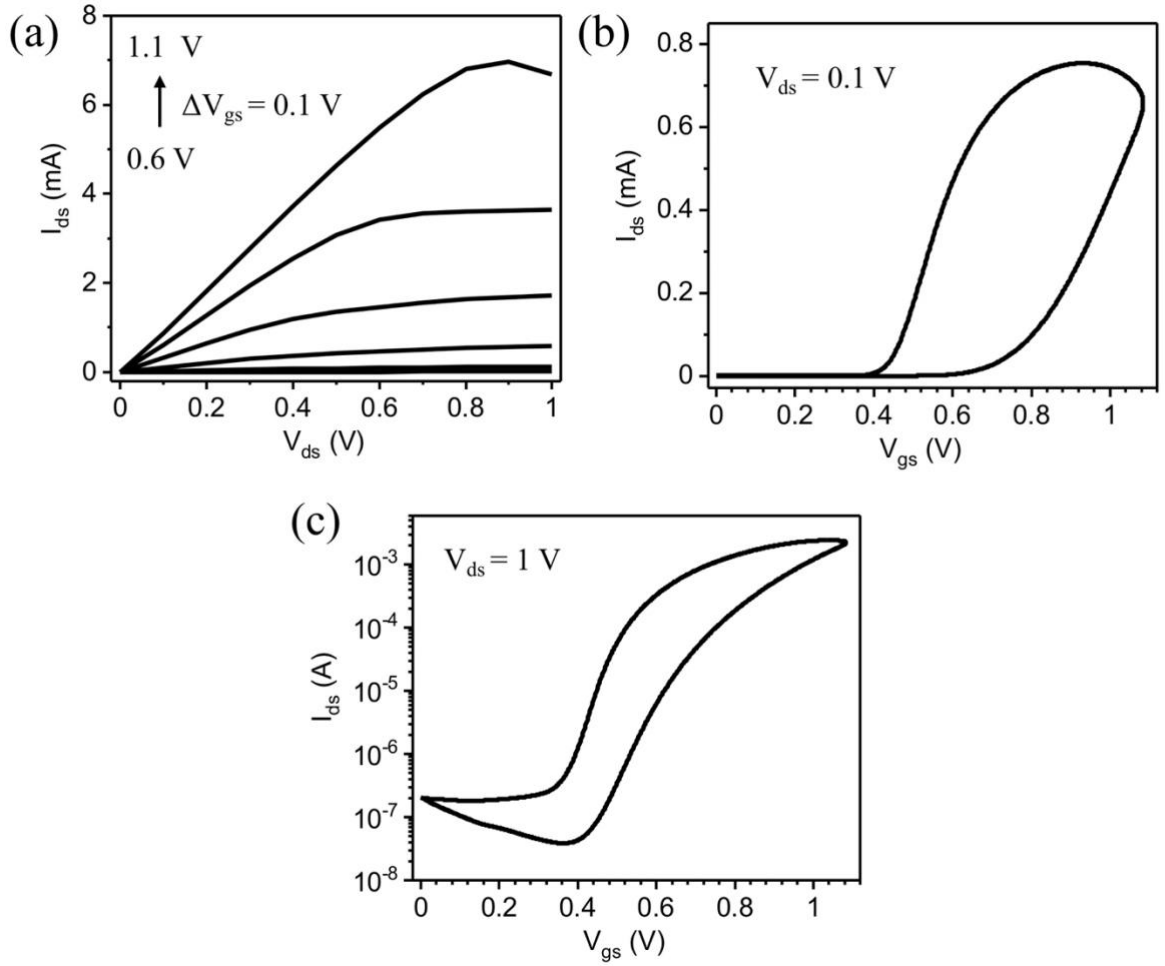

Figure S8. Output (a) and transfer (b,c) characteristics of [EMIM][TFSI]-gated IGTs based on SnO_2 films with Au source/drain electrodes on PET substrates measured in N_2 purged glove box under flat state. The output characteristics were measured at V_{gs} = 0.6, 0.7, 0.8, 0.9, 1.0, 1.1 V with a scan rate of 100 mV/s. The transfer characteristics were measured inr the (b) linear (V_{ds} = 0.1 V) and (c) saturation (V_{ds} = 1 V) regime with a scan rate of 100 mV/s. The linear and saturation transfer characteristics are represented on linear and logarithmic drain–source current (absolute values) scale versus linear gate-source voltage.

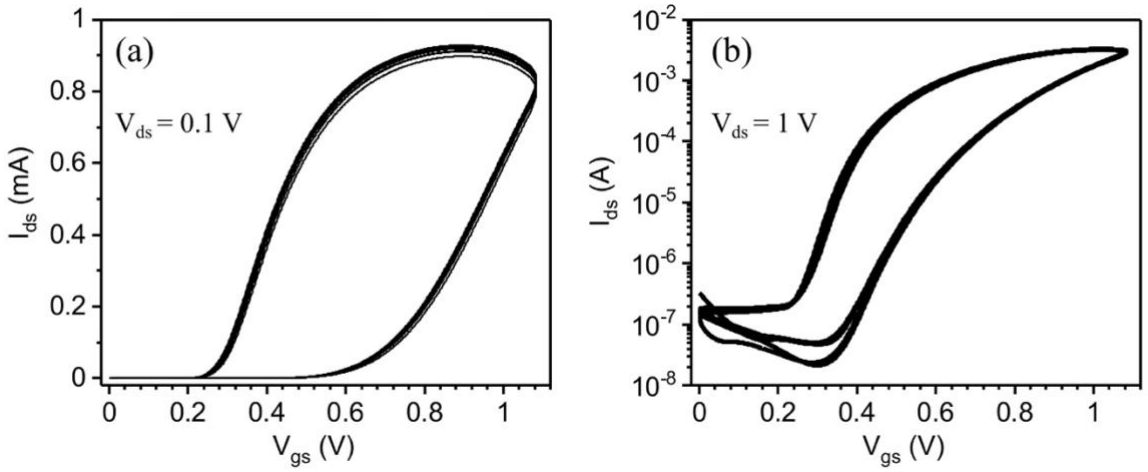

Figure S9. Ten repetitive cycles of transfer characteristics of [EMIM][TFSI]-gated IGTs based on SnO_2 films with Au source/drain electrodes on PET substrates measured in N_2 purged glove box under flat state. The transfer characteristics were measured in the (a) linear (V_{ds} = 0.1 V) and (b) saturation (V_{ds} = 1 V) regime with a scan rate of 50 mV/s. The linear and saturation transfer characteristics are represented on linear and logarithmic drain–source current (absolute values) scale versus linear gate-source voltage.

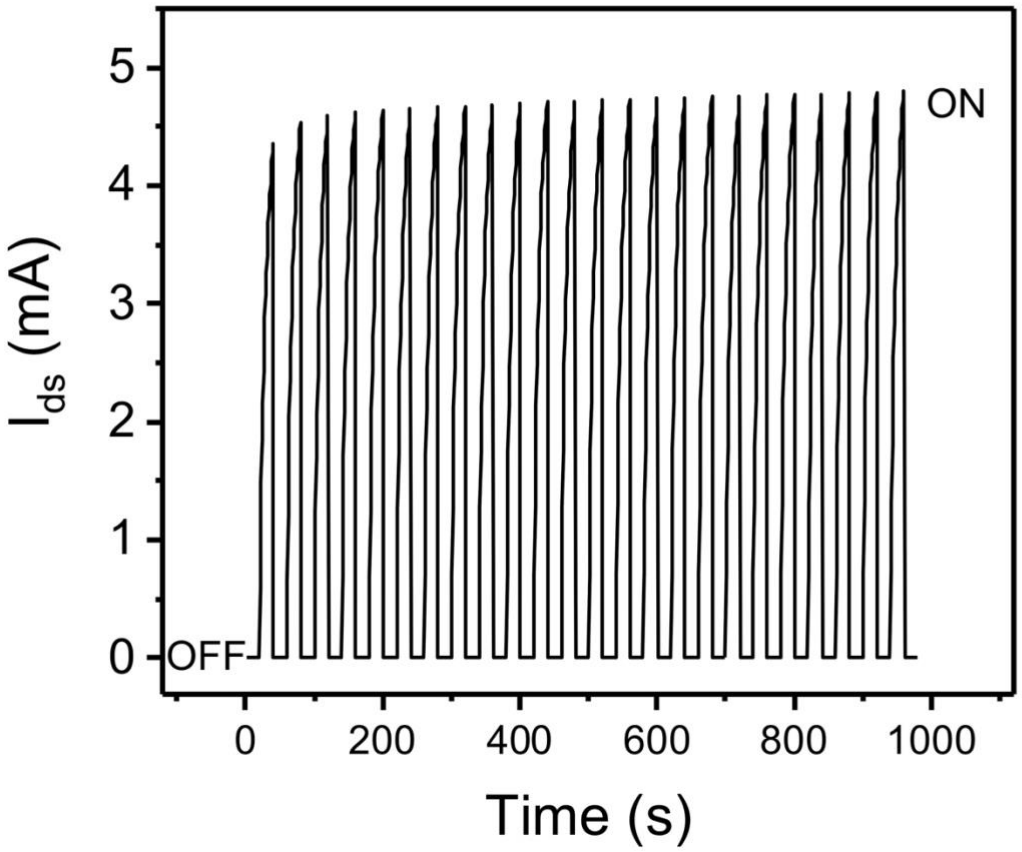

Figure S10. Transient characteristics of [EMIM][TFSI]-gated IGTs based on SnO_2 films with Au source/drain electrodes on PET substrates measured in N_2 purged glove box under OFF state (V_{gs}=0 V, V_{ds} = 1 V) and ON state (V_{gs}=V_{ds}=1V) with an interval of 20 s (24 pulses).

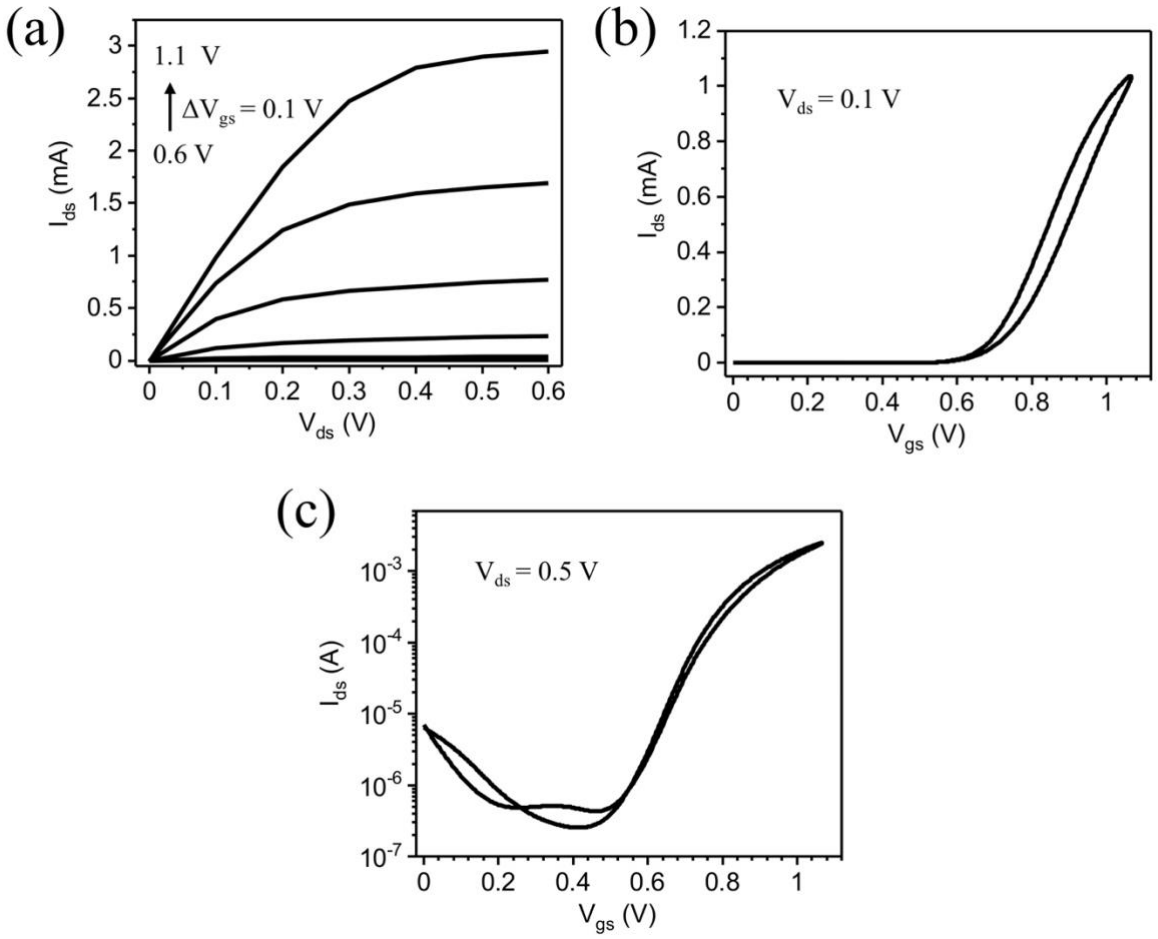

Figure S11. (a) Output and (b, c) transfer characteristics of 0.1M M NaCl aqueous solution gated IGTs based on SnO_2 films with Au source/drain electrodes on PET substrates measured in ambient conditions. Cellulose filter soaked with 0.1M aqueous NaCl solution acted as an ion-gating medium. The output characteristics were measured at V_{gs} = 0.6, 0.7, 0.8, 0.9, 1.0, 1.1 V with a scan rate of 100 mV/s. The transfer characteristics were measured in (b) linear (V_{ds} = 0.1 V) and (c) saturation (V_{ds} = 0.5 V) region with a scan rate of 100 mV/s. The linear and saturation transfer characteristics are represented on linear and logarithmic drain–source current (absolute values) scale versus linear gate-source voltage.

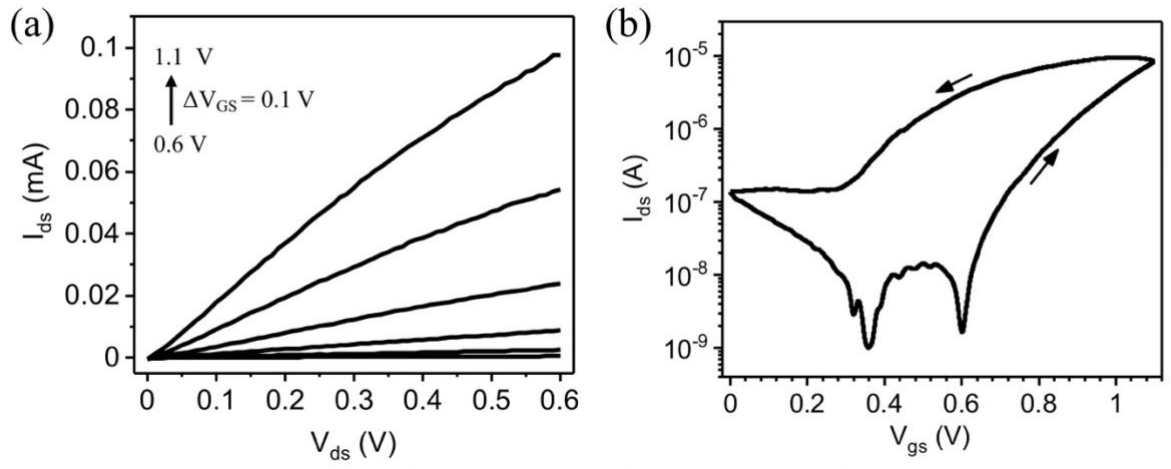

Figure S12. (a) Output and (b) transfer characteristics of [EMIM][TFSI]-gated IGTs based on SnO_2 films with Au source/drain electrodes on glass substrates measured in N_2 purged glove box. The output characteristics were measured at V_{gs} = 0.6, 0.7, 0.8, 0.9, 1.0, 1.1 V and the transfer characteristics at V_{ds} = 0.1 V with a scan rate of 50 mV/s. The transfer characteristics is represented on a logarithmic drain–source current (absolute values) scale versus linear gate-source voltage.

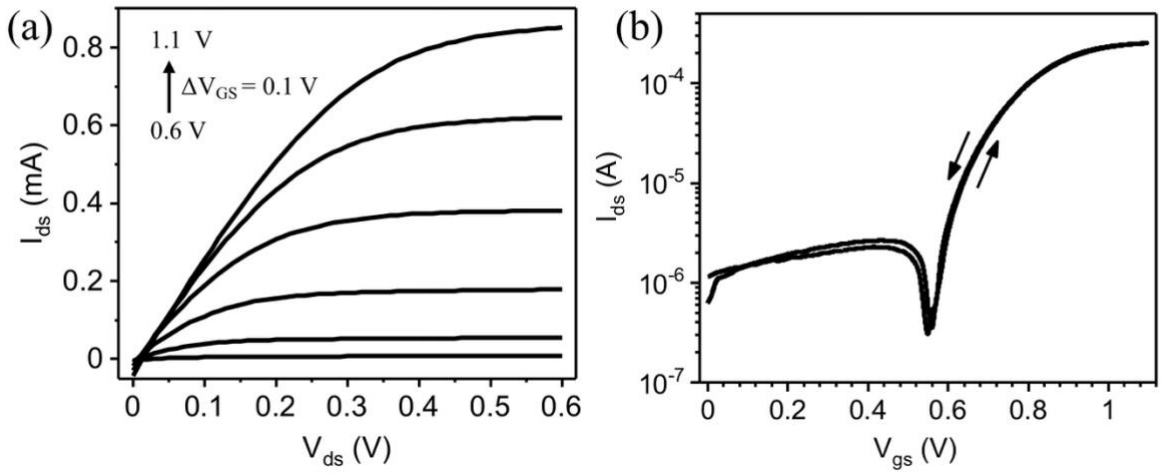

Figure S13. (a) Output and (b) transfer characteristics of the 0.1M NaCl aqueous solution gated IGTs based on SnO_2 films with Au source/drain electrodes on glass substrates measured in ambient conditions. The PDMS well filled with 0.1 M NaCl aqueous solution acted as the gating medium. The output characteristics were measured at V_{gs} = 0.6, 0.7, 0.8, 0.9, 1.0, 1.1 V and the transfer characteristics at V_{ds} = 0.1 V with a scan rate of 50 mV/s. The transfer characteristics are represented on a logarithmic drain–source current (absolute values) scale versus linear gate-source voltage.

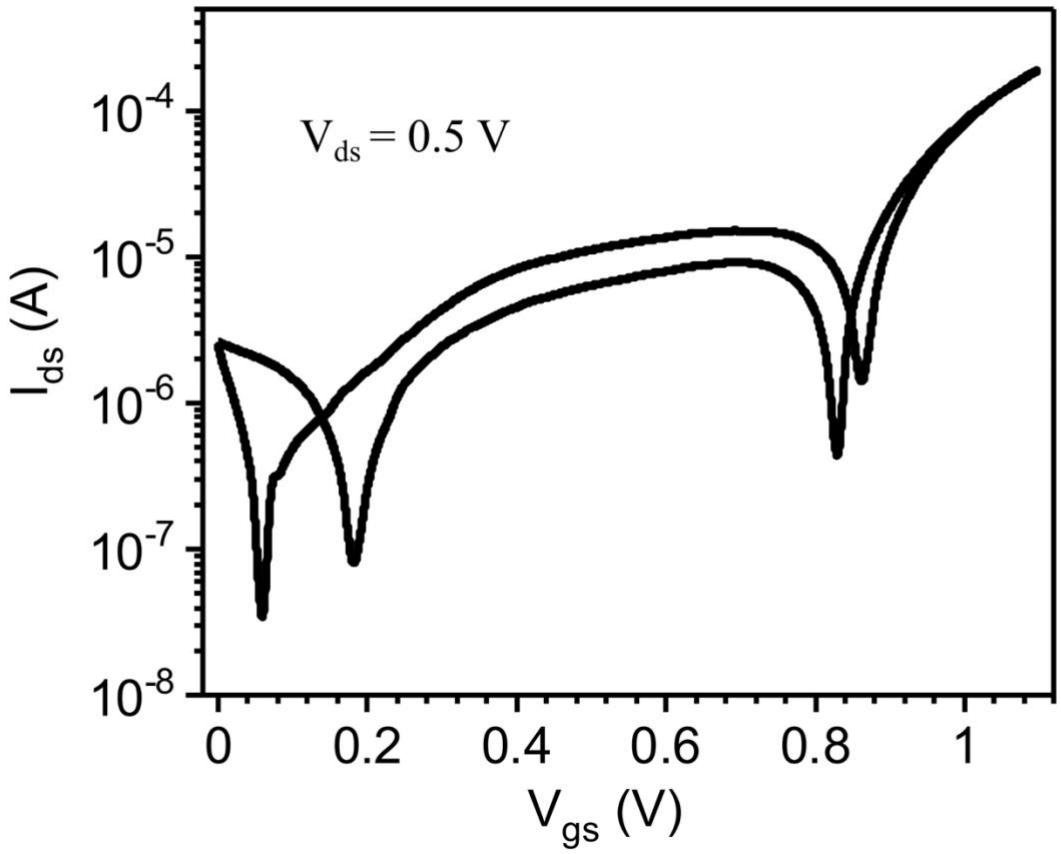

Figure S14. Transfer characteristics of the 0.1 M NaCl aqueous solution gated IGTs based on SnO_2 films with Ag source/drain electrodes on PET substrates measured in ambient conditions. The transfer characteristics were measured at V_{ds} = 0.5 V with a scan rate of 50 mV/s.

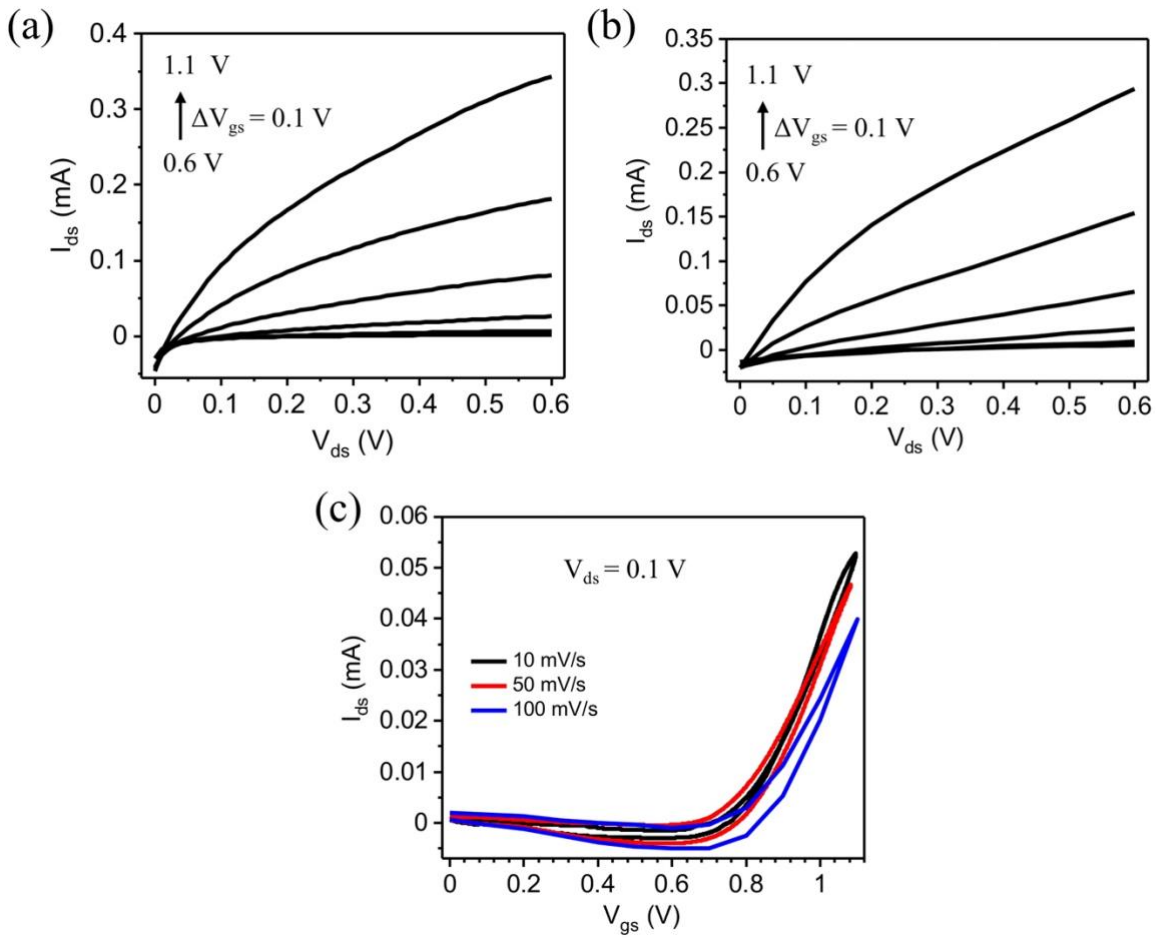

Figure S15. Output (a and b) and (c) transfer characteristics of the 0.1 M NaCl aqueous solution gated IGTs based on SnO_2 films with Ag source/drain electrodes on PET substrates measured in ambient conditions. The output characteristics were measured at V_{gs} = 0.6, 0.7, 0.8, 0.9, 1.0, 1.1 V with a scan rate of (a) 10 mV/s and (b) 100 mV/s. The linear transfer (V_{ds} = 0.1 V) characteristics (c) were measured with a scan rate of 10, 50 and 100 mV/s.

APPENDIX C SUPPLEMENTARY INFORMATION FOR ARTICLE 3: SOLUTION- PROCESSED TITANIUM DIOXIDE ION-GATED TRANSISTORS (IGTS) AND PH SENSORS USING IONIC LIQUID AND AQUEOUS SALINE SOLUTION

Arunprabaharan Subramanian[1], Mona Azimi[1], Cheng Yee Leong[2], Siew Ling Lee[2], Clara Santato[3], Fabio Cicoira[1*]

[1] Department of Chemical Engineering, Polytechnique Montréal, Montreal, Quebec, Canada

[2]Department of Chemistry, University of Technology Malaysia, Johor Bahru, Johor, Malaysia

[3]Department of Engineering Physics, Polytechnique Montréal, Montreal, Quebec, Canada

*** Correspondence:**

Corresponding Author

fabio.cicoira@polymtl.ca

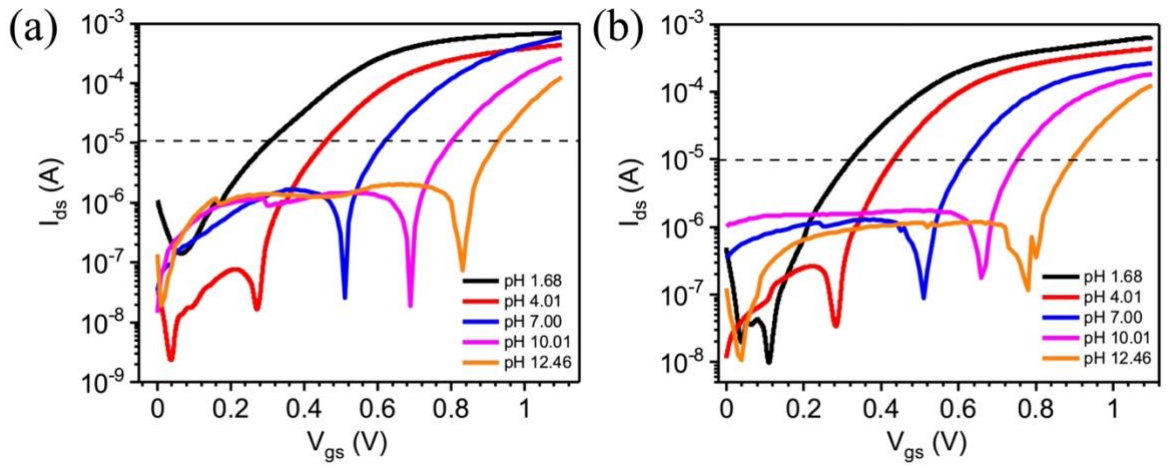

Figure S1. Transfer characteristics (V_{ds} = 0.1 V) of route I TiO_2 films on SiO_2/Si substrates gated with pH buffer (pH 1.68, 4.01, 7.00, 10.01 and 12.46) solutions measured in ambient air. Figure 2 (a) and 2 (b) represents device 2 and device 3.

APPENDIX D LIST OF PUBLICATIONS AT POLYTECHNIQUE MONTREAL NOT INCLUDED IN THE THESIS

1. G. D. O. Silva †, **A. Subramanian**†, X. Meng†, S. Zhang, M. S. Barbosa, B. Baloukas, D. Chartrand, J. C. Gonzáles, M. O. Orlandi, F. Soavi, F. Cicoira and C. Santato, Tungsten oxide ion-gated phototransistors using ionic liquid and aqueous gating media, J. Phys. D: Appl. Phys., **2019**, 52 (30), 305102. *(† equally contributed)*
2. M. Azimi, **A. Subramanian**, N. A. Roslan and F. Cicoira, Flexible organic ion-gated transistors with low operating voltage and light-sensing application, J. Phys. Mater., **2021**, 4 (2), 024001
3. M. Lerond, **A. Subramanian**, W. G. Skene, F. Cicoira, Combining Electrospinning and Electrode Printing for the Fabrication of Stretchable Organic Electrochemical Transistors, Front. Phys., **2021**, 9. 708914.
4. X. Zhou, A. Rajeev, **A. Subramanian**, Y. Li, N. Rossetti, G. Natale, G. A. Lodygensky and F. Cicoira, Self-healing, stretchable, and highly adhesive hydrogels for epidermal patch electrodes, Acta Biomater., **2021**, DOI: 10.1016/j.actbio.2021.07.069

APPENDIX E PARTICIPATION TO CONFERENCES

1. **Subramanian**, M. Azimi, C. Santato and F. Cicoira, Flexible tin dioxide ion-gated transistors using room-temperature ionic liquid and aqueous saline solution, Oral Presentation, Canadian Chemical Engineering Conference, 2021, Montreal
2. **Subramanian**, M. Azimi, C. Santato and F. Cicoira, Tin dioxide ion-gated transistors using ionic liquid and aqueous saline solution, Oral Presentation, IEEE NANO 2021, Montreal
3. **Subramanian**, B. George, S. R. Bobbara, I. Valitova, F. Soavi, C. Santato and F. Cicoira, Effect of channel morphology and gating medium on TiO_2 ion-gated transistors, Poster Presentation, MRS Fall Meeting, 2019, Boston

APPENDIX F SCHOLARSHIPS AND AWARDS RECEIVED AT POLYTECHNIQUE MONTREAL

1. Trottier Scholarship (April 2017), Trottier Energy Institute
2. Québec Government Merit Scholarship Program for Foreign Students (May 2018), Fonds de recherche du Québec - Nature et technologies (Québec-India scholarships)
3. Micro-Nanotechnology Award (October 2017, September 2018, October 2019, February 2021), CMC Microsystems